UNIVERSITY OF SHEFFIELD

NOVEL NUMERICAL PROCEDURES FOR LIMIT ANALYSIS OF STRUCTURES

MESH-FREE METHODS AND MATHEMATICAL PROGRAMMING

by

CANH V. LE

A thesis submitted in partial fulfillment for the
degree of Doctor of Philosophy

in the
Computational Mechanics and Design Research Group
Department of Civil and Structural Engineering

October 2009

Declaration of Authorship

I, Canh Le, declare that this thesis entitled, 'Novel numerical procedures for limit analysis of structures: meshfree methods and mathematical programming' and the work presented in it are my own. I confirm that:

- This work was done wholly or mainly while in candidature for a research degree at this University.
- Where any part of this thesis has previously been submitted for a degree or any other qualification at this University or any other institution, this has been clearly stated.
- Where I have consulted the published work of others, this is always clearly attributed.
- Where I have quoted from the work of others, the source is always given. With the exception of such quotations, this thesis is entirely my own work.
- I have acknowledged all main sources of help.
- Where the thesis is based on work done by myself jointly with others, I have made clear exactly what was done by others and what I have contributed myself.

Signed: _____

Date: _____

SUMMARY

Novel numerical procedures for limit analysis of structures – meshfree methods and mathematical programming

Current research in the field of limit analysis is focussing on the development of numerical tools which are sufficiently efficient and robust to be used in engineering practice. This places demands on the numerical discretisation strategy adopted as well as on the mathematical programming tools applied, which are the key ingredients of a typical computational limit analysis procedure. In this research, the Element-Free Galerkin (EFG) discretisation strategy is used to approximate the displacement and moment fields in plate and slab problems, and second-order cone programming (SOCP) is used to solve the resulting discretised formulations.
A numerical procedure using the EFG method and second-order cone programming for the kinematic limit analysis problem was developed first. The moving least squares technique was used in combination with a stabilised conforming nodal integration scheme, both to keep the size of the optimisation problem small and to provide stable and accurate solutions. The formulation was expressed as a problem of minimizing a sum of Euclidean norms, which was then transformed into a form suitable for solution using SOCP.
To improve the accuracy of solutions and to speed-up the computational process, an efficient h-adaptive EFG scheme was also developed. The naturally conforming property of meshfree approximations (with no nodal connectivity required) facilitates the implementation of h-adaptivity. The error in the computed displacement field was estimated accurately using the Taylor expansion technique. A stabilised conforming nodal integration scheme was also extended to error estimators, leading to an efficient and truly meshfree adaptive method.
To obtain an indication of bounds on the solutions obtained, an equilibrium formulation was also developed. Pure moment fields were approximated using a moving least squares technique. The collocation method was used to enforce the strong form of the equilibrium equations and a stabilised conforming nodal integration scheme was introduced to eliminate numerical instability problems. The von Mises and Nielsen yield criteria were then enforced by introducing second-order cone constraints.

Acknowledgements

The research presented in this thesis has been carried out in the framework of a doctorate at the University of Sheffield, Department of Civil and Structural Engineering, which would not have been possible without help of many, and I am happily in their debt.

I would first like to express my deep gratitude to my supervisors, Matthew Gilbert and Harm Askes, for their scientific and mental support and encouragement during the course of this work. Their invaluable ideas, guidance and trust helped me to overcome a number of difficulties arising in this research.

I would like to acknowledge the financial support received from Ho Chi Minh City Government (300 Masters & Doctors Project) and the University of Sheffield. I would also like to thank to my high-school and university friends for their financial and mental support.

I would like to say thanks to members of the Computational Mechanics and Design research group and my Vietnamese friends in Sheffield for their willingness to help me and for fruitful discussions about a range of topics. Thanks are also extended to Prof. S. Bordas (University of Cardiff), Prof. T. Rabczuk (Bauhaus-University Weimar) and Dr H. Nguyen-Xuan for their discussions on computational aspects of meshfree methods, XFEM and SFEM.

I would like to thank Prof. J. Bonet (University of Swansea) and Prof. E. Maunder (University of Exeter) for having kindly accepted to review this thesis, and Dr T. Bennett (internal coordinator) for conducting the examination.

A special word of thanks also goes to my beloved parents for their love and support. I am definitely indebted to my wife, Yen Nguyen, for her love, understanding, support and patience. She has made me the father of a lovely son, Toan Le. My love for them can not be expressed in words and certainly this thesis is dedicated to them.

Contents

List of Figures

List of Tables

Chapter 1

Introduction

1.1 General

Limit state criteria have been used to design and asses the safety of many engineering components and structures, from simple metal forming problems to large-scale engineering structures and nuclear power plants. A complete elasto-plastic analysis is generally quite complicated due to the need to specify initial stress conditions and to then carry out an analysis in an iterative manner. Difficulties in elasto-plastic analysis and its applications have motivated the development of a simplified direct method, limit analysis, which can be used to identify the collapse load (also known as the limit load, or load carrying capacity, or maximum load intensity) of a structural problem in a simple and more direct manner. By applying the fundamental theorems of plasticity, lower and upper bounds on the load multiplier at the collapse state can be determined directly, without intermediate steps.

The numerical solution process for limit analysis problems generally involves two steps. The *first step* is to discretise the problem fields by introducing a spatial discretisation strategy. One of the most robust and popular discretisation methods is the finite element method (FEM), which decomposes the domain of a continuous problem into a finite number of non-overlapping parts, called elements. Mathematical relations such as complex differential or partial differential governing equations

can be transformed into a set of algebraic equations for each element. Considering the relationship between nodes, a system of algebraic equations that represent the behaviour of the whole continuous domain can be obtained (Zienkiewicz & Taylor, 2000). In the framework of limit analysis, the equations involved may be static equilibrium or kinematical compatibility conditions, together with associated relations.

The *second step* is to formulate a suitable optimisation problem and to apply mathematical programming techniques to obtain a solution. In fact, both static and kinematic theorems can be expressed in the form of an optimisation problem, in which a functional is maximised or minimised, subject to sets of equalities and inequalities. In the kinematic approach, the unknowns in the problem relate to the approximated displacement field, whereas the unknowns are stress parameters in the static approach. Once the stress or displacement fields are approximated and the bound theorems of plasticity theory applied, limit analysis becomes a problem of optimisation involving either linear or nonlinear programming and can respectively be solved using linear or non-linear programming techniques implemented in commercial or in-house optimisation packages.

The two main numerical procedures for limit analysis problems are summarised and shown in Figure 1.1

1.2 Research motivation

Current research in the field of limit analysis is focussing on the development of numerical tools which are sufficiently efficient and robust to be of use to engineers working in practice. These numerical procedures may use continuous, semi-continuous (Krabbenhoft et al., 2005) or truly discontinuous (Smith & Gilbert, 2007) representations of the relevant field parameters; in the present work continuous representations are of particular interest. However, when the FEM is applied some of the well-known characteristics of mesh-based methods can lead to problems: the solutions are often highly sensitive to the geometry of the original mesh,

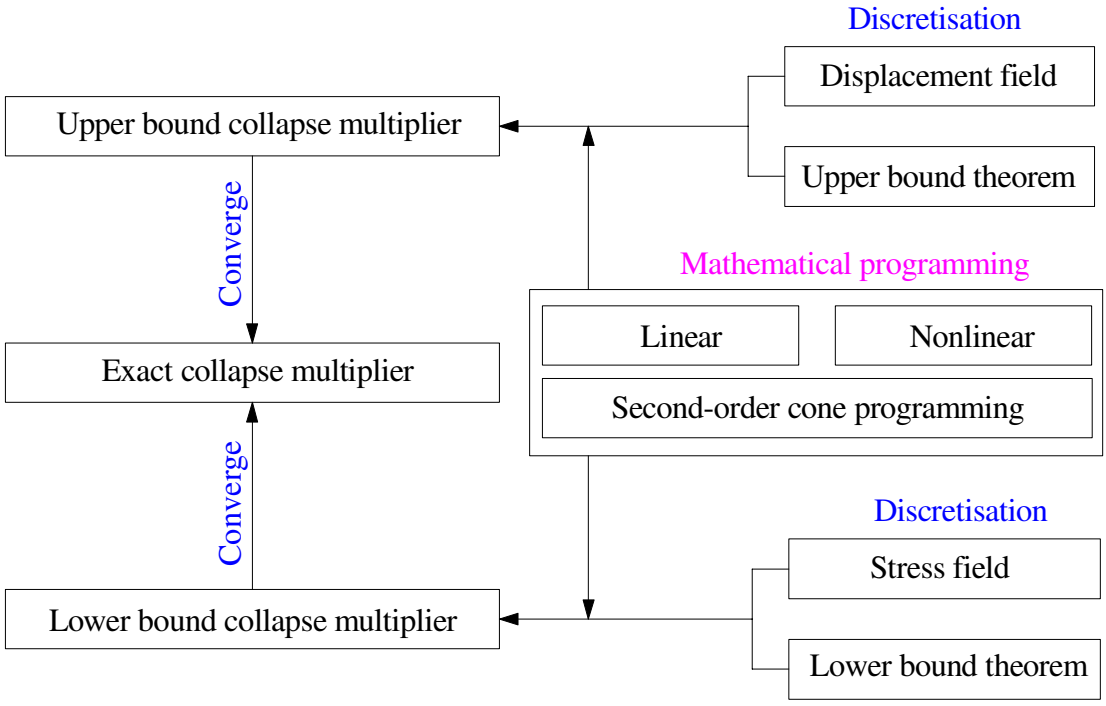

FIGURE 1.1: Limit analysis: numerical procedures

particularly in the region of stress or displacement singularities. Although h-type adaptive refinement schemes (Christiansen & Pedersen, 2001; Borges et al., 2001; Franco et al., 2003; Lyamin & Sloan, 2003; Ciria et al., 2008) have been used in an attempt to overcome such disadvantages, and show immense promise, the schemes quickly become complex and a large number of elements are generally required to obtain accurate solutions.

Moreover, in limit analysis procedures one must solve optimisation problems involving either linear or non-linear programming. When a non-linear yield condition is used, the resulting optimisation problem is non-linear, which presents major difficulties in the solution process. A traditional way of addressing this drawback is to linearise non-linear convex yield criteria, so that the resulting optimisation problem reduces to a linear program. Although this classical linear program can be solved efficiently using Simplex (Anderheggen & Knopfel, 1972; Christiansen, 1981) or interior-point (Andersen & Christiansen, 1995; Christiansen

& Kortanek, 1991) algorithms, a large number of constraints generated in the linearisation process would be needed in order to provide accurate solutions (especially for three-dimensional problems), thereby increasing the computational cost. Attempts have also been made to solve problems involving exact convex yield functions using non-linear programming packages. However, non-linear programming problems are often computationally expensive to solve, with the consequence that often only relatively small problems can be tackled.

The present research focusses both on the discretisation method and on ensuring that the problem is posed in a way that is amenable to rapid solution using an efficient optimisation algorithm. The first aim of the research is to apply so-called 'meshless' methods, which have been developed in recent years to provide a flexible alternative approach to FEM, to the field of limit analysis. These methods use sets of nodes distributed across the problem domain, and also along domain boundaries. One of the first meshless methods developed is the Element-Free Galerkin (EFG) method (Belytschko et al., 1994). The EFG method has been applied successfully to a wide range of computational problems, proving popular due to its rapid convergence characteristics and its ability to obtain highly accurate solutions (Askes, 2000; Liu & Gu, 2005; Chen et al., 2006). Furthermore, the naturally conforming property of meshfree approximations (with no nodal connectivity required) facilitates the implementation of h-adaptivity. Nodes may be moved, discarded or introduced without the need for complex manipulation of the data structures involved. It therefore seems appropriate to investigate the performance of the EFG method when applied to limit analysis problems. Furthermore, in order to obtain efficient meshfree based numerical procedures, a stabilised conforming nodal integration proposed by Chen et al. (2001a) will also be applied within the framework of limit analysis.

The second aim is to increase the efficiency of solving the underlying mathematical optimisation problem generated so that the solutions of large-scale problems in practical engineering can be obtained efficiently. A difficulty present in upper-bound limit analysis problems is that the objective function in the associated optimisation problem is convex, but not everywhere differentiable. One of the most

efficient algorithms to overcome such a difficulty is the primal-dual interior-point method presented in Andersen et al. (2003) and implemented in commercial codes such as the Mosek software package (Mosek, 2008). Furthermore, the algorithm is also suitable for solving lower-bound limit analysis problems since most yield conditions can be described using conic constraints (Makrodimopoulos, 2009). The limit analysis problem involving conic constraints can then be solved by this efficient algorithm (Makrodimopoulos & Martin, 2006b; Krabbenhoft et al., 2007; Ciria et al., 2008; Munoz et al., 2009).

In order to achieve the overall aims, the following tasks will be undertaken:

- Formulate a kinematic limit analysis formulation based on the EFG discretisation strategy and construct a smoothing scheme using a stabilised conforming nodal integration technique.
- Develop a complete solution procedure for the discretised kinematic problem using second-order cone programming.
- Develop an *a posteriori* error estimator based on the stabilised conforming nodal integration scheme. Implement an h-adaptive EFG method to increase the efficiency of the proposed kinematic procedure.
- Develop an EFG based equilibrium limit analysis formulation for application to rigid-perfectly plastic plates and slabs, and solve the resulting static formulation using second-order cone programming.

1.3 Thesis outline

The thesis consists of eight core chapters. Three of these (chapters 4, 5 and 6) are presented as self-contained manuscripts which have been published or submitted for publication. As a result of using this 'three-paper' format, some minor overlap in the content may occur. The contents of each chapter will now be briefly described.

Chapter 2 consists of two main sections which provide a literature review of computational limit analysis and mesh-free methods. The limit analysis section starts with historical remarks and is followed by a brief description and discussion on computational issues. Applications of numerical limit analysis are also outlined, mainly considering application to plates, slabs and geomechanics problems. The second section focusses mainly on mesh-free approximation techniques and numerical implementation details. Applications of mesh-free methods to various engineering problems are also considered.

In chapter 3, a brief description of plasticity relations and limit analysis theory is first provided. Then, a comprehensive discussion of limit analysis formulations and of the mathematical theory of duality is presented. The second part of this chapter starts with a discussion on EFG shape functions and their derivatives. A stabilised conforming nodal integration scheme and an *a posteriori* error estimation scheme are also described. The chapter is closed by providing a brief description of the general framework of conic programming.

Chapter 4 describes a complete numerical procedure to allow computation of approximate upper bounds on the limit load of plates. Three main ingredients are presented: the EFG approximation, a curvature smoothing stabilisation scheme and second-order cone programming. Various numerical examples are examined to test the performance of the proposed procedure. The present solutions are validated against benchmark results from the literature.

In chapter 5, after a brief description of the kinematic formulation which forms the core theoretical part of chapter 4, an error estimator and h-adaptivity scheme for upper bound limit analysis problems are presented. The efficiency of the adaptive procedure is validated by comparing solutions with those obtained using uniform refinement, and with results obtained previously.

In chapter 6, a novel EFG equilibrium model which uses a smoothed moment derivatives stabilisation scheme is described in detail. A discussion of how boundary conditions are enforced is also given. A numerical procedure for static limit analysis problems is completed by introducing second-order cone constraints for

both Nielsen and von Mises yield criteria. The new approach is tested by examining various reinforced concrete slab and metal plate examples. The solutions obtained by the proposed procedure are validated against analytical solutions and benchmark results from the literature.

In chapter 7, some of the broad issues which have come to light in the course of the research are discussed. The convergence characteristics of the methods developed are studied and various computational issues also are discussed.

Finally, key conclusions are drawn and recommendations for future work are presented in chapter 8.

1.4 Publications

Parts of this thesis have been published in or submitted to international journals or presented in conferences. These papers are:

[1] C. V. Le, M. Gilbert and H. Askes. Limit analysis of plates using the EFG method and second-order cone programming. *International Journal for Numerical Methods in Engineering*, 78, 1532–1552, 2009.

[2] C. V. Le, H. Askes and M. Gilbert. A novel numerical procedure for limit analysis of plates: adaptive EFG combined with SOCP. *Proceeding of the 17th UK National Conference on Computational Mechanics in Engineering*, 291–294, 2009.

[3] C. V. Le, H. Askes and M. Gilbert. An adaptive Element-Free Galerkin method applied to limit analysis of plates, *Computer Methods in Applied Mechanics and Engineering*, revising.

[4] C. V. Le, M. Gilbert and H. Askes. Limit analysis of plates and slabs using a meshless equilibrium formulation, *International Journal for Numerical Methods in Engineering*, accepted, 2009.

Chapter 2

Literature review

2.1 Limit analysis

Plastic limit analysis is concerned with the final stage of the plastic response of components and structures, i.e. plastic collapse. It allows the ultimate load-carrying capacity of a solid or structure to be assessed without analysing the entire history of the response, which is required in a conventional incremental elasto-plastic analysis. A great amount of work has been done to develop limit analysis theory and numerical tools for use by engineers working in practice. In this section, both theoretical and computational aspects of limit analysis will be reviewed.

2.1.1 Historical remarks

Based on a rigid-perfectly plastic model of material, the theory of limit analysis has been developed since the early twentieth century. The first complete formulation of the upper and lower bound theorems was introduced by Drucker et al. (1952). Prager (1972) and Martin (1975) also made landmark contributions and since then there has been a continuing interest in the development and application of limit analysis. Significant contributions to the application of limit analysis in

structural engineering were made by Hodge (1959, 1961, 1963). Shortly afterwards, Massonnet & Save (1967) and Save & Massonnet (1972) made further significant progress. Since then, a great deal of attention has been paid to extending both theoretical aspects and its application to various practical engineering problems, see e.g. Chakrabarty (1988); Chen & Han (1988); Lubliner (1990); Kamenjarzh (1996); and more recently Jirasek & Bazant (2002).

2.1.2 Computational limit analysis

Limit analysis makes use of the fundamental theorems of plastic analysis to provide a powerful means of estimating the maximum load sustainable by a solid or structure. However, exact analytical solutions have been determined for only a limited class of problems, usually those with a regular geometry and simple loading. An exact solution is rarely obtainable for most practical problems with arbitrary geometry and boundary conditions, and numerical approximations must therefore be developed.

The progress of numerical limit analysis strongly relies on the development of both discretisation methods and mathematical programming techniques. Over the past four decades, many numerical solution methods for limit analysis problems have been developed, and in parallel significant progress has been made in developing powerful numerical analysis and optimisation techniques. The first attempt to solve two-dimensional plastic limit analysis of continua problems appears to have been made by Koopman & Lance (1965). In their investigations a finite difference method was employed to approximate the stress fields, and equilibrium equations were enforced at all points in a grid. A well-known drawback of the finite difference method is that its formulation is not well-suited to problems with arbitrary geometry and loading conditions. Consequently, discretisation by finite elements has become an indispensable and universal alternative numerical analysis tool.

It can be noted from the literature that limit analysis problems can be tackled using two different numerical approaches. The first method is based on incremental evaluations of the nonlinear stress-strain relations of flow theory, and may be

performed either using the iterative Newton-Raphson method (e.g. Argyris (1967); Marcal & King (1967); Zienkiewicz et al. (1969)) or using mathematical programming (e.g. Maier (1968); Cohn & Maier (1979)). However, incremental methods may be computationally expensive because of the need to perform an analysis in an iterative manner. The second approach, based on the fundamental limit theorems of plasticity, determines directly the limit load factor without intermediate steps by combining mathematical programming and (usually) a finite element discretisation. The method has become a powerful tool of solving problems of arbitrary geometry thanks to dramatic developments in computer technology. The development of the direct method has been the result of pioneering works by Brion & Hodge (1967); Hodge & Belytschko (1968); Neal (1968); Maier (1970); Nguyen-Dang (1976); Christiansen (1980); Casciaro & Cascini (1982), amongst others.

Key features of the direct limit analysis approach are:

- application of variational principles;
- spatial discretisation techniques;
- ways of enforcing the yield condition;
- choice of optimisation algorithm.

2.1.2.1 Variational principles

Markov (Markov, 1947) and Hill's principles (Hill, 1950) are the two main variational principles used in engineering mechanics, expressed in terms of strains and stresses respectively (see Section 3.1.2 for further details). The direct consequences of these minimisation principles for the case of proportional loading are respectively the fundamental upper and lower bound theorems of plastic limit analysis (Save & Massonnet, 1972), see Section 3.1.3 for further details. These one-field principles provide the theoretical foundations to enable pure spatial discretisation in the displacement or equilibrium models. In other words, if the displacement field is approximated and the upper-bound theorem is applied, an upper-bound on

the actual collapse multiplier can be determined, while the lower-bound solution can be obtained as a result of employing an equilibrium model and the lower-bound theorem. On the other hand, an approximation of the collapse multiplier can also be achieved with the use of two-field principles which gives rise to the saddle-point problem (min-max) obtained by modifying Markov's principle. Such mixed-approaches provide the theoretical foundation for the use of mixed or hybrid finite elements.

2.1.2.2 Spatial discretisation techniques

The finite element method is the most universal numerical analysis technique applicable to problems involving complex geometries, boundary conditions and material properties. It is, therefore, understandable that finite elements have been the subject of numerous publications not only in the field of plastic limit analysis but also in physical and engineering models in general. In the literature there are three main types of finite element models, which use either displacement, equilibrium and mixed formulations.

Numerical procedures for lower-bound limit analysis using equilibrium finite elements have been developed by several investigators (Hodge & Belytschko, 1968; Nguyen-Dang, 1976; Bottero et al., 1980; Krabbenhoft & Damkilde, 2002; Lyamin & Sloan, 2002a). In the equilibrium finite element formulation, the assumed stress or moment fields within each element are expressed in terms of spatial coordinates and parameters that are usually associated with nodal stress/moment values. These approximated fields are also required to satisfy *a priori* the boundary equilibrium conditions (relations between the external load and internal stress distribution) and equilibrium at interfaces between continuous finite elements. Therefore, a set of linear conditions on the stress/moment parameters have to be introduced in order to satisfy static admissibility. Due to these additional conditions, construction of such fields is often more difficult than construction of the dual fields - the displacement or velocity fields.

In displacement finite elements, the velocity fields are represented by a continuous function expressed in terms of spatial coordinates and nodal velocities. Compared with equilibrium models, the displacement formulation is more popular as: (i) the internal compatibility condition can be satisfied straightaway in the assembly scheme, and (ii) boundary conditions can be enforced directly. Displacement finite elements have been applied to limit analysis problems by workers such as Hodge & Belytschko (1968); Anderheggen (1976); Capsoni & Corradi (1997) and Krabbenhoft et al. (2005).

Mixed finite elements have been also developed for limit analysis problems (Christiansen, 1981, 1996; Capsoni, 1999; Yu & Tin-Loi, 2006). The attractive features of the mixed formulation are that it allows both stresses and displacements to be determined directly, and volumetric locking can be avoided. The only drawback of such mixed approaches is the lack of information on the status of the solutions obtained, that is, it is *a priori* unclear whether the solution will be an upper bound or a lower bound. Another discretisation method, the Boundary Element Method (BEM), has been also applied to limit analysis problems, see e.g. Maier & Polizzotto (1983); Panzeca (1992); Liu et al. (2004) and Zhang et al. (2004). However, a drawback of the BEM is that a fundamental solution/Green function of the problem must be known.

2.1.2.3 Enforcement of the yield condition

In order to obtain a true lower-bound, it is vital to enforce the yield criterion everywhere in the problem domain. Hodge & Belytschko (1968) introduced a method to treat plate problems using quadratic moment fields. In their paper, the constraints are imposed only at points where the yield condition is likely to be most important, e.g relative maxima points. The location of these relative maxima points is calculated within each step of the mathematical programming algorithm. This process is time-consuming and complicated, and the relative maxima points may not exist, or may be located outside an element.

An alternative method is to fulfill the yield condition only at a number of selected points in each element (Zavelani-Rossi, 1974). However, the optimal solution so obtained cannot be considered as a true lower-bound. To address this, an *a posteriori* check is performed on the solution, using a sufficiently large number of points within elements. Constraints at points where the yield condition is violated can then be added to the optimisation problem. The process is repeated until the yield criterion is satisfied at all points evaluated, so as to obtain a truly statically admissible field. Alternatively, if only linear shape functions are used, the yield condition only needs to be checked at nodal points (e.g. Lysmer (1970); Lyamin & Sloan (2002b) and Ciria et al. (2008)).

2.1.2.4 Mathematical programming

The efficiency of any numerical procedure for limit analysis problems usually relies on the choice of mathematical programming algorithm used to enable a solution to be obtained. From a mathematical point of view, Linear Programming (LP) is very attractive, and has been widely applied to limit analysis problems, as in the following references (Anderheggen & Knopfel, 1972; Cohn & Maier, 1979; Grierson, 1977; Nguyen-Dang, 1984; Sloan, 1988). Typically this involves a piecewise linear approximation of non-linear yield surfaces, see e.g. Maier (1970); Laudiero (1972); Tin-Loi (1990) and Christiansen (1996). Existing optimisation algorithms, such as the simplex method or the more recently developed family of interior point methods can then be applied.

By means of a Newton type scheme, von Mises or other nonlinear yield functions can be used directly in nonlinear programming formulations. An important step in most algorithms designed to solve non-linear problems is to eliminate linear or non-linear constraints by introducing Lagrangian multipliers. The problem then becomes an unconstrained functional, and several iterative methods have been proposed to treat such problems, see for example Gaudrat (1991); Zouain et al. (1993); Liu et al. (1995) and Andersen (1996).

As a direct method for use with nonlinear programming solvers, the elastic compensation method modifies the Young's modulus of each element. The optimised statically admissible stress field is obtained in each iteration of a linear-elastic finite element solution scheme. The development and application of the method in practical computation has been addressed by Mackenzie & Boyle (1992); Ponter & Carter (1997); Ponter et al. (2000); Chen & Ponter (2001); Maier et al. (2003); Boulbibane & Ponter (2005) and Boulbibane & Ponter (2006).

2.1.3 Applications of numerical limit analysis

Applications of limit analysis can be found in various engineering sectors. For example, limit analysis can be applied to problems involving metal forming, plates and shells, masonry structures and geotechnical materials. However, perhaps the two most significant applications in civil engineering will be reviewed in the following sections.

Application to plates and slabs

The yield line method has been shown to provide an effective means of performing plastic analysis of slabs and plates (Wood, 1961; Johansen, 1962). This well-known method can predict accurate upper bounds on the actual collapse multiplier for many practical engineering problems. However, as it is fundamentally a hand-based analysis method, difficulties are encountered when treating problems of arbitrary geometry, especially when the problems involve columns or holes. Consequently, various computational limit analysis procedures which use finite elements and mathematical programming have been developed over the past few decades. The first, ground-breaking, numerical procedure for rigid-plastic limit analysis problems was developed by Hodge & Belytschko (1968). In their paper, the problem field was approximated using finite elements and the Sequential Unconstrained Minimisation Technique (SUMT) was employed to solve the resulting optimisation problem. Surprisingly, their results remained for a long time the

best available and were referred to as such in reviews compiled by Save & Massonnet (1972) and Save (1995), despite the fact that relatively coarse meshes and incompatible finite elements were used.

Another method based on a class of mixed finite element discretisations was proposed by Christiansen & Larsen (1983). A dual limit analysis formulation for plate bending problems was described and mixed displacement and moment finite elements were used. The mixed method provides simultaneous approximations of the collapse multiplier, and both moment and displacement fields are determined directly. The von Mises yield criterion for plate bending was linearised and the resulting optimisation problem can be solved by using a general linear programming package. However, a solution which involves linearisation of the yield surface is not as accurate as when using the exact non-linear yield condition. Consequently, since then attention has focussed on developing non-linear optimisation algorithms to enable a solution to be obtained in an efficient way. Capsoni & Corradi (1997) presented a direct iterative algorithm for the kinematic formulation of plane strain problems. The algorithm was then adopted to solve both thin and thick plate problems (Capsoni & Corradi, 1999).

In parallel, limit analysis procedures for perfectly plastic slabs have been developed for use in design over a period of several decades. Chan (1972) was the first to use finite elements and mathematical programming to calculate bounds on the collapse load of a reinforced concrete slab. In the paper, both moment and velocity fields were discretised using finite elements and the resulting nonlinear optimisation problem was solved using the SUMT algorithm. At around the same time, Anderheggen & Knopfel (1972) presented a numerical procedure based on mixed finite elements and linear programming to determine the collapse loads of plates. The model requires the assumption of parametric stress and displacement fields, and linearisation of the yield condition. In Faccioli & Vitiello (1973), with the use of linear moment distribution finite elements and linearised yield criteria, lower bounds on the collapse load of thin plates were determined using linear programming. A useful discussion of the various options for equilibrium triangular plate elements to be used in a linear programming formulation of plate bending

problems was described in Krenk et al. (1994). In order to avoid linearising the yield criteria, Krabbenhoft & Damkilde (2002) proposed an optimisation algorithm to solve a lower-bound limit analysis problem with non-linear criteria. Using the analogy between the mathematical duality and the dual principle of limit analysis, they also demonstrated that a collapse mechanism could be extracted from a lower bound solution.

It is important to point out that for reinforced concrete slabs the yield condition proposed by Nielsen (1964) and Wolfensberger (1964), which is commonly known as Nielsen's yield criterion, is often used. In fact, this yield criterion consists of two intersecting cones, and this therefore results in difficulties in deriving the expression of the dissipation function and the set of the plastically admissible strains/curvatures for kinematic limit analysis problems. Consequently, the square yield condition is usually used in upper-bound limit analysis of slabs. Chan (1972) proposed a kinematic formulation based on discontinuous finite elements in which potential hinge/yield lines were placed at the boundaries of triangular elements. The method was also adopted by Munro & Fonseca (1978). With the use of finite elements and linear programming, the method can be used to identify the most critical arrangement of yield-lines, and can potentially be applied to practical engineering problems. However, the success of the method depends on how well the critical yield line pattern can be approximated using the given mesh; in other words the solution is sensitive to the layout of the mesh. Attempts have been made by Johnson (1995, 2001) and Thavalingam et al. (1998) and others to overcome such difficulties, but further developments are required to make this approach practicable.

Application in geomechanics

Computational limit analysis has become a powerful tool for analysing the stability of problems in soil mechanics, and a huge amount of work has been done in the field over last few decades. Lysmer (1970) originally proposed a numerical procedure using finite elements and linear programming to compute lower bound limit loads in soil mechanics. In the paper, the soil mass was discretised into a number of 3-noded triangular elements, the nodal stresses being the unknowns,

and in contrast to standard finite element formulation each node was unique to a particular element. This meant that more than one node could share the same coordinate, a key feature of discontinuous finite element methods.

Together with the development of finite element technology and mathematical programming algorithms, limit analysis techniques for geotechnical problems have been developed by many researchers over the last two decades. Significant work in the field has been carried out by Sloan and his collaborators, i.e. Sloan (1988, 1989); Yu & Sloan (1994); Lyamin & Sloan (2002a) and Zhao et al. (2007). In Sloan (1989), an upper bound analysis was carried out using constant strain triangles and the finite meshes were arranged in a specific manner to avoid volumetric locking problems. Yu et al. (1994) used linear strain triangles with straight edges. In this paper, the shearing direction between elements was specified in advance in order to avoid locking problems. More recently, Makrodimopoulos & Martin (2006b) developed simplex strain elements for use in combination with second-order cone programming algorithms to apply to upper bound limit analysis problems. Two and three dimensional bearing capacity of footings in sand problem have recently been investigated by Lyamin et al. (2007).

As an alternative, a truly discontinuous model called Discontinuity Layout Optimisation (DLO) was proposed by Smith & Gilbert (2007). In fact, a successful discontinuous limit analysis procedure is able to identify the critical arrangement of discontinuities in a problem from a wide, preferably near infinite, number of possibilities. The problem is thus similar to the problem of identifying the optimum layout of gridlike structures. Figure 2.1 illustrates the analogy between a truss layout optimisation and a strip footing bearing capacity problem in geomechanics.

The DLO procedure can overcome both the volumetric locking and stress/velocity singularity limitations of finite element limit analysis. The method has now been developed into a commercial software application for geomechanics problems. Apart from application in geomechanics problems, the DLO numerical analysis procedure is potentially applicable to various engineering problems, such as the

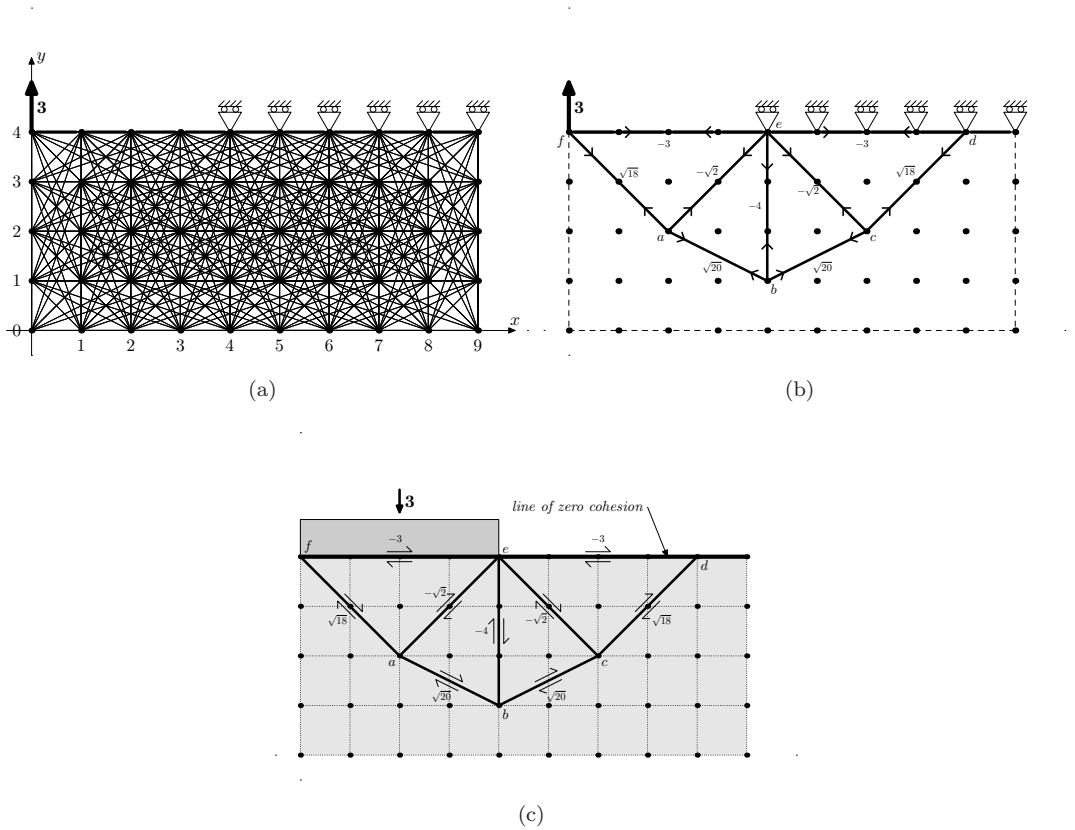

FIGURE 2.1: Analogy between truss and discontinuity layout optimisation (Smith and Gilbert 2007). (a) Truss layout problem: loading and supports, ground structure and locations of pre-existing bars, (b) optimal layout of truss bars for problem (a), (c) discontinuity layout problem: imposed displacement conditions and optimal layout of slip-lines, i.e. as (b)

determination of critical yield line patterns in concrete slabs, and identification of critical slip-line patterns in metal forming problems.

2.1.4 Computational mechanics aspects

Various aspects of computational limit analysis have been investigated in order to provide more robust and efficient numerical tools to enable solutions to practical engineering problems to be obtained. Two well-known issues involving finite element discretisation will be discussed below.

Volumetric locking

Nagtegaal et al. (1974) were the first to point out the isochoric or volumetric locking problem which can occur in plane strain and 3D elastic perfectly-plastic analyses. It is emphasised that this sort of locking problem is purely due to an inability of the approximations to describe exact velocity modes (Askes et al., 1999). When lower-order elements are used, the kinematic constraint (sometimes called the divergence-free or incompressibility condition) leads to a reduction of the available number of degrees of freedom, and therefore the exact velocities cannot be described. To illustrate this volumetric locking behaviour, the plain strain problem in Figure 2.2 is modelled with one quadrilateral finite element and four nodes. Let $\dot{u}_x$ and $\dot{u}_y$ be the components of the imposed velocity $\dot{\mathbf{u}}$, so that the strain rate vector reads

$$\begin{bmatrix} \dot{\epsilon}_{xx} \\ \dot{\epsilon}_{yy} \\ \dot{\epsilon}_{zz} \\ \dot{\gamma}_{xy} \end{bmatrix} = \begin{bmatrix} y\dot{u}_x \\ x\dot{u}_y \\ 0 \\ x\dot{u}_x + y\dot{u}_y \end{bmatrix} \tag{2.1}$$

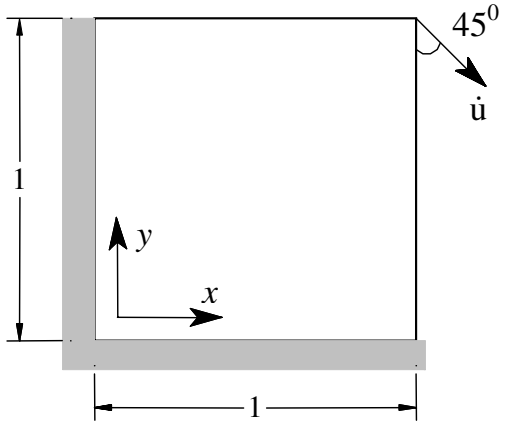

FIGURE 2.2: Patch-problem statement

The incompressibility condition in terms of the volumetric strain rate $\dot{\epsilon}_v$ reads

$$\begin{aligned} \dot{\epsilon}_v &= \dot{\epsilon}_{xx} + \dot{\epsilon}_{yy} + \dot{\epsilon}_{zz} \\ &= y\dot{u}_x + x\dot{u}_y \\ &= y\frac{1}{2}\sqrt{2}\dot{u} - x\frac{1}{2}\sqrt{2}\dot{u} \\ &= (y-x)\frac{1}{2}\sqrt{2}\dot{u} = 0 \end{aligned} \tag{2.2}$$

which can only be satisfied for arbitrary x and y if $\dot{u} = 0$. Due to the characteristics of the bi-linear shape functions of this element, the imposed velocities of Figure 2.2 cannot be described.

In the context of limit analysis, for the cases where an unbounded yield criterion is used, an infinite number of linear constraints on nodal velocities must be introduced in the kinematic formulation (Andersen et al., 1998; Tin-Loi & Ngo, 2003). Consequently, the collapse mechanism cannot be described and no limit load can be found, leading to so-called volumetric locking.

Various solutions have been proposed in the literature to overcome this problem. These include the use of special element patches (Nagtegaal et al., 1974); reduced or selective integration (Zienkiewicz et al., 1971; Hughes, 1980); augmenting the strain field (Simo & Rifai, 1990). The most robust and effective method is probably the application of higher-order displacement-based elements (de Borst, 1982; Sloan & Randolph, 1982). More recently, Tin-Loi & Ngo (2003) used the p-version finite element method to overcome the well-known locking behaviour in limit analysis problems. However, there are drawbacks to using higher-order elements: mesh generation requires complex algorithms and computational costs increase. As an alternative to higher-order elements, the Element-Free Galerkin (EFG) method can be used (Belytschko et al., 1994). Due to the high-order shape functions used in the EFG method the volumetric locking problem can be suppressed (Dolbow & Belytschko, 1999; Askes et al., 1999), though not entirely removed (Huerta & Fernandez-Mendez, 2001).

Error estimation and adaptivity

The objective of using error estimation and adaptivity is to improve the accuracy of the solution, to speed-up the computational process, or both. It is well-known that the accuracy of the finite element solution depends on how the problem is discretised. Automatic refinement strategies based on *a posteriori* error estimators are often used. The *a posteriori* error estimators can be categorised into two main classes: *recovery-type* (Zienkiewicz & Zhu, 1987, 1992) and *residual-type* (Babuska & Rheinboldt, 1978; Zhu & Zhang, 1999). The *recovery-type* error estimators measure the smoothness of stresses between adjacent elements without solving the error equations. They are simple and preferable in many practical engineering problems. Borges et al. (2001) adopted a recovery scheme to estimate the interpolation error for limit analysis problems. With the use of a Taylor expansion, the local error for each element could be estimated by

$$\|u^h(\mathbf{x}) - u(\mathbf{x})\|_{L^2(\Omega)} \simeq C\|\mathscr{H}(u^h(\mathbf{x})) \cdot (\mathbf{x} - \mathbf{x}_0)^2\|_{L^2(\Omega)} \tag{2.3}$$

where C is a constant and $\mathscr{H}(u^h(\mathbf{x}))$ is the recovered Hessian matrix obtained from the finite element solution u^h.

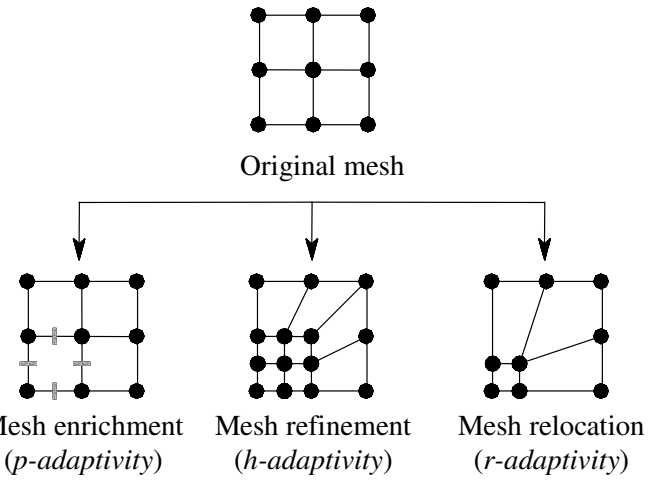

FIGURE 2.3: Remeshing strategies

Once the error information is obtained, the mesh can be adapted. The mesh should be improved in regions where the local error is large. There are several techniques

for remeshing, for instance, *mesh refinement* (h-adaptivity), *mesh enrichment* (p-adaptivity), *mesh relocation* (r-adaptivity) or combinations of any two of these (Askes, 2000; Pannachet, 2006), Figure 2.3. From an intuitive point of view, the simplest strategy is probably h-adaptivity. Consequently, h-adaptivity has been applied to a wide range of problems in engineering practice, particularly for plastic limit analysis problems. Borges et al. (2001) and Lyamin et al. (2005) performed h-adaptivity based on the advancing front technique, which is able to capture discontinuities arising from localised plastic deformations during plastic collapse. In Ciria et al. (2008) and Munoz et al. (2009), a novel method for h-adaptivity meshing based on the gap between upper and lower bounds was introduced.

2.2 Mesh-free methods: state of the art

2.2.1 Introduction

Numerical methods are indispensable for the successful simulation of physical and engineering problems usually described by underlying partial differential equations. Current research in computational mechanics is focussing on the development of numerical tools which are sufficiently efficient and robust to enable solutions of practical problems to be obtained. However, there are many problems of industrial and academic interest which cannot be treated efficiently using conventional numerical methods such as finite elements, finite volumes or finite differences. For instance, consider simulation of manufacturing processes where there is a need to deal with extremely large deformations of the mesh, or simulation of failure where simulation of propagating cracks with arbitrary and complex paths is needed, or simulation of strain localisation problems. These problems are not well suited to classical mesh-based methods. Consequently, so-called meshless or meshfree methods (MMs) have been developed to eliminate at least part of this mesh dependence by constructing the approximation entirely in terms of nodes (often called particles in mesh-free methods, Huerta et al. (2004)).

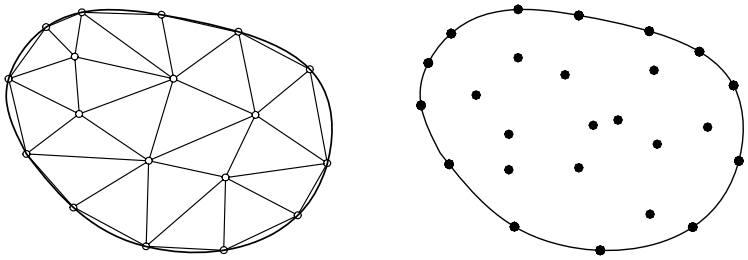

(a) Finite element method (b) Mesh-free methods

FIGURE 2.4: Discretisation strategies

Mesh-free methods use sets of nodes scattered within the problem domain as well as on the boundaries to represent the domain and its boundaries, Figure 2.4. There is no need for a mesh or elements; instead the relation between nodes is handled via so-called domains of influence. The naturally conforming property of the mesh-free methods results in many computational advantages which may be summarised as follows:

- The absence of a mesh is the most attractive and important feature of the MMs. The connectivity of the nodes can be generated at run-time and may change with time, and therefore the MMs facilitates the implementation of h-adaptivity. In MMs there is no mesh-alignment sensitivity problem, a well-known drawback of mesh-based methods (Li & Liu, 2002). Furthermore, for problems with large deformations or moving discontinuities, MMs show great advantages since no remeshing is necessary.

- The shape functions of MMs can easily be constructed to have any desired order of continuity (Fries & Matthies, 2003), thus no post-processing is needed to obtain smooth stress distributions etc.

- The convergence characteristics of MMs are often considerably better than those obtained when using mesh-based shape functions (Li & Liu, 1996; Liu, 2003). Moreover, the accuracy of MMs solutions can be controlled more easily (Li & Liu, 2002), and this may result in efficiencies of error estimation and adaptivity.

In general, MMs can be classified based on two main criteria: approximation/interpolation techniques(Fries & Matthies, 2003; Liu & Gu, 2005; Nguyen et al., 2008), and computational formulation (Li & Liu, 2002; Liu & Gu, 2005). Systematic classification of MMs can be found in these papers. However, some important aspects of MMs such as approximation techniques, numerical implementation and applications will be emphasised in the following sections.

2.2.2 Approximation techniques

The method of function approximation/interpolation based on a set of arbitrary nodes is a key issue in MMs; various methods have been developed. Before introducing some popular approximation functions, it is appropriate to mention the essential conditions required for convergence, namely: consistency, completeness or reproducing capacity, and the concept of partition of unity.

Consistency and completeness

For any numerical method to converge, it must be consistent and stable. The consistency of an approximation is defined by its ability to represent a differential equation (Fries & Matthies, 2003), or in a mathematical sense, a scheme $L^h u = f$ is consistent of order $p > 0$ with the differential equation $Lu = f$ if $\|Lu - L^h u\| = O(h^p)$, where h is a parameter that reflects the refinement of grid/mesh. It is obvious that the approximation error $\|Lu - L^h u\|$ goes to zero when $h \to 0$. The consistency term is usually applied to finite difference and collocation methods which discretise the strong form of a partial differential equation (PDE) (Belytschko et al., 1998). When the PDE is transformed into its associated weak form and is solved by a Galerkin method, the completeness and reproducing terms are used in the study of convergence. A set of functions $\Phi_I(\mathbf{x})$ is complete to order s if any polynomial up to degree s is exactly reproduced as

$$\sum_I x^p \Phi_I(\mathbf{x}) = x^p \quad \text{for} \quad 0 \leq p \leq s \tag{2.4}$$

or

$$\sum_I \mathbf{p}(\mathbf{x}_I)\Phi_I(\mathbf{x}) = \mathbf{p}(\mathbf{x}) \quad \forall \mathbf{x} \in \Omega \tag{2.5}$$

where $\mathbf{p}(\mathbf{x})$ contains the basis functions.

The terms completeness and reproducing ability are very closely related to consistency, and it has been shown in Belytschko et al. (1998) that in the analysis for convergence the role of completeness (i.e. reproducing conditions) in Galerkin methods parallels the role of consistency in finite difference methods.

Partition of Unity (PU)

A partition of unity is a paradigm in which a domain Ω is covered by overlapping patches, or subdomains Ω_I, each of which is associated with a function $\Phi_I(\mathbf{x})$ which is nonzero only in Ω_I, Figure 2.5, and has the property

$$\sum_I \Phi_I(\mathbf{x}) = 1 \quad \text{in } \Omega_I \tag{2.6}$$

If the set of $\Phi_I(\mathbf{x})$ satisfy the equation (2.4), it is called a partition of unity of order s (Fries & Matthies, 2003).

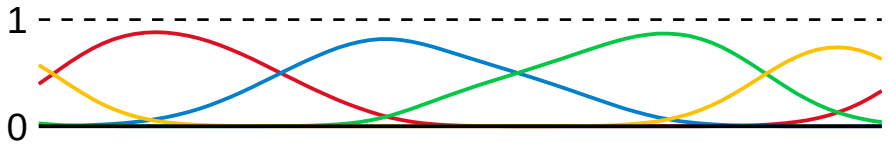

FIGURE 2.5: Illustration of interpolants that form a Partition of Unity (Wikipedia)

2.2.2.1 Smooth Particle Hydrodynamics method

The idea of meshless methods was originally developped by Lucy (1977) and Gingold & Monaghan (1977). The so-called Smooth Particle Hydrodynamics (SPH) method was used for modelling astrophysical phenomena without boundaries such

as exploding stars and dust clouds. Monaghan (1988) proposed a more rational basis with a kernel approximation, and the SPH approximation for a single function $u(\mathbf{x})$ in a domain Ω is given by

$$u^h(\mathbf{x}) = \int_\Omega w(\mathbf{x}-\mathbf{x}', h)u(\mathbf{x}')\ \mathrm{d}\Omega_{\mathbf{x}'} \tag{2.7}$$

where $u^h(\mathbf{x})$ is the approximation, $w(\mathbf{x}-\mathbf{x}', h)$ is a kernel or weight function, and h is the measure of the size of support.

For the purposes of numerical evaluations, the discrete form of (2.7) is needed and can be obtained by numerical quadrature of the right-hand side:

$$u^h(\mathbf{x}) = \sum_I w(\mathbf{x}-\mathbf{x}_I, h)u_I\Delta V_I = \sum_I \Phi_I(\mathbf{x})u_I \tag{2.8}$$

where ΔV_I is some measure of the domain surrounding of node I, and $\Phi_I(\mathbf{x}) = w(\mathbf{x}-\mathbf{x}', h)\Delta V_I$ are the SPH shape functions of the approximation.

It has been shown by Belytschko et al. (1996a) that the linear consistency conditions do not hold for either uniform or non-uniform nodal distributions in SPH. Nevertheless SPH methods have provided good solutions to second-order PDEs.

2.2.2.2 Reproducing Kernel Particle Method

The Reproducing Kernel Particle Method (RKPM) is an improved version of the continuous SPH approximation. In order to ensure a certain order of consistency of the SPH approximation, a correction function $C(\mathbf{x}, \mathbf{x}')$ is added to the approximation as (Liu et al., 1995a)

$$u^h(\mathbf{x}) = \int_\Omega C(\mathbf{x}, \mathbf{x}')w(\mathbf{x}-\mathbf{x}', h)u(\mathbf{x}')\ \mathrm{d}\Omega_{\mathbf{x}'} \tag{2.9}$$

where $C(\mathbf{x}, \mathbf{x}')$ is obtained by imposing the reproducing conditions.

By performing numerical integration, the discrete version of (2.9) can be expressed as

$$u^h(\mathbf{x}) = \sum_I C(\mathbf{x}, \mathbf{x}_I) w(\mathbf{x} - \mathbf{x}_I, h) u_I \Delta V_I = \sum_I \Phi_I(\mathbf{x}) u_I \tag{2.10}$$

It is interesting to note that if ΔV_I is chosen to be unity, the RKPM is identical to the Moving Least Squares approximation which will be presented in the following section.

2.2.2.3 Moving Least Squares Approximation

The Moving Least Squares (MLS) approximation, originated by mathematicians for data fitting and surface construction, can be categorised as a method of finite series representation of functions. An excellent description of MLS is given by Lancaster & Salkauskas (1981). Nayroles et al. (1992) were the first to use a MLS approximation to construct shape function for their diffuse element method for mechanics problems. The approximation technique was further developed by Belytschko et al. (1994), who named it the Element-Free Galerkin (EFG) method. In MLS, the function of the field variable $u(\mathbf{x})$ in the domain Ω can be approximated at point $\mathbf{x}$ as

$$u^h(\mathbf{x}) = \sum_{i=1}^{m} p_i(\mathbf{x}) a_i(\mathbf{x}) \equiv \mathbf{p}^T(\mathbf{x}) \mathbf{a}(\mathbf{x}) \tag{2.11}$$

where m is the number of terms in the basis, $p_i(\mathbf{x})$ are monomial basis functions, and $a_i(\mathbf{x})$ are their coefficients, which are functions of the spatial coordinates $\mathbf{x}$. The complete polynomial basis of degree s is given by

$$\mathbf{p}^T(\mathbf{x}) = \begin{cases} \mathbf{p}^T(x) = (1, x, x^2, \ldots, x^s) & \text{in 1D} \\ \mathbf{p}^T(x, y) = (1, x, y, xy, x^2, y^2, \ldots, x^s, y^s) & \text{in 2D} \\ \mathbf{p}^T(x, y, z) = (1, x, y, z, xy, yz, zx, x^2, y^2, z^2, \ldots, x^s, y^s, z^s) & \text{in 3D} \end{cases} \tag{2.12}$$

which can be build using the Pascal pyramid as shown in Figure 2.6.

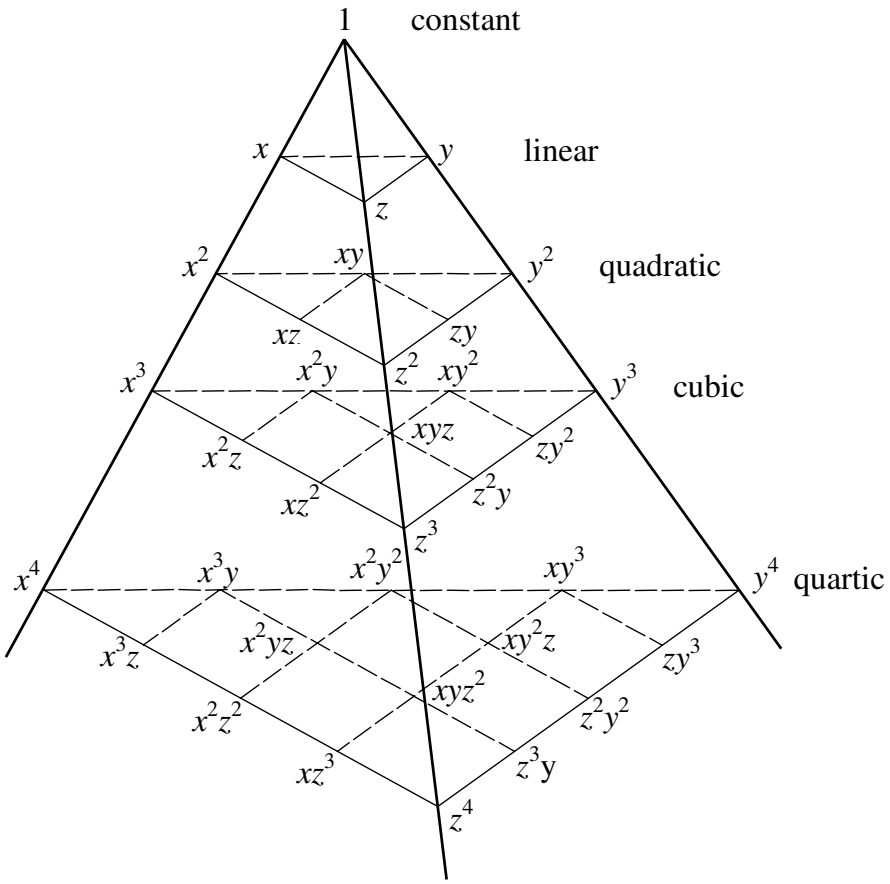

FIGURE 2.6: Pascal pyramid of monomials

A local approximation is defined by Lancaster & Salkauskas (1981) as

$$u^h(\mathbf{x}, \mathbf{x}_I) = \sum_{i=1}^{m} p_i(\mathbf{x}_I) a_i(\mathbf{x}) = \mathbf{p}^T(\mathbf{x}_I)\mathbf{a}(\mathbf{x}) \tag{2.13}$$

The coefficients $a_i(\mathbf{x})$ are obtained at any point $\mathbf{x}$ by carrying out a weighted least squares fit for the local approximation, which is achieved by minimizing the difference between the local approximation and the function, Figure 2.7. This

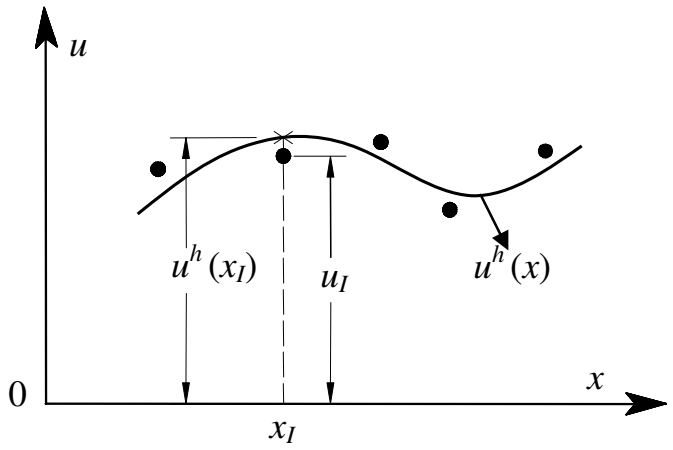

FIGURE 2.7: The approximation function $u^h(x)$ and the nodal parameters u_I in the MLS approximation

yields the quadratic form as follows

$$\begin{aligned} J &= \sum_I^n w(\mathbf{x}-\mathbf{x}_I)\left(u^h(\mathbf{x},\mathbf{x}_I)-u(\mathbf{x}_I)\right)^2 \\ &= \sum_I^n w(\mathbf{x}-\mathbf{x}_I)\left[\mathbf{p}^T(\mathbf{x}_I)\mathbf{a}(\mathbf{x})-u_I\right]^2 \end{aligned} \tag{2.14}$$

where $w(\mathbf{x}-\mathbf{x}_I)$ is a weighting function with compact support, u_I is the nodal parameter of the field variable at node I and n is the number of points in the neighbourhood of $\mathbf{x}$. The minimisation condition requires

$$\frac{\partial J}{\partial \mathbf{a}} = 0 \tag{2.15}$$

which leads to the following system of linear equations

$$\mathbf{A}(\mathbf{x})\mathbf{a}(\mathbf{x}) = \mathbf{B}(\mathbf{x})\mathbf{u} \tag{2.16}$$

where $\mathbf{A}$ and $\mathbf{B}$ are given by

$$\mathbf{A}(\mathbf{x}) = \sum_I^n w(\mathbf{x}-\mathbf{x}_I)\mathbf{p}(\mathbf{x}_I)\mathbf{p}^T(\mathbf{x}_I) \tag{2.17}$$

$$\mathbf{B}(\mathbf{x}) = [w(\mathbf{x}-\mathbf{x}_1)\mathbf{p}(\mathbf{x}_1), w(\mathbf{x}-\mathbf{x}_2)\mathbf{p}(\mathbf{x}_2), \ldots, w(\mathbf{x}-\mathbf{x}_n)\mathbf{p}(\mathbf{x}_n)] \tag{2.18}$$

Solving the equation (2.16) for $\mathbf{a}(\mathbf{x})$, we obtain

$$\mathbf{a}(\mathbf{x}) = \mathbf{A}^{-1}(\mathbf{x})\mathbf{B}(\mathbf{x})\mathbf{u} \tag{2.19}$$

The approximation $u^h(\mathbf{x})$ can then be expressed as

$$u^h(\mathbf{x}) = \sum_I^n \Phi_I(\mathbf{x}) u_I \tag{2.20}$$

where the shape functions $\Phi_I(\mathbf{x})$ are given by

$$\Phi_I(\mathbf{x}) = \mathbf{p}^T(\mathbf{x})\mathbf{A}^{-1}(\mathbf{x})\mathbf{B}_I(\mathbf{x}) \tag{2.21}$$

The consistency of order s of the MLS approximations can be achieved if the basis is complete in the polynomials of order s. In fact, any function which appears in the basis can be reproduced exactly by a MLS approximation. If $\mathbf{p}(\mathbf{x}) = 1$, the resulting MLS shape functions is given by

$$\Phi_I^0(\mathbf{x}) = \frac{w(\mathbf{x} - \mathbf{x}_I)}{\sum_I^n w(\mathbf{x} - \mathbf{x}_I)} \tag{2.22}$$

which is known as the Shepard function, the lowest order form of MLS shape functions.

Other important properties of MLS approximation can be seen:

- The dashed line in Figure 2.8 shows that the sum of the shape functions $\sum_I \Phi_I(\mathbf{x})$ equals 1 in the whole domain $\Omega = [-5,\ 5]$, thus $\Phi_I(\mathbf{x})$ forms a PU, and the first derivatives of the MLS-PU build Partition of Nullities (PNs), $\sum_I \Phi_{I,x}(\mathbf{x}) = 0$ as shown in Figure 2.9.

- The MLS technique can provide high-order shape functions, and therefore in general can result in better convergence rates compared to mesh-based FEM approximations with an equivalent basis. However, this property may

cause problems in evaluating the integral expressions of the weak form since a large number of integration points are required to ensure that accurate solutions are obtained.

- The MLS shape functions do not possess the Kronecker delta property. This non-interpolant character makes imposition of essential boundary conditions difficult.

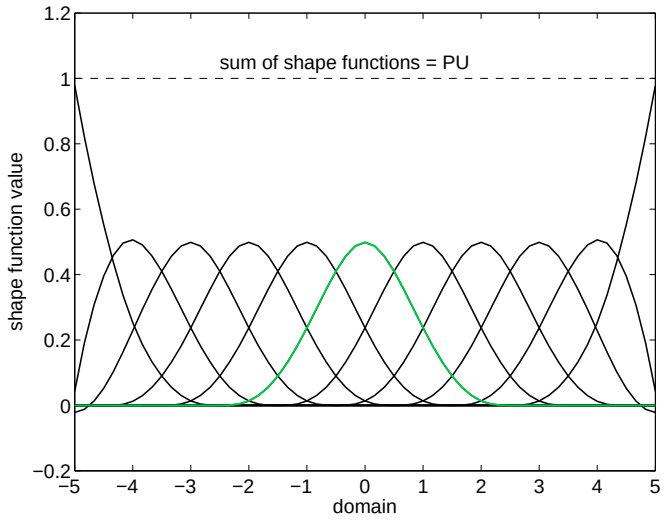

FIGURE 2.8: Partition of Unity functions with MLS technique

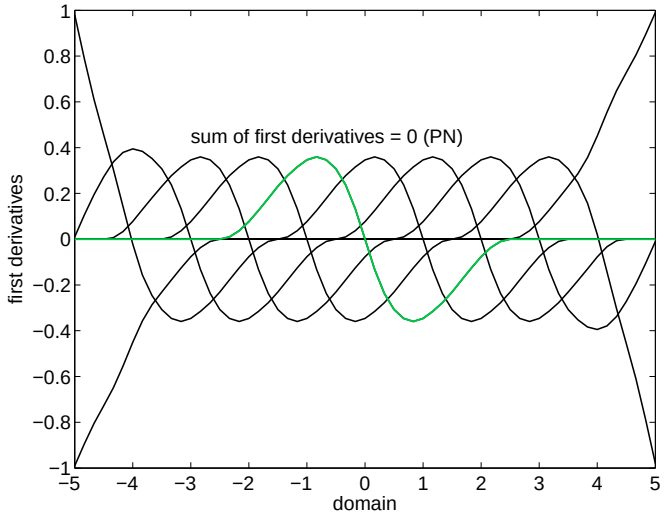

FIGURE 2.9: Partition of Nullity (PN) functions with MLS technique

2.2.2.4 Partition of Unity Methods

Melenk & Babuska (1996) and Duarte & Oden (1996) have shown that mesh-free methods can also be based on partitions of unity. This viewpoint has led to several approximations for mesh-free methods. Melenk & Babuska (1996) introduced approximations of the form

$$\begin{aligned} u^h(\mathbf{x}) &= \sum_I \Phi_I^0(\mathbf{x})(a_{0I} + a_{1I}x + \cdots + a_{sI}x^s + b_{1I}\sinh nx + b_{2I}\cosh nx) \\ &= \sum_I \Phi_I^0(\mathbf{x}) \left(\sum_i p_i(\mathbf{x})\beta_{iI} \right) = \sum_I \Phi_I^0(\mathbf{x})\boldsymbol{\beta}_{iI}\mathbf{p}(\mathbf{x}) \end{aligned} \tag{2.23}$$

with

$$\boldsymbol{\beta}_{iI} = [a_{0I}, a_{1I}, \ldots, a_{sI},\ b_{1I}, b_{2I}] \tag{2.24}$$

$$\mathbf{p}^T(\mathbf{x}) = [1, x, \ldots, x^s, \sinh nx, \cosh nx] \tag{2.25}$$

where $\Phi_I^0(\mathbf{x})$ is the Shepard function. The coefficients $\boldsymbol{\beta}_{iI}$ are the unknowns of the approximation and can be determined by a Galerkin or collocation procedure. The *intrinsic* basis function $\mathbf{p}^T(\mathbf{x})$ consists of special enhancement functions, usually a known feature of the sought solution. The order of consistency of the approximation depends on the number of terms x^s.

Duarte & Oden (1996) used the PU concept in a more general manner by constructing it from an MLS shape function of order s, and their approximation is

$$u^h(\mathbf{x}) = \sum_I \Phi_I^s(\mathbf{x}) \left(u_I + \sum_i^m b_{iI} q_i(\mathbf{x}) \right) \tag{2.26}$$

with $q_i(\mathbf{x})$ can be a monomial basis of any order greater than s and can be either high-order monomial or are *enhancement/enrichment functions*, called this the *extrinsic* basis. In this approximation, special properties such as discontinuities, singularities, boundary layers, or other relevant features of a solution can be introduced via *enhancement/enrichment functions*.

Based on the PU concept, Belytschko & Black (1999) presented a method where discontinuous enrichment functions are added to the finite element approximation so that crack problems can be solved with minimal remeshing. The method was then improved by Moes et al. (1999) and called the eXtended Finite Element Method (XFEM). The method is well-suited to problems involving discontinuities or singularities because it allows for the entire crack to be represented independently of the mesh, and enrichment functions can be added locally to the approximations in the interaction of the crack geometry with the mesh.

2.2.3 Numerical implementation details

All approximation/interpolation functions presented in section (2.2.2) can be employed in the resolution of a PDE boundary value problem. Usually SPH methods are used in combination with a collocation technique, while approximations based on a MLS development are often combined with a Galerkin formulation. Considering a partial differential equation on a domain Ω with essential boundary Γ_u defined by

$$Lu(\mathbf{x}) = f(\mathbf{x}) \text{ in } \Omega \tag{2.27}$$

$$\mathbf{u} = \overline{\mathbf{u}} \quad \text{on } \Gamma_u \tag{2.28}$$

where L is the differential operator and $\mathbf{u}$ may contain both displacement and rotation degrees of freedom. In the following sections, implementation aspects of the collocation techniques and weak-form procedures to solve this problem are described.

2.2.3.1 Collocation methods

Consider an approximation of a set of n_N nodes in the form

$$u^h(\mathbf{x}) = \sum_{I=1}^{n_N} \Phi_I(\mathbf{x}) u_I \tag{2.29}$$

where $\Phi_I(\mathbf{x})$ is the shape function obtained by any approximation techniques described in section (2.2.2), and u_I are nodal values to be determined.

In collocation methods, the PDE (2.27) is fulfilled at nodes within the domain Ω and equation (2.28) is imposed at nodes on the essential boundary. The discrete equations can be written as

$$Lu^h(\mathbf{x}_J) = f(\mathbf{x}_J) \;\; \forall \; J \in \Omega \tag{2.30}$$

$$\mathbf{u}^h(\mathbf{x}_K) = \overline{\mathbf{u}}_K \quad \forall \; K \in \Gamma_u \text{ and } J + K = n_N \tag{2.31}$$

The above is a set of n_N equations with n_N unknown u_I.

The presented collocation procedure is applicable to any mesh-free method based on partition of unity. Two major advantages of the method are: (i) the final system of equations can be obtained efficiently since no integration is required, and (ii) shape functions are only evaluated at nodes rather than at integration points as in other methods based on weak-form of the PDE. However, the stability of solutions is not guaranteed.

2.2.3.2 Galerkin method

The Galerkin method can be viewed as a particular weighted residual method which is general and provides a powerful means of obtaining approximate solutions for ordinary differential equations (ODE) or PDE. Before describing the important features of the Galerkin method, it is necessary to recall some basic concepts of the weighted residual method. If the PDE is discretised numerically, the unknown field u is approximated by a so-called trial function $u^h(\mathbf{x})$, and the residual error $\mathscr{R}$ is determined by

$$\mathscr{R} = Lu^h(\mathbf{x}) - f(\mathbf{x}) \tag{2.32}$$

The weak form of equation (2.27) is

$$\int_\Omega \varphi \mathscr{R} \, \mathrm{d}\Omega \equiv \int_\Omega \varphi \left(Lu^h(\mathbf{x}) - f(\mathbf{x}) \right) \, \mathrm{d}\Omega = 0 \tag{2.33}$$

where an arbitrary function φ is called the test function or weight function (which is a different meaning from the weight function used in MMs).

In general, the order of smoothness required for the trial function depends on the order of a PDE (L), i.e. if n_L is the order derivatives occur in L, then the trial must be C_{n_L-1} ($n_L - 1$ continuous derivatives). Usually, integration by parts is applied to (2.33) in order to reduce the order of the differential operator L, and therefore the requirement on continuity of the trial space is weakened, and the requirement on continuity of the test space is made severe. If L contains even-order derivatives, integration by parts can be applied such that the same continuity requirements hold for test and trial spaces. The resulting formulation is called the *weak-form* associated with the *strong-form* given by (2.27).

Note that the fundamental difference between methods based on the weighted residual approach rests on the choice of the test function. If the test function φ is chosen to be the Dirac delta $\delta(\mathbf{x} - \mathbf{x}_I)$, the equation (2.33) reduces to the strong form (2.30) in the collocation method.

In many cases, the Galerkin method results in the same formulations obtained by variational principles, and therefore it has some physical foundations. In addition, the method can provide stable solutions and its system matrix is symmetric, for finite element formulations with symmetric differential operator L. Consequently, the Galerkin method is regarded so far as the most effective version of the weighted residual method, and is widely used in numerical procedures.

Mesh-free methods based on the Galerkin formulation have been reported by several authors, e.g. Belytschko et al. (1994); Duarte & Oden (1996); Melenk & Babuska (1996) and Liu et al. (1995a). An important aspect of these methods is the evaluation of integrals in the weak form equations. Gauss integration is one of the most commonly used techniques. However, a background mesh must be employed in this quadrature scheme, and therefore this is not really a truly mesh-free method. Furthermore, a large number of integration points would be needed in order to obtain accurate solutions because high-order shape functions are used. As a result, the computational cost of mesh-free methods using Gauss integration

is relatively high. The direct nodal integration method, wherein the integrals of the weak form are evaluated at the nodes only, can be used to overcome these difficulties. There is no need for cell structures or background meshes in this approach. It is therefore a truly mesh-free method and it is also faster. However, it results in spatial instabilities due to vanishing derivatives of mesh-free shape functions at the nodes. Beissel & Belytschko (1996) proposed a scheme to modify the potential energy functional by adding to it the square of the residual of the equilibrium equation, so that singular modes are eliminated. Another scheme called stabilised conforming nodal integration was proposed by Chen et al. (2001a). In this scheme, nodal strains are computed by a divergence counterpart of a spatial averaging of strains. The derivatives of shape functions are evaluated at vertices of a representative nodal domain, not at the nodes, and therefore spurious modes are eliminated. It has been shown that the scheme can be applied to a wide range of problems (Sze et al., 2004; Wang & Chen, 2004). The method is also applied to FEM and is called the smoothed finite element method (SFEM), i.e. Liu et al. (2007a) and Liu et al. (2007b). More recently, Fries & Belytschko (2008) and Duan & Belytschko (2009) proposed a stabilised stress-point integration scheme to improve convergence and stability properties.

2.2.3.3 Enforcement of essential boundary conditions

In general, most mesh-free approximations do not satisfy the Kronecker delta property (i.e. $\Phi_I(\mathbf{x}_J) \neq \delta_{IJ}$), or in other words, do not pass through the nodal parameter values. This leads to difficulties in imposing the boundary conditions. Some possibilities to overcome such difficulties are: (1) Lagrangian multiplier approaches (Belytschko et al., 1994; Duarte & Oden, 1996; Melenk & Babuska, 1996; Liu et al., 1995a); (2) Modified variational principles (Lu et al., 1994); (3) Penalty methods (Zhu & Atluri, 1998; Atluri & Zhu, 2000); (4) Point collocation methods (Zhu & Atluri, 1998); (5) Coupling to finite elements (Belytschko et al., 1996a; Huerta & Fernandez-Mendez, 2000); or (6) use of specially modified shape functions (Wagner & Liu, 2000), among others.

Among the above-mentioned methods, the Lagrangian multiplier method is viewed as the most accurate one for enforcing essential boundary conditions. However, one possible disadvantage of the method is that the discrete equations for a linear self-adjoint PDE are no longer positive definite nor banded (Belytschko et al., 1996a). The approach based on the modified variational principle results in banded equations, but with lesser accuracy in the boundary conditions. Compared with the Lagrangian multiplier method, the Penalty method can yield a banded, symmetric and positive definite system matrix, which is a significant advantage in practical applications. However, the success of the Penalty method relies on the use of large absolute values of the penalty parameter. Note that the penalty parameter may be a positive or negative number (Askes & Pannachet, 2005). The system stiffness matrix may become ill-conditioned when increasing the absolute value of the penalty parameter. Based on the Kronecker delta property of FEM shape functions, boundary conditions may be imposed easily when coupling to the finite element method. The disadvantage is that the coupling method leads to a somewhat complicated code structure due to the need to generate transition regions. Alteratively the boundary collocation method allows enforcement of boundary conditions efficiently. Although boundary conditions are enforced exactly only at a finite number of boundary points, the collocation method is a straightforward generalisation of the imposition of essential boundary conditions in the finite element method. Moreover, the method results in a set of equality constraints which can be treated efficiently in the framework of limit analysis. Therefore, this method will be used throughout this research.

2.2.4 Applications

One of the early objectives of developing mesh-free methods was to allow simulation of crack problems without meshes or remeshing. As noted in the previous sections, in mesh-free approximations the connectivity of nodes is generated at run-time and can vary with time and space. This flexible mesh-free feature considerably simplifies the simulation of fracture, free surfaces and crack propagation. In these problems, mesh-free methods have significant advantages when dealing with

evolving moving discontinuities compared with mesh-based methods. Belytschko and his co-workers have systematically applied the EFG method to simulate crack growth/propagation problems (Lu et al., 1995; Belytschko et al., 1996; Belytschko & Tabbara, 1996), where a constant crack-tip velocity was assumed. An extension to allow application to process zone models with mixed-mode dynamic crack propagation in concrete was proposed by Belytschko et al. (2000).

Large deformation analysis is another main application area for mesh-free methods, where the methods have a clear edge over the finite element computations. Mesh-free methods require no explicit mesh in the computation process, and therefore avoid mesh distortion difficulties in large deformation analysis. Chen and his co-workers proposed a Lagrangian formulation in combination with RKPM to simulate several large deformation problems, such as metal forming, extrusion (Chen et al., 1998), large deformation of rubber materials (Chen et al., 1997), soil mechanics problems (Chen et al., 2001). In Jun et al. (1998) and Li & Liu (2000), an explicit RKPM has been also developed for large deformation problems. It has been reported in these simulations that the main advantages of using mesh-free methods in large deformation analysis are (i) no need for remeshing; (ii) absence of volumetric locking for suitable choice of support size of shape function; and (iii) no complicated mixed formulations.

Mesh-free methods based on MLS approximations are very attractive for plate and shell structures because the C^1 continuity requirement can easily be achieved by its approximation. Krysl and Belytschko were the first to apply the EFG method to the analysis of thin plates and shells with C^1 approximations (Krysl & Belytschko, 1995, 1996). In their simulations, background quadrature cells were used for numerical integration and the essential boundary conditions were enforced by Lagrangian multipliers. It was demonstrated that the performance of the method is efficient and insensitive to irregular nodal distributions. It was also found that membrane locking can be removed completely with the use of a quadratic polynomial basis. Donning & Liu (1998) developed a mesh-free method to analyse moderately thick and thin structures using Mindlin-Reissner theory. It was proved that shear and membrane locking are completely eliminated at the

point-wise approximation level using cardinal splines. Leitao (2001) presented a mesh-free method based on the use of radial basis functions to build an approximation of the general solution of the partial differential equations governing the Kirchhoff plate bending problem. Linear and non-linear analysis of laminate plates using the EFG method has also been reported by Belinha & Dinis (2006) and Belinha & Dinis (2007). Instead of using thin-shell theory, Li et al. (2000) presented an approach to perform a large deformation analysis of thin-shell structures using a mesh-free approximation of a 3D problem. Due to the smoothness of mesh-free approximations, one can accurately capture the gradient in the thickness direction, and avoid both shear locking as well as volumetric locking.

Multiple scale computations using mesh-free methods can be rewarding as well. Liu and his co-workers were the first to use mesh-free approximation in multi-scale computations (Liu et al., 1996a,b; Liu & Jun, 1998). In mesh-free approximation functions, dilation parameters or weight/kernel functions can be chosen differently, therefore the approximations may be viewed as filters with different length scales, and one can formulate multi-scale formulations. Multi-scale RKPM have been applied in many applications including those involving wave propagation (Liu & Chen, 1995), fluid dynamics (Liu et al., 1997a), large deformation (Liu & Jun, 1998), strain localisation (Li & Liu, 1999) and damage (Liu et al., 1999). Zhang et al. (2000) used the EFG method to model rock structures.

Chapter 3

Fundamentals

In this chapter, theoretical foundations which are necessary for the developments described in subsequent chapters are presented. The chapter starts with a brief description of plasticity relations and limit analysis theory, and is followed by a brief description and discussion of the computational issues associated with meshfree methods.

3.1 Plasticity relations and limit analysis theory

Plasticity theory is long-established and has been applied to various problems in engineering practice. Foundations and applications of plastic theory are described in Save & Massonnet (1972); Lubliner (1990); Kamenjarzh (1996) and Jirasek & Bazant (2002). In this section, some of the main ingredients, including consideration of the material model and variational principles, are presented. Details of the limit analysis theorems and the mathematical theory of duality are also provided.

3.1.1 Material model

The mechanical behaviour of rate-independent plastic and non-hardening solids or structures can be idealised by an elastic-perfectly plastic model, Figure 3.1. In this model, the material behaves elastically if the stress intensity is below the yield stress; otherwise plastic deformation appears if the yield stress is reached. In fact the elastic strains are significantly smaller than the plastic ones, and it can be shown that, in a state of the so-called *unrestricted plastic flow*, the elastic characteristics may be ignored. Consequently, limit analysis solutions of rigid-perfectly plastic bodies are theoretically also valid for elastic-plastic bodies.

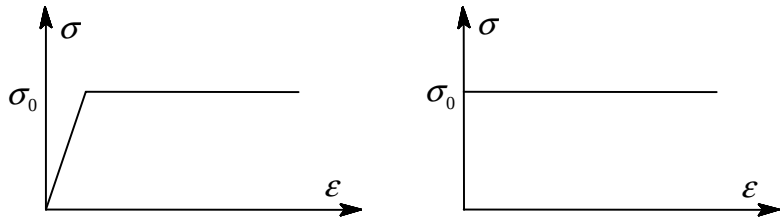

FIGURE 3.1: Material models: elastic-perfectly plastic (left) and rigid-perfectly plastic (right)

In the framework of a limit analysis problem, only plastic strain rates are considered and are assumed to obey an associated flow law

$$\dot{\boldsymbol{\epsilon}} = \dot{\mu}\frac{\partial \psi}{\partial \boldsymbol{\sigma}} \tag{3.1}$$

where the plastic multiplier $\dot{\mu}$ is non-negative and $\psi(\boldsymbol{\sigma})$ is the yield function that represents the time-independent yield surface such that

- $\psi(\boldsymbol{\sigma}) < 0$ corresponds to elastic behaviour
- $\psi(\boldsymbol{\sigma}) = 0$ corresponds to the appearance of plastic deformations
- $\psi(\boldsymbol{\sigma}) > 0$ corresponds to the inaccessible region

The material model must also obey two important laws of plasticity, namely, Drucker's stability postulate and its important consequences, namely convexity and the normality rule.

Drucker's stability postulate

For a rigid-perfectly plastic model, the material is stable in Drucker's sense during a complete cycle of loading and unloading: *"Over the cycle of application and removal of the set of forces, the new work performed by the external agency on the changes in the displacements it produces is non-negative"* Martin (1975).

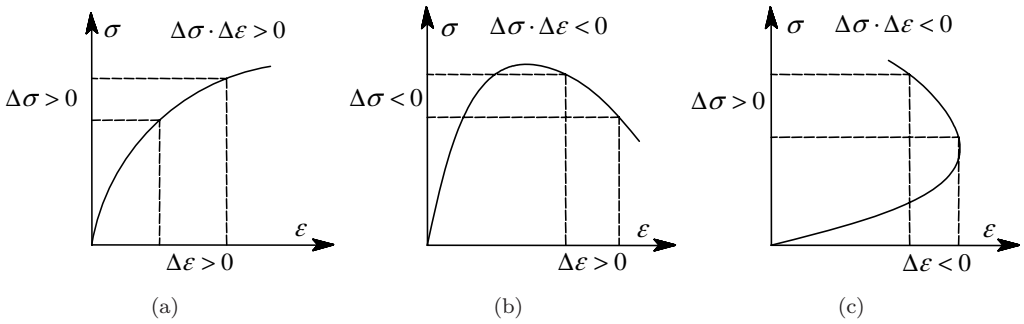

FIGURE 3.2: Stable (a) and unstable (b, c) materials

The postulate is illustrated graphically in Figure 3.2. The mathematical expression of the postulate is as follows

$$\oint (\boldsymbol{\sigma} - \boldsymbol{\sigma}^0) \mathrm{d}\boldsymbol{\epsilon} \geq 0 \tag{3.2}$$

where $\oint$ is the integral taken over a cycle of applying and removing the added stress set, $\boldsymbol{\sigma}$ is the stress tensor on the yield surface satisfying the yield condition $\psi(\boldsymbol{\sigma}) = 0$, and $\boldsymbol{\sigma}^0$ is plastically admissible stress tensor such that $\psi(\boldsymbol{\sigma}^0) < 0$. Drucker's postulate has the following important consequences (Lubliner, 1990):

Principle of maximum plastic dissipation

Drucker's stability postulate may be expressed as

$$(\boldsymbol{\sigma} - \boldsymbol{\sigma}^0) \dot{\boldsymbol{\epsilon}} \geq 0 \tag{3.3}$$

which is sometimes known simply as *Drucker's inequality*, and is valid for both hardening and perfectly plastic materials.

Normality rule

At any point on the smooth yield surface $\psi(\boldsymbol{\sigma}) = 0$, plastic strain rates are normal to the yield yield surface or, in other words, proportional to the gradient of ψ in stress space , $\partial\psi/\partial\boldsymbol{\sigma}$. If the yield surface is not everywhere smooth but has one or more singular points (corners) at which the normal direction is not unique, the plastic strain rates lie between adjacent normals at the corners, Figure 3.3. When n differentiable surfaces intersect at a singular point, the relation (3.1) is replaced by

$$\dot{\boldsymbol{\epsilon}}_p = \sum_{i=1}^{n} \dot{\mu}_i \frac{\partial \psi_i}{\partial \boldsymbol{\sigma}} \tag{3.4}$$

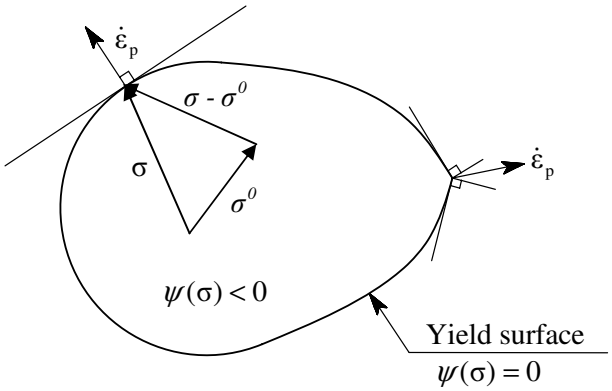

FIGURE 3.3: Normality rule

Convexity of yield surface

It can be seen from Figure 3.3 that if there are any $\boldsymbol{\sigma}^0$ lying on the outward side of the tangent, inequality (3.3) is violated. In other words, the entire elastic region must lie to one side of the tangent, and consequently the yield surface is convex. It has been recognised that this is one of the most important consequences in plasticity theory (Lubliner, 1990). It permits the use of convex programming tools for limit and shakedown analysis problems.

Yield criteria

The yield condition defines the elastic limits of a material under a complex stress state. For isotropic materials, this condition may be expressed as a symmetric function of the principal stresses

$$\psi(\sigma_1, \sigma_2, \sigma_3) = k \tag{3.5}$$

where k is a material constant and is connected with the yield limit.

Since the yield function is symmetric in its arguments, the stress components can be replaced by their invariants, and the yield criterion can be written in the form

$$\psi(I_1, J_2, J_3) = k \tag{3.6}$$

where I_1 is the first invariant of the stress tensor, whilst J_2 and J_3 are the second and the third invariants of the deviatoric stress tensor.

In many problems, the influence of hydrostatic stress is negligible, and therefore the yield criterion is independent of I_1. The von Mises yield criterion is one of the most commonly used yield criteria which is independent of hydrostatic pressure. The von Mises yield criterion states that yielding will begin when the octahedral shearing stress reaches the critical value k_v such that

$$J_2 - k_v = 0 \tag{3.7}$$

where $k_v = \frac{\sigma_0}{\sqrt{3}}$, and σ_0 is the yield stress obtained from a uniaxial tension test.

3.1.2 Variational principles

This section presents a general overview of the fundamental variational principles which govern limit analysis theory. Let Ω denote the domain of an elastic-perfectly plastic or rigid-perfectly plastic body, and Γ its boundary, which consists of a Dirichlet portion Γ_u where displacement boundary conditions are prescribed and

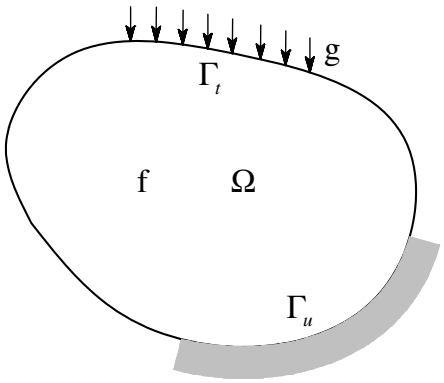

FIGURE 3.4: Structural model

a Neumann portion Γ_t where stress boundary conditions are assumed, so that $\Gamma = \Gamma_u \cup \Gamma_t$ and $\Gamma_u \cap \Gamma_t = \oslash$, as shown in Figure 3.4. These variational principles can be stated in terms of a *statically admissible field* and a *kinematically admissible field*, which are defined as follows

The stress field $\boldsymbol{\sigma}$ is

- *statically admissible* if it satisfies the equilibrium equation and stress boundary conditions

$$\begin{aligned} -\mathbf{L}^T \cdot \boldsymbol{\sigma} &= \mathbf{f} \quad \text{in } \Omega \\ \mathbf{n} \cdot \boldsymbol{\sigma} &= \mathbf{g} \quad \text{on } \Gamma_t \end{aligned} \tag{3.8}$$

  where $\mathbf{L}$ denotes the differential operator

$$\mathbf{L}^T = \begin{bmatrix} \dfrac{\partial}{\partial x} & 0 & 0 & \dfrac{\partial}{\partial y} & 0 & \dfrac{\partial}{\partial z} \\ 0 & \dfrac{\partial}{\partial y} & 0 & \dfrac{\partial}{\partial x} & \dfrac{\partial}{\partial z} & 0 \\ 0 & 0 & \dfrac{\partial}{\partial z} & 0 & \dfrac{\partial}{\partial y} & \dfrac{\partial}{\partial x} \end{bmatrix} \tag{3.9}$$

  $\mathbf{n}$ is the matrix containing the components of the outward normal vector to Ω

$$\mathbf{n} = \begin{bmatrix} n_x & 0 & 0 & n_y & 0 & n_z \\ 0 & n_y & 0 & n_x & n_z & 0 \\ 0 & 0 & n_z & 0 & n_y & n_x \end{bmatrix} \tag{3.10}$$

$\mathbf{f}$ is the volume force and $\mathbf{g}$ is the surface load acting on Γ_t.

- *plastically admissible* if nowhere violates the yield condition, $\psi(\boldsymbol{\sigma}) \leq 0$.

The strain rate field $\dot{\boldsymbol{\epsilon}}$ is

- *kinematically admissible* if it satisfies the compatibility and kinematical boundary conditions

$$\begin{aligned} \dot{\boldsymbol{\epsilon}} &= \mathbf{L}\dot{\mathbf{u}} \quad \text{in } \Omega \\ \dot{\mathbf{u}} &= 0 \qquad \text{on } \Gamma_u \end{aligned} \tag{3.11}$$

- *plastically admissible* if the strain rate vectors belong to the set of normals to the yield surface and the external power of the load is positive

$$\int_{\Omega} \mathbf{f} \cdot \dot{\mathbf{u}} \, \mathrm{d}\Omega + \int_{\Gamma_t} \mathbf{g} \cdot \dot{\mathbf{u}} \, \mathrm{d}\Gamma \geq 0 \tag{3.12}$$

Markov's principle:

Among all kinematically and plastically admissible strain rate fields, the actual field makes the following functional an absolute minimum

$$\Psi(\dot{\mathbf{u}}) = \underbrace{\int_{\Omega} D_p(\dot{\boldsymbol{\epsilon}}) \mathrm{d}\Omega}_{W_{int}} - \underbrace{\left(\int_{\Omega} \mathbf{f} \cdot \dot{\mathbf{u}} \, \mathrm{d}\Omega + \int_{\Gamma_t} \mathbf{g} \cdot \dot{\mathbf{u}} \, \mathrm{d}\Gamma \right)}_{W_{ext}} \tag{3.13}$$

where $D_p(\dot{\boldsymbol{\epsilon}})$ is the plastic dissipation function defined by

$$D_p(\dot{\boldsymbol{\epsilon}}) = \max_{\boldsymbol{\sigma}} \ \boldsymbol{\sigma} \cdot \dot{\boldsymbol{\epsilon}} \quad \text{subject to} \quad \psi(\boldsymbol{\sigma}) \leq 0 \tag{3.14}$$

or

$$D_p(\dot{\boldsymbol{\epsilon}}) = \boldsymbol{\sigma}_{(\epsilon)} \cdot \dot{\boldsymbol{\epsilon}} \tag{3.15}$$

where $\boldsymbol{\sigma}_{(\epsilon)}$, is the value of $\boldsymbol{\sigma}$ solving the problem (3.14), that is a stress state associated to $\dot{\boldsymbol{\epsilon}}$ through the normality rule. The plastic dissipation function is a uniquely defined function of strain rates; however explicit expressions for $D_p(\dot{\boldsymbol{\epsilon}})$

are not available in general terms and must be constructed on the basis of the specific form of yield function used.

Hill's principle:

Among all statically and plastically admissible stress fields, the actual field makes the following functional an absolute minimum

$$\Pi(\boldsymbol{\sigma}) = -\int_{\Gamma_u} (\mathbf{n} \cdot \boldsymbol{\sigma}) \cdot \dot{\mathbf{u}} \, \mathrm{d}\Gamma \tag{3.16}$$

It is important to note that direct consequences of the Markov and Hill's principles, applied to the particular case of proportional loading, are theorems providing upper and lower bounds on the actual collapse load.

3.1.3 Limit analysis theorems and their duality

Let us consider a rigid-perfectly plastic body subjected to external loading $(\mathbf{f}, \mathbf{g})$ which is assumed to be governed by a proportional load multiplier λ and can be written as $(\lambda \mathbf{f}_0, \lambda \mathbf{g}_0)$. If the value of λ is sufficiently small, the body behaves elastically, i.e. no plastic deformation is observed. When λ increases and reaches a significant value, yielding occurs at some points in the body, but is not sufficient to cause collapse. Further increasing λ, the plastic regions will grow until finally a collapse mechanism forms. The corresponding value of λ is called the plastic collapse multiplier. The aim of limit analysis is to determine this collapse multiplier. A limit analysis problem can be formulated using either the static theorem or kinematical theorem.

Static theorem (lower-bound limit analysis)

A *statically and plastically admissible stress state* is described by a stress field $\boldsymbol{\sigma}$ and a load multiplier λ^- such that

$$\begin{aligned} -\mathbf{L}^T \cdot \boldsymbol{\sigma} &= \lambda^- \mathbf{f} \quad \text{in } \Omega \\ \mathbf{n} \cdot \boldsymbol{\sigma} &= \lambda^- \mathbf{g} \quad \text{on } \Gamma_t \\ \psi(\boldsymbol{\sigma}) &\leq 0 \quad \text{in } \Omega \end{aligned} \tag{3.17}$$

For convenience, let us denote the set of all plastically admissible stress fields by

$$\mathcal{B} = \{\boldsymbol{\sigma} \,|\, \psi(\boldsymbol{\sigma}(\mathbf{x})) \leq 0 \;\; \forall\, \mathbf{x} \in \Omega\} \tag{3.18}$$

The lower-bound theorem of limit analysis can be stated as

The exact collapse load multiplier λ is the largest one among all possible static solutions λ^- corresponding to the set of all statically and plastically admissible stress fields $\boldsymbol{\sigma}$, that is

$$\lambda^- \leq \lambda \tag{3.19}$$

The demonstration of this theorem involves application of the principle of virtual work and the property of convexity of the yield surface, see Hodge (1963); Save & Massonnet (1972) and Lubliner (1990). The static limit analysis problem can be formulated in the form of a mathematical programming problem as

$$\lambda \;=\; \max\, \lambda^- \quad \text{s.t} \begin{cases} -\mathbf{L}^T \cdot \boldsymbol{\sigma} = \lambda^- \mathbf{f} & \text{in } \Omega \\ \mathbf{n} \cdot \boldsymbol{\sigma} = \lambda^- \mathbf{g} & \text{on } \Gamma_t \\ \boldsymbol{\sigma} \in \mathcal{B} \end{cases} \tag{3.20}$$

Kinematic theorem (upper-bound limit analysis)

A *kinematically and plastically admissible velocity state* is described by a displacement rate field $\dot{\mathbf{u}}$ and a plastic strain rate field $\dot{\boldsymbol{\epsilon}}$ such that

$$\begin{aligned} &\dot{\boldsymbol{\epsilon}} = \mathbf{L}\dot{\mathbf{u}} \quad \text{in } \Omega \\ &\dot{\mathbf{u}} = 0 \quad \text{on } \Gamma_u \\ &W_{ext} > 0 \end{aligned} \tag{3.21}$$

From the equation of virtual work (or strictly speaking, work rate) which states that the internal work rate and the external work rate must be equal, the corresponding kinematically admissible multiplier λ^+ can be evaluated as

$$\lambda^+ = \frac{W_{int}}{W_{ext}} \tag{3.22}$$

The upper-bound theorem of limit analysis can be stated as

The exact collapse load multiplier λ is the smallest one among all possible kinematic solutions λ^+ corresponding to the set of all kinematically and plastically admissible velocity fields $\dot{\mathbf{u}}$, that is

$$\lambda \leq \lambda^+ \tag{3.23}$$

The upper-bound on the actual collapse load multiplier can be obtained by solving the following optimisation problem (in normalised form)

$$\lambda = \min W_{int} \quad \text{s.t} \begin{cases} \dot{\boldsymbol{\epsilon}} = \mathbf{L}\dot{\mathbf{u}} & \text{in } \Omega \\ \dot{\mathbf{u}} = 0 & \text{on } \Gamma_u \\ W_{ext} = 1 \end{cases} \tag{3.24}$$

Mathematical framework of duality formulations

In this part, a mathematical description of the duality problem of limit analysis is presented briefly; more details can be found in Christiansen (1996). Let X denote an appropriate space of a statically admissible stress state, whereas Y is an appropriate space of a kinematically admissible velocity state. For smooth fields $\boldsymbol{\sigma}$ and $\dot{\mathbf{u}}$, the classical form of the equilibrium equation (3.8) can always be transformed to a more precise variational form as

$$a(\boldsymbol{\sigma}, \dot{\mathbf{u}}) = W_{ext}(\dot{\mathbf{u}}), \quad \forall\, \dot{\mathbf{u}} \in Y \tag{3.25}$$

where the internal work rate a is rewritten as a function of $\boldsymbol{\sigma}$ and $\dot{\mathbf{u}}$

$$a(\boldsymbol{\sigma}, \dot{\mathbf{u}}) = -\int_{\Omega} (\mathbf{L}^T \cdot \boldsymbol{\sigma}) \cdot \dot{\mathbf{u}} \, \mathrm{d}\Omega + \int_{\Gamma_t} (\mathbf{n} \cdot \boldsymbol{\sigma}) \cdot \dot{\mathbf{u}} \, \mathrm{d}\Gamma \tag{3.26}$$

and the external work rate W_{ext} is

$$W_{ext}(\dot{\mathbf{u}}) = \int_{\Omega} \mathbf{f} \cdot \dot{\mathbf{u}} \, \mathrm{d}\Omega + \int_{\Gamma_t} \mathbf{g} \cdot \dot{\mathbf{u}} \, \mathrm{d}\Gamma \tag{3.27}$$

The static principle of limit analysis (3.20) can be now expressed as

$$\begin{aligned} \lambda \;=\; & \max\ \lambda^{-} \\ & \text{s.t} \begin{cases} a(\boldsymbol{\sigma}, \dot{\mathbf{u}}) = \lambda^{-} W_{ext}(\dot{\mathbf{u}}), \forall\, \dot{\mathbf{u}} \in Y \\ \exists\, \boldsymbol{\sigma} \in \mathcal{B}, \quad \mathcal{B} = \{\boldsymbol{\sigma} \in X \,|\, \psi(\boldsymbol{\sigma}(\mathbf{x})) \leq 0 \ \ \forall\, \mathbf{x} \in \Omega\} \end{cases} \end{aligned} \tag{3.28}$$

Due to the fact that both a and W_{ext} are linear functions of $\dot{\mathbf{u}}$, the equation (3.28) can be cast as (Christiansen, 1996)

$$\lambda \;=\; \max_{\boldsymbol{\sigma} \in \mathcal{B}} \ \min_{\dot{\mathbf{u}} \in C} \ a(\boldsymbol{\sigma}, \dot{\mathbf{u}}) \tag{3.29}$$

where the set C is defined by $C = \{\dot{\mathbf{u}} \in Y \,|\, W_{ext}(\dot{\mathbf{u}}) = 1\}$

If expressing the plastic dissipation rate in terms of $\boldsymbol{\sigma}$ and $\dot{\mathbf{u}}$ as

$$W_{int}(\dot{\mathbf{u}}) = \max_{\boldsymbol{\sigma} \in \mathcal{B}} \ a(\boldsymbol{\sigma}, \dot{\mathbf{u}}), \tag{3.30}$$

the kinematic principle of limit analysis (3.24) can be written

$$\begin{aligned} \lambda &= \min_{\dot{\mathbf{u}} \in C} W_{int}(\dot{\mathbf{u}}) \\ &= \min_{\dot{\mathbf{u}} \in C} \max_{\boldsymbol{\sigma} \in \mathcal{B}} a(\boldsymbol{\sigma}, \dot{\mathbf{u}}) \end{aligned} \tag{3.31}$$

It is clear from equation (3.29) and (3.31) that strong duality holds as

$$\max_{\boldsymbol{\sigma} \in \mathcal{B}} \min_{\dot{\mathbf{u}} \in C} a(\boldsymbol{\sigma}, \dot{\mathbf{u}}) = \min_{\dot{\mathbf{u}} \in C} \max_{\boldsymbol{\sigma} \in \mathcal{B}} a(\boldsymbol{\sigma}, \dot{\mathbf{u}}) \tag{3.32}$$

In summary, the exact collapse load multiplier can be obtained by solving one of the following optimisation problems

$$\lambda = \max \{\lambda^- \mid \exists\, \boldsymbol{\sigma} \in \mathcal{B} :\ a(\boldsymbol{\sigma}, \dot{\mathbf{u}}) = \lambda^- W_{ext}(\dot{\mathbf{u}}), \forall\, \dot{\mathbf{u}} \in Y\} \tag{3.33}$$

$$= \max_{\boldsymbol{\sigma} \in \mathcal{B}} \min_{\dot{\mathbf{u}} \in C} a(\boldsymbol{\sigma}, \dot{\mathbf{u}}) \tag{3.34}$$

$$= \min_{\dot{\mathbf{u}} \in C} \max_{\boldsymbol{\sigma} \in \mathcal{B}} a(\boldsymbol{\sigma}, \dot{\mathbf{u}}) \tag{3.35}$$

$$= \min_{\dot{\mathbf{u}} \in C} W_{int}(\dot{\mathbf{u}}) \tag{3.36}$$

In any numerical procedure for limit analysis problems, the problem spaces must be discretised by numerical methods. For the static approach (3.33) or the kinematic formulation (3.36), only one field need be discretised; that is the stress or displacement field, respectively. On the other hand, the mixed formulations (3.34, 3.35) require the approximation of both stress and displacement fields, and therefore mixed finite elements can be used (Anderheggen & Knopfel, 1972; Christiansen, 1981; Casciaro & Cascini, 1982; Christiansen, 1996).

3.1.4 Formulation for plates

Next, the general plasticity formulations of Section 3.1.3 are applied to thin plates in particular.

Basic relations

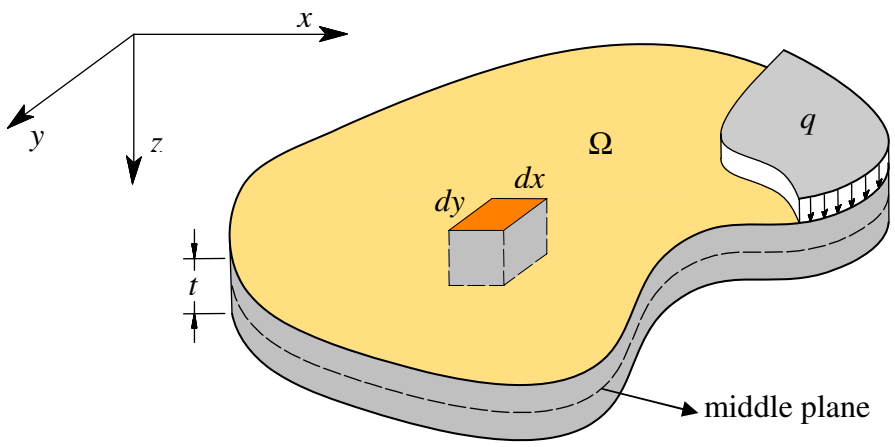

FIGURE 3.5: Kirchhoff plate subjected to transverse load

Consider a rigid-perfectly plastic plate of uniform thickness t, which is bounded by a curve enclosing a plane area Ω with kinematical boundary Γ_u and static boundary Γ_m, and subjected to a transverse load q, Figure 3.5. The plastic behaviour of thin plates may be analysed under Kirchhoff's assumption that the normals to the middle plane of the plate remain straight and normal to the deformed middle plane. If $\dot{u}$ denotes the transverse displacement rate, the strain rates can be expressed by relations

$$\dot{\boldsymbol{\epsilon}} = z\dot{\boldsymbol{\kappa}} \tag{3.37}$$

with the vectors of strain and curvature rates defined by

$$\dot{\boldsymbol{\epsilon}} = \begin{bmatrix} \dot{\epsilon}_{xx} \\ \dot{\epsilon}_{yy} \\ \dot{\gamma}_{xy} \end{bmatrix} ; \quad \dot{\boldsymbol{\kappa}} = - \begin{bmatrix} \dot{\kappa}_{xx} \\ \dot{\kappa}_{yy} \\ \dot{\kappa}_{xy} \end{bmatrix} = - \begin{bmatrix} \dfrac{\partial^2}{\partial x^2} \\ \dfrac{\partial^2}{\partial y^2} \\ 2\dfrac{\partial^2}{\partial x \partial y} \end{bmatrix} \dot{u} = -\nabla^2 \dot{u} \tag{3.38}$$

Let $\mathbf{m}$ denote a vector consisting of the bending and twisting moments per unit width of the plate, and is defined as

$$\mathbf{m} = \begin{bmatrix} m_{xx} \\ m_{yy} \\ m_{xy} \end{bmatrix} = \int_{-t/2}^{t/2} \begin{bmatrix} \sigma_{xx} \\ \sigma_{yy} \\ \sigma_{xy} \end{bmatrix} z \, \mathrm{d}z = \int_{-t/2}^{t/2} \boldsymbol{\sigma} z \, \mathrm{d}z, \tag{3.39}$$

where stress sign conventions are shown in Figure 3.6.

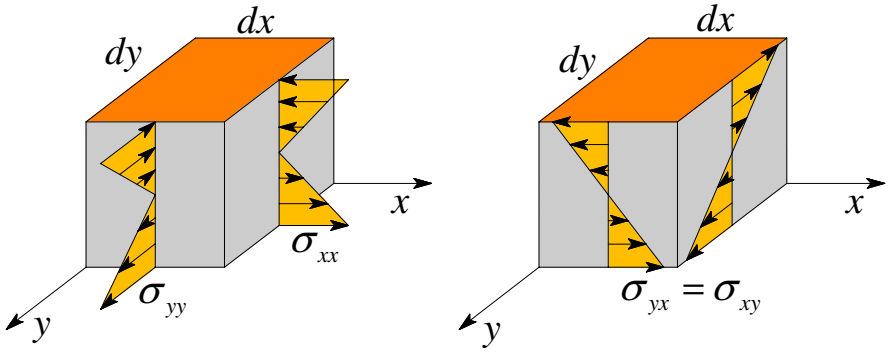

FIGURE 3.6: Kirchhoff stresses: sign conventions

The differential equation of equilibrium can be written as

$$(\nabla^2)^T \mathbf{m} + q = 0 \tag{3.40}$$

Because we actually consider each layer of thickness dz to be in a state of plane stress, the yield condition is

$$\psi(\boldsymbol{\sigma}) \leq 0 \tag{3.41}$$

The stresses $\boldsymbol{\sigma}$ are of constant magnitude in a fully plastic cross section, and can be expressed in terms of the bending and twisting moments as (Save et al., 1997, section 5.4)

$$\boldsymbol{\sigma} = \frac{4}{t^2}\mathbf{m}, \tag{3.42}$$

hence the corresponding yield criterion for the plate is

$$\psi\left(\frac{4}{t^2}\mathbf{m}\right) \leq 0 \tag{3.43}$$

The von Mises failure criterion for plane stress problems is given as

$$\psi(\boldsymbol{\sigma}) \equiv \sqrt{\boldsymbol{\sigma}^T\ \mathbf{P}\ \boldsymbol{\sigma}} - \sigma_0 \leq 0 \tag{3.44}$$

where σ_0 is the yield stress and

$$\mathbf{P} = \frac{1}{2}\begin{bmatrix} 2 & -1 & 0 \\ -1 & 2 & 0 \\ 0 & 0 & 6 \end{bmatrix} \tag{3.45}$$

Combining equations (3.42) and (3.44), the criterion takes the form

$$\psi(\mathbf{m}) \equiv \sqrt{\mathbf{m}^T\ \mathbf{P}\ \mathbf{m}} - m_p \leq 0 \tag{3.46}$$

where $m_p = \sigma_0 t^2/4$ is the plastic moment of resistance per unit width of the plate.

The relations between the curvature rates and the moments are determined from the normality rule as

$$\dot{\boldsymbol{\kappa}} = \dot{\mu}\frac{\partial \psi}{\partial \mathbf{m}} \equiv \dot{\mu}\frac{\mathbf{P}\mathbf{m}}{m_p} \tag{3.47}$$

Because the matrix $\mathbf{P}$ is invertible, the moments $\mathbf{m}$ can be expressed in terms of the curvature rates as

$$\mathbf{m} = \frac{m_p}{\dot{\mu}}\mathbf{P}^{-1}\dot{\boldsymbol{\kappa}} \tag{3.48}$$

Substituting (3.48) into (3.46), the plastic multiplier $\dot{\mu}$ is calculated by

$$\dot{\mu} = \sqrt{\dot{\boldsymbol{\kappa}}^T\mathbf{Q}\ \dot{\boldsymbol{\kappa}}} \tag{3.49}$$

where

$$\mathbf{Q} = \mathbf{P}^{-1} = \frac{1}{3}\begin{bmatrix} 4 & 2 & 0 \\ 2 & 4 & 0 \\ 0 & 0 & 1 \end{bmatrix} \tag{3.50}$$

In the plastic limit state, only plastic strain rates are considered, and therefore the dissipation rate per unit area of plate can be calculated by

$$D_p = \int_{-t/2}^{t/2} \boldsymbol{\sigma}\dot{\boldsymbol{\epsilon}}\,\mathrm{d}z = \mathbf{m}\dot{\boldsymbol{\kappa}} \tag{3.51}$$

Applying the normal rule and taking relation (3.49) into account, equation (3.51) becomes

$$D_p = \dot{\mu}\mathbf{m}\frac{\partial\psi}{\partial\mathbf{m}} = m_p\dot{\mu} = m_p\sqrt{\dot{\boldsymbol{\kappa}}^T\mathbf{Q}\;\dot{\boldsymbol{\kappa}}} \tag{3.52}$$

Hence, the internal dissipation power of the two-dimensional plate domain Ω can be written as

$$\dot{W}_{int}(\dot{\boldsymbol{\kappa}}) = \int_\Omega D_p\;\mathrm{d}\Omega = m_p\int_\Omega\sqrt{\dot{\boldsymbol{\kappa}}^T\mathbf{Q}\;\dot{\boldsymbol{\kappa}}}\;\mathrm{d}\Omega \tag{3.53}$$

Finally, bound theorems for plate and slab problems are summarised below.

Static approach (lower bound)

$$\begin{aligned} \lambda \;=\; & \max\;\lambda^- \\ & \text{s.t}\begin{cases} (\nabla^2)^T\mathbf{m} + \lambda^- q = 0 \quad \text{in}\;\;\Omega \\ \psi(\mathbf{m}) \le 0 \end{cases} \end{aligned} \tag{3.54}$$

Kinematic approach (upper bound)

$$\begin{aligned} \lambda \;=\; & \min\;m_p\sqrt{\dot{\boldsymbol{\kappa}}^T\mathbf{Q}\;\dot{\boldsymbol{\kappa}}} \\ & \text{s.t}\begin{cases} \dot{\boldsymbol{\kappa}} = -\nabla^2\dot{u} \quad \text{in}\;\;\Omega \\ W_{ext} = 1 \end{cases} \end{aligned} \tag{3.55}$$

3.2 Mesh-free method

In this section, a brief description and discussion of computational issues associated with meshfree methods, including computation of EFG shape functions, domain of influence, stabilised conforming nodal integration and *a posteriori* error estimation, are presented.

3.2.1 Computation of shape functions and its derivatives

The moving least square (MLS) approximation presented in the previous chapter is utilised to construct an approximation function $u^h(\mathbf{x})$ that fits a discrete set of data so that

$$u^h(\mathbf{x}) = \sum_{I=1}^{n} \mathbf{\Phi}_I(\mathbf{x})\mathbf{u}_I \tag{3.56}$$

$$\mathbf{\Phi}_I(\mathbf{x}) = \mathbf{p}^T(\mathbf{x})\mathbf{A}^{-1}(\mathbf{x})\mathbf{B}_I(\mathbf{x}) \tag{3.57}$$

$$\mathbf{A}(\mathbf{x}) = \sum_{I=1}^{n} w_I(\mathbf{x})\mathbf{p}(\mathbf{x}_I)\mathbf{p}^T(\mathbf{x}_I) \tag{3.58}$$

$$\mathbf{B}_I(\mathbf{x}) = w_I(\mathbf{x})\mathbf{p}(\mathbf{x}_I) \tag{3.59}$$

where $\mathbf{p}(\mathbf{x})$ is a set of basis functions and $w_I(\mathbf{x})$ is a weight function associated with node I.

For fourth-order problems, the polynomial basis function $\mathbf{p}(\mathbf{x})$ must at least be quadratic (Krysl & Belytschko, 1995). In this work, the quadratic basis for 1D and 2D bending problems is defined by

$$\mathbf{p}^T(\mathbf{x}) = \begin{cases} \mathbf{p}^T(x) = (1, x, x^2) & \text{for beams} \\ \mathbf{p}^T(x, y) = (1, x, y, xy, x^2, y^2) & \text{for plates} \end{cases} \tag{3.60}$$

The weight function $w_I(\mathbf{x})$ plays an important rule in the performance of meshfree methods. If the weight function and its derivatives are continuous, then the shape function and its derivatives will be continuous, and if the weight function

is chosen to be piecewise constant over each sub-domain or element the standard FEM shape functions will be obtained. To provide adequate local character to the MLS approximation and sparse system equations, the weight function should be chosen to be positive over each sub-domain and be zero outside. One of the most common weight functions, used in the conventional EFG method, is the isotropic quartic spline function given as

$$w_I(\mathbf{x}) = \begin{cases} 1 - 6s_I^2 + 8s_I^3 - 3s_I^4 & \text{if } s_I \leq 1 \\ 0 & \text{if } s_I > 1 \end{cases} \tag{3.61}$$

with $s_I = \frac{\|\mathbf{x}-\mathbf{x}_I\|}{R_I}$, R_I is the support radius of node I.

We will need the expression of the first and second partial derivatives of the shape function with respect to $\mathbf{x}$. The first order derivative is given by

$$\mathbf{\Phi}_{I,j}(\mathbf{x}) = \mathbf{p}_{,j}^T \mathbf{A}^{-1}\mathbf{B}_I + \mathbf{p}^T \mathbf{A}_{,j}^{-1}\mathbf{B}_I + \mathbf{p}^T \mathbf{A}^{-1}\mathbf{B}_{I,j} \tag{3.62}$$

with $\mathbf{A}_{,j}^{-1}$ computed by

$$\mathbf{A}_{,j}^{-1} = -\mathbf{A}^{-1}\mathbf{A}_{,j}\mathbf{A}^{-1} \tag{3.63}$$

It is important to note that the second term in equation (3.62) is expensive to calculate due to the term $\mathbf{A}_{,j}^{-1}$. Therefore, the main disadvantage of the standard EFG method appears to be the additional computation time associated with the construction of shape functions and their derivatives. Moreover, when a quadratic basis function is used, the matrix $\mathbf{A}$ rapidly becomes poorly conditioned (Belytschko et al., 1996a), as shown in Figure 3.7. This may provide inaccurate solutions because of the use of matrix inversion.

In practice, it is seldom necessary to form the explicit inverse of a matrix. A better way, both from an execution time and a numerical accuracy standpoint, is to use LU factorisation associated with Gaussian elimination. Here, an efficient approach to compute the shape functions and their derivatives is presented. The

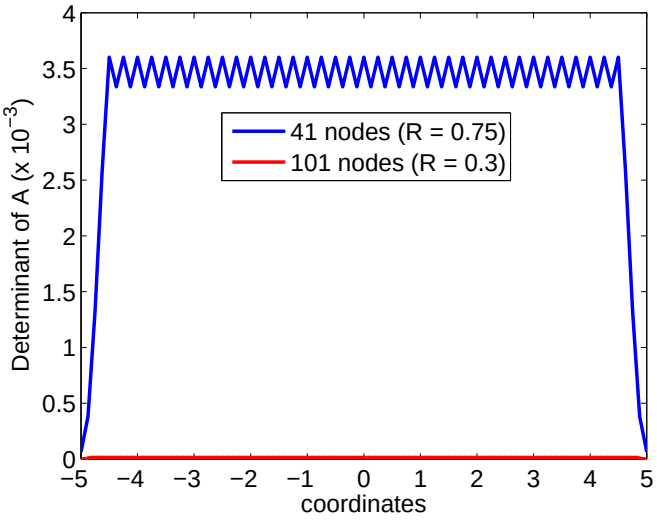

FIGURE 3.7: Condition of the matrix A vs the number of nodes ($R = 3 \times \frac{10}{(n-1)}$) for a 1D domain of length 10 units with uniform spacing of nodes

shape function in equation (3.57) can be written as

$$\mathbf{\Phi}_I(\mathbf{x}) = \mathbf{p}^T(\mathbf{x})\mathbf{A}^{-1}(\mathbf{x})\mathbf{B}_I(\mathbf{x}) = \gamma^T(\mathbf{x})\mathbf{B}_I(\mathbf{x}) \tag{3.64}$$

This leads to the relationship

$$\mathbf{A}(\mathbf{x})\gamma(\mathbf{x}) = \mathbf{p}(\mathbf{x}) \tag{3.65}$$

The coefficients $\gamma(\mathbf{x})$ can be determined using LU decomposition of the matrix $\mathbf{A}$ and back-substitution.

The first and second derivatives of $\gamma(\mathbf{x})$ are achieved by taking the derivatives of equation (3.65) and rearranging the terms which are known to the right-hand side

$$\mathbf{A}\gamma_{,j} = \mathbf{p}_{,j} - \mathbf{A}_{,j}\gamma \tag{3.66}$$

$$\mathbf{A}\gamma_{,jk} = \mathbf{p}_{,jk} - (\mathbf{A}_{,j}\gamma_{,k} + \mathbf{A}_{,k}\gamma_{,j} + \mathbf{A}_{,jk}\gamma) \tag{3.67}$$

The equations (3.65), (3.66), (3.67) can be solved for γ, $\gamma_{,j}$, $\gamma_{,jk}$ and the shape functions and their derivatives are then given by

$$\mathbf{\Phi}_I = \gamma^T \mathbf{B}_I \tag{3.68}$$

$$\mathbf{\Phi}_{I,j} = \gamma_{,j}^T \mathbf{B}_I + \gamma^T \mathbf{B}_{I,j} \tag{3.69}$$

$$\mathbf{\Phi}_{I,jk} = \gamma_{,jk}^T \mathbf{B}_I + \gamma_{,j}^T \mathbf{B}_{I,k} + \gamma_{,k}^T \mathbf{B}_{I,j} + \gamma^T \mathbf{B}_{I,jk} \tag{3.70}$$

The above technique for constructing the shape function and their derivatives is approximately two and a half times as fast as using the standard EFG method due to the fact that using LU decomposition instead of inversion to solve a linear system of equation is two to three times as fast (irrespective of the platform). In addition, the LU decomposition technique produces residuals of the order of machine accuracy, relative to the magnitude of the data. A sample shape function and its derivatives is shown in Figure 3.8. In Section 3.2.3, a technique will be presented that allows the required order of differentiation to be reduced by one.

Note that another technique to avoid loss of accuracy due to roundoff error in EFG is to shift the origin to the evaluation point. The argument $\mathbf{x}$ should be replaced by a simple linear transformation $\bar{\mathbf{x}} = \mathbf{x} - \mathbf{x}_{orig}$. Terms in the equations from (3.65) to (3.70) are determined as

$$\mathbf{A}(\mathbf{x}) = \sum_{I=1}^{n} w_I(\mathbf{x}) \mathbf{p}^T(\mathbf{x}_I - \mathbf{x}_{orig}) \mathbf{p}(\mathbf{x}_I - \mathbf{x}_{orig}) \tag{3.71}$$

$$\mathbf{B}_I(\mathbf{x}) = w_I(\mathbf{x}) \mathbf{p}(\mathbf{x}_I - \mathbf{x}_{orig}) \tag{3.72}$$

$$\mathbf{p}(\mathbf{x}) = \mathbf{p}(0);\ \mathbf{p}_{,j}(\mathbf{x}) = \mathbf{p}_{,j}(0);\ \mathbf{p}_{,jk}(\mathbf{x}) = \mathbf{p}_{,jk}(0) \tag{3.73}$$

3.2.2 Domain of influence

Each node is assigned a so-called domain of influence which can have an arbitrary shape, though circular domains are most commonly used. The concept of the

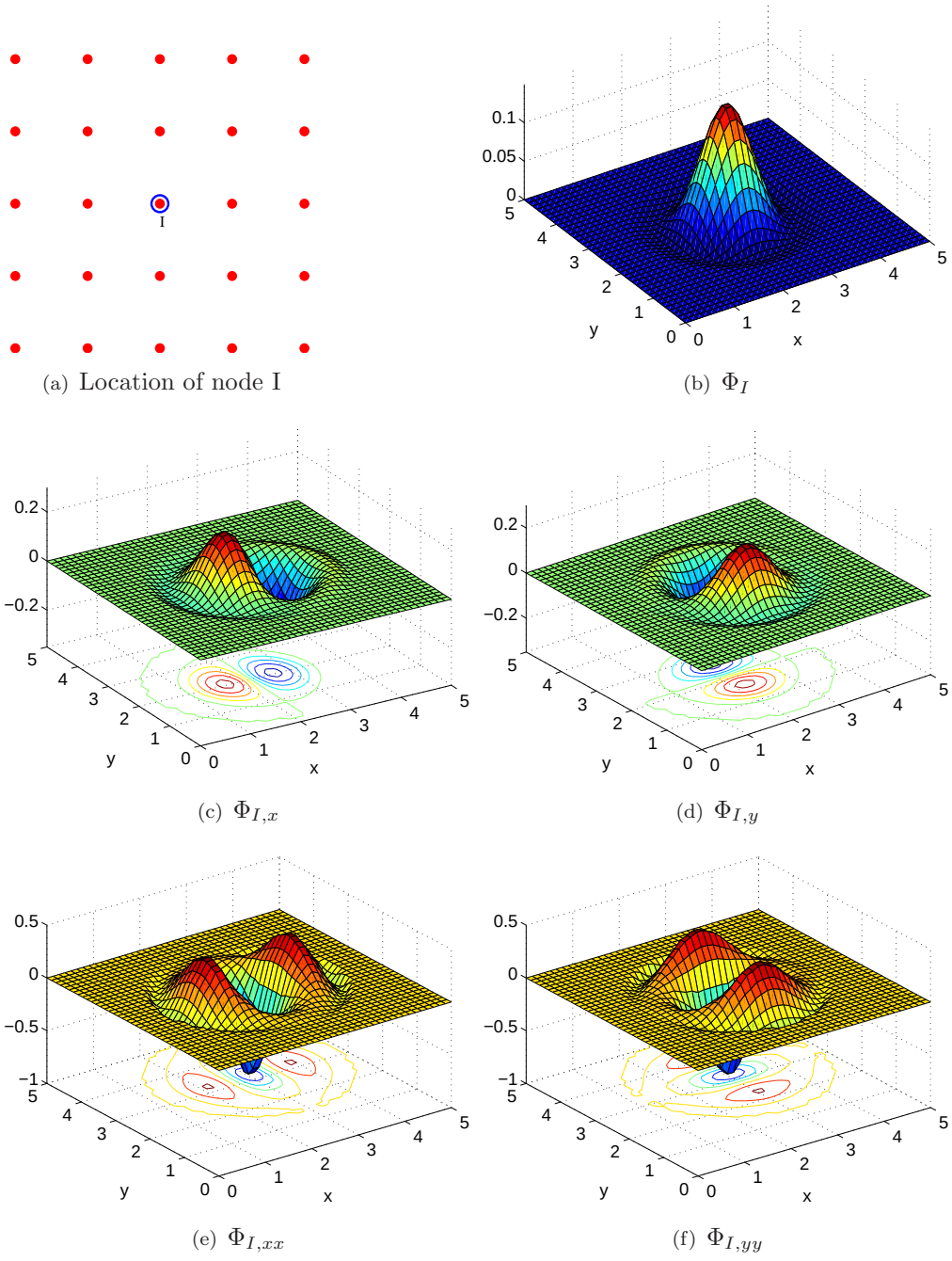

(a) Location of node I

(b) Φ_I

(c) $\Phi_{I,x}$

(d) $\Phi_{I,y}$

(e) $\Phi_{I,xx}$

(f) $\Phi_{I,yy}$

FIGURE 3.8: Sample shape function and derivatives ($\beta = 6$)

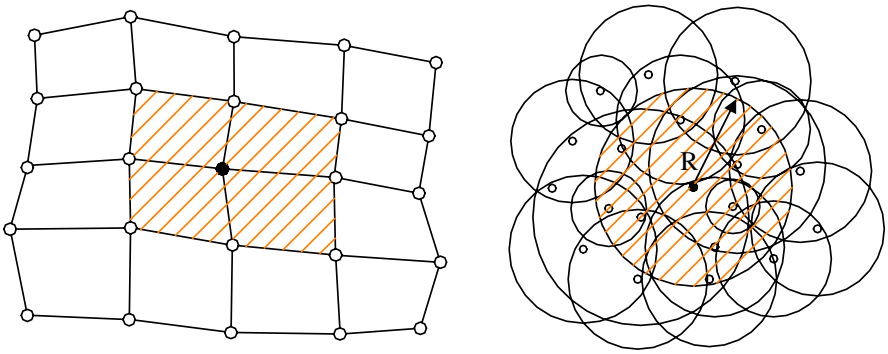

FIGURE 3.9: Domain of influence for finite element shape functions (left) and for mesh-free shape functions (right)

domain of influence for finite element and mesh-free shape functions is illustrated in Figure 3.9.

The support, or the domain of influence, of the weight function associated with node I is chosen to satisfy the following requirements (Chen et al., 2006)

- The support, as set by the radius R_I, should be large enough to ensure that the matrix $\mathbf{A}$ can be inverted, in other words, to provide a sufficient number of nodes inside the domain of influence (which is greater than the number of terms in $\mathbf{p}$).
- The support should not be too large to ensure there is adequate local character to the approximation and for the sake of computational cost (building shape functions).

The size of the compact support of the weight function at node I is determined by

$$R_I = \beta \cdot h_I \tag{3.74}$$

where β is the dimensionless size of influence domain and h_I is the nodal spacing when nodes were distributed regularly, or the maximum distance to neighbouring nodes when nodes are distributed irregularly. For the irregular nodal layout case, the size of the influence domain needs to be locally determined. Based on Voronoi

cell information (see 3.2.3), the neighbouring nodes of node I can be identified and grouped as

$$\begin{aligned} N_I &= \{P_J : V(P_J) \cap V(P_I) \neq \oslash\} \\ &= \{p_1, p_2, p_3, p_4, p_5, p_6, p_7\} \end{aligned} \tag{3.75}$$

where $V(P_I)$ is the Voronoi cell of node P_I.

The maximum distance is then determined by

$$h_I = \max\{d_J : d_J = \overline{P_I P_J}, \forall P_J \in N_I\} \tag{3.76}$$

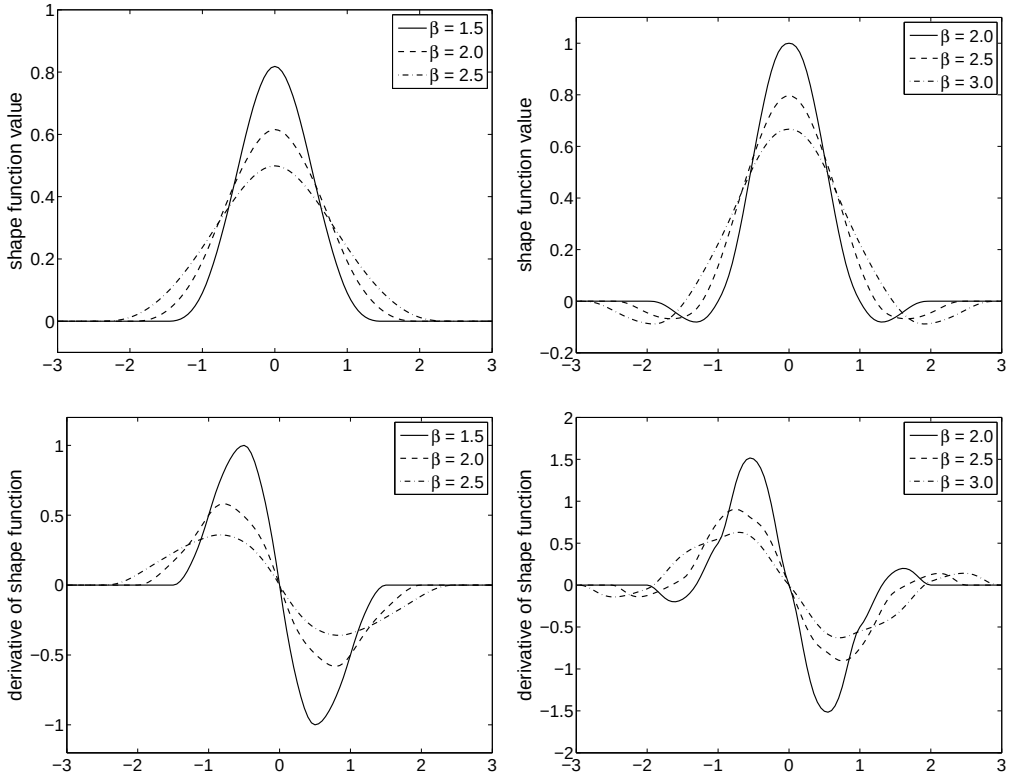

FIGURE 3.10: MLS shape functions and its derivatives with $\mathbf{p}^T = [1, x]$ (left column) and $\mathbf{p}^T = [1, x, x^2]$ (right column)

Together with the basis function $\mathbf{p}$ and the weight function w, the size of the domain of influence determines the character of the MLS shape functions. In

Figure 3.10 one-dimensional MLS shape functions are plotted for different values of β, using Equation (3.61) and with the complete linear and quadratic basis vector $\mathbf{p}$. It can be observed from the figure that when relatively small values of β are used, the MLS shape functions and their derivatives behave in a manner similar to finite element shape functions. For large values of β the MLS shape functions behave more like higher-degree polynomials, and are smoother. The question which arises is how large should the value β be? Usually in practice, the optimal value of β is chosen by carrying out numerical experiments, i.e. for elasticity problems, $\beta = 2 \rightarrow 3$ leads to good results (Liu, 2003; You et al., 2003).

3.2.3 Stabilised conforming nodal integration

The stabilised conforming nodal integration (SCNI) scheme proposed by Chen et al. (2001a) is one of the most efficient integration techniques for mesh-free methods. The SCNI scheme allows evaluation of (smoothed values of) integrals at nodes; therefore it is cheap and fast, and can provide stable solutions. In the SCNI scheme, there is a need to generate representative domains associated with a set of regular/irregular nodes. Voronoi diagrams are amongst the most fundamental and useful constructs to define an irregular set of nodes. In this section, we first present a brief description of Voronoi diagrams before describing the context of the smoothing technique.

Voronoi diagram

Consider a set of distinct nodes $N_v = \{n_1, n_2, \ldots, n_v\}$ in two-dimensional Euclidean space $\mathbb{R}^2$. The Voronoi diagram of the set N_v is a subdivision of the plane into cells Ω which are either closed and convex or unbounded. Each Voronoi cell Ω is associated with node n_I, such that any point in Ω is closer to n_I than any other node $n_J \in N_v$, $I \neq J$. The mathematical definition of the Voronoi polygon Ω is expressed as (de Berg et al., 2008)

$$\Omega = \{\mathbf{x} \in \mathbb{R}^2 \mid d(\mathbf{x}, \mathbf{x}_I) < d(\mathbf{x}, \mathbf{x}_J),\ I \neq J\} \tag{3.77}$$

where $d(\mathbf{x}, \mathbf{x}_I)$ is the distance between the point $\mathbf{x}$ and the node n_I. An example of a Voronoi diagram and its dual, a Delaunay triangulation, for a set of eight nodes is shown in Figure 3.11. It can be seen from the figure that for all nodes inside the convex hull[1] the Voronoi cells are closed and bounded and for all nodes on the boundary of the convex hull the cells are unbounded

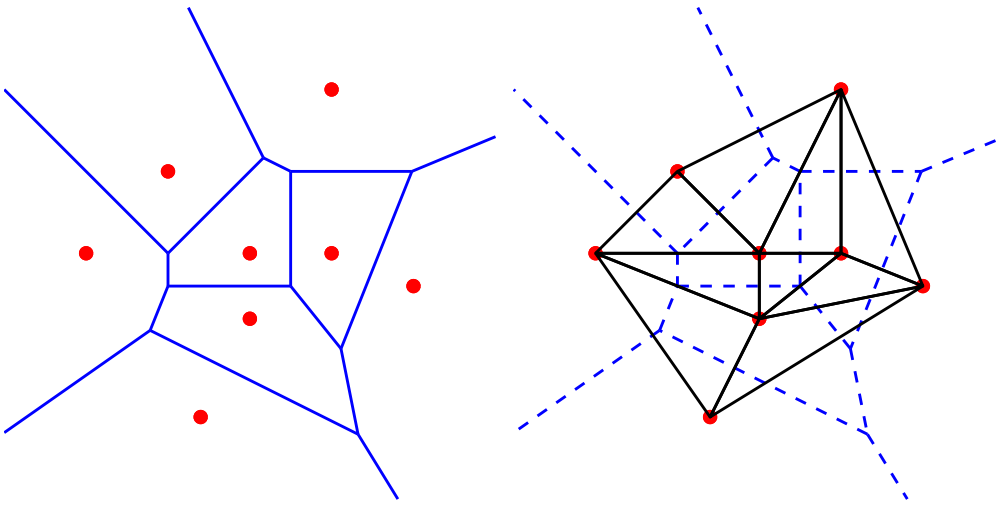

(a) Voronoi diagram (b) Delaunay triangulation

FIGURE 3.11: Geometric structures for a set of eight nodes

Several algorithms have been developed to generate Delaunay triangulations or Voronoi diagrams (Fortune, 1995). In this work, the function *voronoi* in Matlab is used in a two-dimensional framework.

Strain smoothing stabilisation

A strain smoothing method was firstly presented in Chen et al. (2000) for regularisation of material instabilities. The strain smoothing stabilisation method was then modified for use in nodal integration schemes by (Chen et al., 2001a)

$$\tilde{\epsilon}_{ij}^{h}(\mathbf{x}_J) = \int_{\Omega_J} \epsilon_{ij}^{h}(\mathbf{x}) \varphi(\mathbf{x}, \mathbf{x} - \mathbf{x}_J) \, \mathrm{d}\Omega \tag{3.78}$$

[1]The smallest convex domain containing the set of nodes N_v

where $\tilde{\epsilon}_{ij}^h$ is the smoothed value of strains ϵ_{ij}^h at node J, and φ is a distribution (or smoothing) function that has to satisfy the following properties (Chen et al., 2000; Yoo et al., 2004)

$$\varphi \geq 0 \quad \text{and} \quad \int_{\Omega_J} \varphi \, \mathrm{d}\Omega = 1 \tag{3.79}$$

For simplicity, the smoothing function φ is assumed to be a piecewise constant function and is given by

$$\varphi(\mathbf{x}, \mathbf{x} - \mathbf{x}_J) = \begin{cases} 1/a_J, & \mathbf{x} \in \Omega_J \\ 0, & \mathbf{x} \notin \Omega_J \end{cases} \tag{3.80}$$

where a_J is the area of the representative domain of node J.

Substituting equation (3.80) into the equation (3.78), and applying the divergence theorem, gives the following equation

$$\begin{aligned} \tilde{\epsilon}_{ij}^h(\mathbf{x}_J) &= \frac{1}{a_J} \int_{\Omega_J} \frac{1}{2}(u_{i,j}^h + u_{j,i}^h) \, \mathrm{d}\Omega \\ &= \frac{1}{2a_J} \oint_{\Gamma_J} \left(u_i^h n_j + u_j^h n_i \right) \, \mathrm{d}\Omega \end{aligned} \tag{3.81}$$

where Γ_J is the boundary of the representative domain Ω_J.

Now introducing a moving least squares approximation of the displacement fields, the smooth version of the strains can be expressed as

$$\tilde{\boldsymbol{\epsilon}}^h(\mathbf{x}_J) = \begin{bmatrix} \tilde{\epsilon}_{xx}^h(\mathbf{x}_J) \\ \tilde{\epsilon}_{yy}^h(\mathbf{x}_J) \\ 2\tilde{\epsilon}_{xy}^h(\mathbf{x}_J) \end{bmatrix} = \tilde{\mathbf{B}}\mathbf{d} \tag{3.82}$$

where

$$\mathbf{d}^T = [u_1, u_2, \ldots, u_n, v_1, v_2, \ldots, v_n] \tag{3.83}$$

$$\tilde{\mathbf{B}} = \begin{bmatrix} \tilde{\Phi}_{1,x} & \tilde{\Phi}_{2,x} & \ldots & \tilde{\Phi}_{n,x} & 0 & 0 & \ldots & 0 \\ 0 & 0 & \ldots & 0 & \tilde{\Phi}_{1,y} & \tilde{\Phi}_{2,y} & \ldots & \tilde{\Phi}_{n,y} \\ \tilde{\Phi}_{1,y} & \tilde{\Phi}_{2,y} & \ldots & \tilde{\Phi}_{n,y} & \tilde{\Phi}_{1,x} & \tilde{\Phi}_{2,x} & \ldots & \tilde{\Phi}_{n,x} \end{bmatrix} \tag{3.84}$$

with

$$\begin{aligned} \tilde{\Phi}_{I,\alpha}(\mathbf{x}_J) &= \frac{1}{a_J} \oint_{\Gamma_J} \Phi_I(\mathbf{x}_J) n_\alpha(\mathbf{x}) \mathrm{d}\Gamma \\ &= \frac{1}{2a_J} \sum_{k=1}^{ns} \left(n_\alpha^k \, l^k + n_\alpha^{k+1} \, l^{k+1} \right) \Phi_I(\mathbf{x}_J^{k+1}) \end{aligned} \tag{3.85}$$

where $\tilde{\Phi}$ is the smoothed version of Φ; ns is the number of segments of a Voronoi nodal domain Ω_J as shown in the Figure 3.12; $\mathbf{x}_J^k$ and $\mathbf{x}_J^{k+1}$ are the coordinates of the two end points of boundary segment Γ_J^k which has length l^k and outward surface normal n^k.

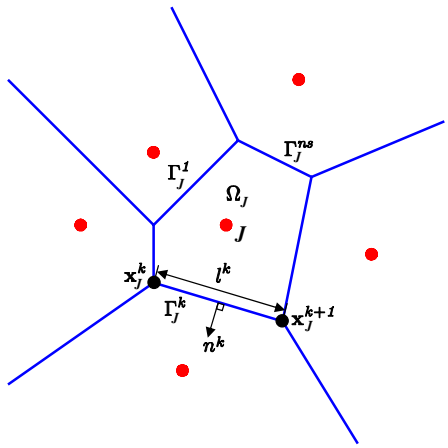

FIGURE 3.12: Geometry definition of a representative nodal domain

3.2.4 A posteriori error estimation

An important ingredient of any adaptive analysis procedure is how to assess accurately the approximation error in numerical solutions. This error information is normally used as a guide to enhance the quality of the discrete model so as to increase the accuracy of solutions, as well as to reduce computational cost. *A posteriori* error estimations which approximate the actual error at the end of each computation step have become an essential part of many numerical procedures.

In a typical computational situation, the approximation error is defined as

$$e := u - u^h \tag{3.86}$$

where u is the exact solution to the mathematical model and u^h is the numerical approximation of u.

The error e in Equation (3.86) cannot be calculated directly since the exact solution u is, in general, unknown. However, as a more refined/enriched discretisation can provide a better approximation to the actual solution, the actual value of e can be estimated by using a very fine discretisation. Another approach to approximate the error is to replace the exact solution by a recovered one based on the superconvergence property of some sample points in the problem domain (Zienkiewicz & Zhu, 1992). The solution obtained from a recovered scheme, or from a very fine discretisation, is called the reference solution which can be used instead of the exact solution. In Chung & Belytschko (1998) the reference stresses (or derivatives) were obtained by using a MLS approximation with a domain of influence which is significantly smaller than the one used when constructing the shape functions. This method is simple and fast, but has to date not yet been applied to a wide variety of problems.

An *a posteriori* error estimator based on approximation error estimation, which has been applied successfully to various linear and non-linear problems (Liu et al., 1997; Krongauz & Belytschko, 1997; Haussler-Combe & Korn, 1998; Rabczuk & Belytschko, 2005), will be described briefly in the remainder of this section. For

simplicity, the approximation error for linearly complete polynomials in two dimensions is presented. Let $u(\mathbf{x})$ be a function that can be developed into a Taylor series expansion. Then the nodal values can be written in terms of the (unknown) exact solution and its derivatives as

$$\begin{aligned} u_I &= u(\mathbf{x}_I) = u(\mathbf{x}) + u_{,x}(\mathbf{x})(x_I - x) + u_{,y}(\mathbf{x})(y_I - y) + \frac{1}{2}u_{,xx}(\mathbf{x})(x_I - x)^2 \\ &+ u_{,xy}(\mathbf{x})(x_I - x)(y_I - y) + \frac{1}{2}u_{,yy}(\mathbf{x})(y_I - y)^2 + O(h^3) \end{aligned} \tag{3.87}$$

Ignoring higher order terms, the approximation error can be written as

$$\begin{aligned} u^h(\mathbf{x}) - u(\mathbf{x}) &= \sum_I \Phi_I(\mathbf{x})u_I - u(\mathbf{x}) \\ &= u(\mathbf{x}) \cdot \left(\sum_I \Phi_I(\mathbf{x}) - 1 \right) + u_{,x}(\mathbf{x}) \cdot \sum_I \Phi_I(\mathbf{x})(x_I - x) \\ &+ u_{,y}(\mathbf{x}) \cdot \sum_I \Phi_I(\mathbf{x})(y_I - y) + \frac{1}{2}u_{,xx}(\mathbf{x}) \cdot \sum_I \Phi_I(\mathbf{x})(x_I - x)^2 \\ &+ u_{,xy}(\mathbf{x}) \cdot \sum_I \Phi_I(\mathbf{x})(x_I - x)(y_I - y) + \frac{1}{2}u_{,yy}(\mathbf{x}) \cdot \sum_I \Phi_I(\mathbf{x})(y_I - y)^2 \end{aligned} \tag{3.88}$$

For linearly complete shape functions, consistency conditions are

$$\begin{aligned} \sum_I \Phi_I(\mathbf{x}) &= 1 \\ \sum_I \Phi_I(\mathbf{x}) \cdot x_I &= x \\ \sum_I \Phi_I(\mathbf{x}) \cdot y_I &= y \end{aligned} \tag{3.89}$$

Applying Equations (3.89) to Equation (3.88), one can obtain

$$\begin{aligned} u^h(\mathbf{x}) - u(\mathbf{x}) &= \frac{1}{2}u_{,xx}(\mathbf{x}) \cdot \sum_I \Phi_I(\mathbf{x})(x_I - x)^2 \\ &+ u_{,xy}(\mathbf{x}) \cdot \sum_I \Phi_I(\mathbf{x})(x_I - x)(y_I - y) \\ &+ \frac{1}{2}u_{,yy}(\mathbf{x}) \cdot \sum_I \Phi_I(\mathbf{x})(y_I - y)^2 \end{aligned} \tag{3.90}$$

Since all shape functions are bounded, that is $|\Phi_I(\mathbf{x})| \leq c$ where c is a constant, and have compact support ($|x_I - x| \leq R_I,\ |y_I - y| \leq R_I$), taking the L^2-norm of Equation (3.90) the error estimate is

$$\|u^h(\mathbf{x}) - u(\mathbf{x})\|_{L^2(\Omega)} \leq cR_I^2 \left\| \frac{1}{2}u_{,xx}(\mathbf{x}) + u_{,xy}(\mathbf{x}) + \frac{1}{2}u_{,yy}(\mathbf{x}) \right\|_{L^2(\Omega)} \tag{3.91}$$

Similarly, the approximation error associated with the derivatives can be estimated. The error in the first derivative is expressed as

$$\|u^h_{,x}(\mathbf{x}) - u_{,x}(\mathbf{x})\|_{L^2(\Omega)} \leq cR_I \left\| \frac{1}{2}u_{,xx}(\mathbf{x}) + u_{,xy}(\mathbf{x}) + \frac{1}{2}u_{,yy}(\mathbf{x}) \right\|_{L^2(\Omega)} \tag{3.92}$$

3.3 Conic programming

A set $\mathscr{K}$ is called a cone if $\forall \mathbf{x} \in \mathscr{K}$ and $\eta \geq 0$, $\eta\mathbf{x} \in \mathscr{K}$. The cone $\mathscr{K}$ is pointed if it includes the origin, and is nonempty and closed under the following condition: $\mathbf{x}, \mathbf{x}' \in \mathscr{K} \Rightarrow \mathbf{x} + \mathbf{x}' \in \mathscr{K}$. The most relevant cones having these properties are (Ben-Tal & Nemirovski, 2001; Ciria et al., 2008)

- The nonnegative orthant:

$$\mathscr{K} \equiv \mathbb{R}^n_+ = \{\mathbf{x} \in \mathbb{R}^n \,|\, x_i \geq 0,\ \forall\, i = 1 \to n\} \tag{3.93}$$

- The Lorentz (or second-order, or ice-cream) cone:

$$\mathscr{K} \equiv \mathscr{L}^n_q = \left\{ \mathbf{x} \in \mathbb{R}^n \,|\, x_1 \geq \sqrt{\sum_{i=2}^{n} x_i^2} = \|\mathbf{x}_{2\to n}\|_{L^2} \right\} \tag{3.94}$$

- The rotated quadratic cone:

$$\mathscr{K} \equiv \mathscr{L}^n_r = \left\{ \mathbf{x} \in \mathbb{R}^n \,|\, x_1 x_2 \geq \sum_{i=3}^{n} x_i^2 = \|\mathbf{x}_{3\to n}\|^2_{L^2},\ x_1, x_2 \geq 0 \right\} \tag{3.95}$$

- The semi-definite cone:

$$\mathscr{K} \equiv S_+^n = \left\{ \mathbf{X} \in \mathbb{R}^{n \times n} \,|\, \mathbf{X} \succeq 0,\, \mathbf{X} = \mathbf{X}^T \right\} \tag{3.96}$$

  where the symbol '$\succeq$' denotes that the matrix is positive semi-definite. For instance, a matrix $\mathbf{X} \in \mathbb{R}^{3\times 3}$ belongs to S_+^3, $\mathbf{X} \in S_+^3$, meaning that

$$\mathbf{X} = \begin{bmatrix} x_1 & x_4 & x_6 \\ x_4 & x_2 & x_5 \\ x_6 & x_5 & x_3 \end{bmatrix} \succeq 0 \quad \text{or} \quad \mathbf{z}^T\mathbf{X}\mathbf{z} \geq 0,\, \mathbf{z} \in \mathbb{R}^3 \tag{3.97}$$

Let $\mathscr{K}^*$ denote the dual cone of $\mathscr{K}$, and $\mathscr{K}^*$ is defined as

$$\mathbf{x}^T\mathbf{y} \geq 0,\, \forall \mathbf{x} \in \mathscr{K} \Leftrightarrow \mathbf{y} \in \mathscr{K}^* \tag{3.98}$$

Figure 3.13 illustrates the primal cone $\mathscr{K}$ and its dual cone $\mathscr{K}^*$.

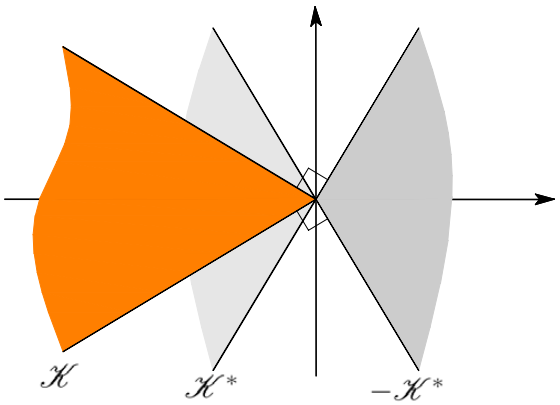

FIGURE 3.13: Primal and dual cones

A conic programming problem is an optimisation problem with linear objective function and conic constraints (Ben-Tal & Nemirovski, 2001). The mathematical formulation of a standard conic optimisation problem can be expressed as

$$\begin{aligned} &\min\ \mathbf{c}^T\mathbf{x} \\ &\text{s.t} \begin{cases} \mathbf{A}\mathbf{x} = \mathbf{b} \\ \mathbf{x} \in \mathscr{K} = \mathscr{K}_1 \times \mathscr{K}_2 \times \cdots \times \mathscr{K}_N \end{cases} \end{aligned} \tag{3.99}$$

where $\mathbf{x} \in \mathbb{R}^n$ are the optimisation variables, and the problem coefficients are $\mathbf{c} \in \mathbb{R}^n$, $\mathbf{A} \in \mathbb{R}^{m \times n}$, $\mathbf{b} \in \mathbb{R}^m$. The dual formulation corresponding to (3.99) is

$$\begin{aligned} &\max\ \mathbf{b}^T\mathbf{y} \\ &\text{s.t} \begin{cases} \mathbf{A}^T\mathbf{y} + \mathbf{s} = \mathbf{c} \\ \mathbf{s} \in \mathscr{K}^* = \mathscr{K}_1^* \times \mathscr{K}_2^* \times \cdots \times \mathscr{K}_N^* \end{cases} \end{aligned} \tag{3.100}$$

with $\mathbf{s} \in \mathbb{R}^n$ is a vector of slack variables and $\mathbf{y} \in \mathbb{R}^n$.

Subclasses of conic programming methods include linear programming (LP) when $\mathscr{K} \equiv \mathbb{R}^n_+$, second-order cone programming (SOCP) when $\mathscr{K} \equiv \mathscr{L}^n_q$ or $\mathscr{K} \equiv \mathscr{L}^n_r$ as defined in Equations (3.94) and (3.95), and semi-definite programming (SDP) when $\mathscr{K} \equiv S^n_+$ as defined in Equation (3.96). Note that LP is a particular case of SOCP, and both can always be cast in the form of a SDP.

Chapter 4

Limit analysis of plates using the EFG method and second-order cone programming[1]

The meshless Element-Free Galerkin (EFG) method is extended to allow computation of the limit load of plates. A kinematic formulation which involves approximating the displacement field using the moving least squares technique is developed. Only one displacement variable is required for each EFG node, ensuring that the total number of variables in the resulting optimisation problem is kept to a minimum, with far fewer variables being required compared with finite element formulations using compatible elements. A stabilised conforming nodal integration scheme is extended to plastic plate bending problems. The evaluation of integrals at nodal points using curvature smoothing stabilisation both keeps the size of the optimisation problem small and also results in stable and accurate solutions. Difficulties imposing essential boundary conditions are overcome by enforcing displacements at the nodes directly. The formulation can be expressed as

[1]based on C.V. Le, M. Gilbert and H. Askes, Limit analysis of plates using the EFG method and second-order cone programming, International Journal for Numerical Methods in Engineering, 78, 1532–1552, 2009.

the problem of minimizing a sum of Euclidean norms subject to a set of equality constraints. This non-smooth minimiation problem can be transformed into a form suitable for solution using second-order cone programming (SOCP). The procedure is applied to several benchmark beam and plate problems and is found in practice to generate good upper bound solutions for benchmark problems.

4.1 Introduction

Limit state criteria are applied to the safety assessment and design of many engineering structures. Considering the ultimate limit state, a traditional and popular approach is to perform a complete elastoplastic analysis. However, an elastoplastic analysis procedure tends to be quite complex due to the need carry this out in an iterative and incremental manner. Alternatively, by applying the fundamental theorems of plasticity, limit analysis can be used to directly identify upper and lower bounds on the load multiplier at collapse, without intermediate steps. There has been a resurgence in interest in computational limit analysis procedures in recent years, principally thanks to the availability of highly efficient optimisation algorithms, which have been developing rapidly.

Computational limit analysis generally involves two steps: (i) numerical discretisation; and (ii) mathematical programming to enable a solution to be obtained. Computational limit analysis approaches based on the finite element method (FEM) are particularly well established; significant contributions include Hodge & Belytschko (1968); Nguyen-Dang (1976); Capsoni & Corradi (1997) and Christiansen & Andersen (1999). Once the stress or displacement fields are approximated and the bound theorems applied, limit analysis becomes a problem of optimisation involving either linear or nonlinear programming. (Note that, for convenience, the term 'displacement' is here used as shorthand for 'displacement rate'.) Problems involving piecewise linear yield functions or nonlinear yield functions can, respectively, be solved using linear or non-linear programming techniques (Gaudrat, 1991; Christiansen & Kortanek, 1991; Zouain et al., 1993; Liu et al., 1995; Andersen, 1996; Andersen et al., 1998; Vicente da Silva & Antao, 2007).

Current research is focussing on the development of limit analysis tools which are sufficiently efficient and robust to be of use to engineers working in practice, and a diverse range of numerical procedures are being investigated. These procedures may use continuous, semi-continuous (Krabbenhoft et al., 2005) or truly discontinuous (Smith & Gilbert, 2007) representations of the relevant field parameters; in the present work continuous representations are of particular interest. However, when FEM is applied some of the well-known characteristics of mesh-based methods can lead to problems: the solutions are often highly sensitive to the geometry of the original mesh, particularly in the region of stress or displacement singularities. Although h-type adaptive refinement schemes (Christiansen & Pedersen, 2001; Borges et al., 2001; Franco et al., 2003; Lyamin & Sloan, 2003; Ciria et al., 2008) have been used to try to overcome such disadvantages, and show immense promise, the schemes quickly become complex and a large number of elements are generally required to obtain accurate solutions. On the other hand, the objective function in the associated optimisation problem is convex, but not everywhere differentiable. One of the most efficient algorithms to overcome this difficulty is the primal-dual interior-point method presented in Andersen et al. (2003) and implemented in commercial codes such as the Mosek software package (Mosek, 2008). The limit analysis problem involving conic constraints can then be solved by this efficient algorithm (Makrodimopoulos & Martin, 2006b; Krabbenhoft et al., 2007; Ciria et al., 2008).

In recent years so-called 'meshless' methods have been developed to provide a flexible alternative approach to FEM. The methods use sets of nodes distributed across the problem domain, and also along domain boundaries. One of the first meshless methods developed is the Element-Free Galerkin (EFG) method (Belytschko et al., 1994). The EFG method has been applied successfully to a wide range of computational problems, proving popular due to its rapid convergence characteristics and its ability to obtain highly accurate solutions. It therefore seems appropriate to investigate the performance of the EFG method when applied to limit analysis problems. Recently, a numerical procedure for lower-bound limit analysis was presented by Chen et al. (2008). In the paper, a self-equilibrium stress basis vector at each Gaussian point is computed using the EFG method. Although this does not

guarantee a strict lower-bound, a reliable estimate of the limit load factor can be obtained when the discretisation is sufficiently fine. It is shown that the solutions obtained for a number of 2D problems are in good agreement with other solutions in the literature.

In this paper a numerical procedure based on the EFG method for upper-bound limit analysis of rigid-perfectly plastic plates governed by the von Mises criterion is proposed. Nodal collocation is used to impose essential boundary conditions. A stabilised conforming nodal integration (SCNI) scheme is used to evaluate the integral of both internal dissipation power and work rate of external load. This results in a truly meshless method and reduces computational effort. Attention is also focussed on formulating the plate limit analysis problem as one of minimizing a sum of Euclidean vector norms, which can be solved efficiently by a primal-dual interior-point method (Andersen et al., 2003), such as second-order cone programming (SOCP). To illustrate the method it is then applied to a series of bending problems, including those for which solutions already exist in the literature.

4.2 Limit analysis of plates - kinematic formulation

Consider a rigid-perfectly plastic plate subjected to a distributed load $\lambda^+ q$ and with a constrained boundary Γ_u. According to Kirchhoff's hypothesis, if u^h denotes the transverse displacement, the strain rates can be expressed by relations

$$\dot{\boldsymbol{\epsilon}} = z\dot{\boldsymbol{\kappa}} \tag{4.1}$$

with the vectors of strains and curvatures

$$\dot{\boldsymbol{\epsilon}} = \left[\begin{array}{ccc} \dot{\epsilon}_{xx} & \dot{\epsilon}_{yy} & \dot{\gamma}_{xy} \end{array} \right]^T \tag{4.2}$$

$$\dot{\boldsymbol{\kappa}} = -\nabla^2 \dot{u}^h = - \left[\begin{array}{ccc} \dfrac{\partial^2 \dot{u}^h}{\partial x^2} & \dfrac{\partial^2 \dot{u}^h}{\partial y^2} & 2\dfrac{\partial^2 \dot{u}^h}{\partial x \partial y} \end{array} \right]^T \tag{4.3}$$

In the framework of a limit analysis problem, only plastic strains are considered and are assumed to obey the normality rule

$$\dot{\boldsymbol{\epsilon}} = \dot{\mu}\frac{\partial \psi}{\partial \boldsymbol{\sigma}} \tag{4.4}$$

where the plastic multiplier $\dot{\mu}$ is non-negative and the yield function $\psi(\boldsymbol{\sigma})$ is convex. In this study, the von Mises failure criterion is used

$$\psi(\boldsymbol{\sigma}) = \sqrt{\boldsymbol{\sigma}^T\ \mathbf{P}\ \boldsymbol{\sigma}} - \sigma_0 \leq 0 \tag{4.5}$$

where σ_0 is the yield stress and

$$\boldsymbol{\sigma} = \begin{bmatrix} \sigma_{xx} & \sigma_{yy} & \tau_{xy} \end{bmatrix}^T \tag{4.6}$$

$$\mathbf{P} = \frac{1}{2}\begin{bmatrix} 2 & -1 & 0 \\ -1 & 2 & 0 \\ 0 & 0 & 6 \end{bmatrix} \tag{4.7}$$

The plastic dissipation is expressed by

$$D_p = \max(\boldsymbol{\sigma}^*\boldsymbol{\epsilon}) \equiv \boldsymbol{\sigma}_\epsilon\ \boldsymbol{\epsilon} \tag{4.8}$$

where $\boldsymbol{\sigma}^*$ represents the admissible stresses contained within the convex yield surface and $\boldsymbol{\sigma}_\epsilon$ represents the stresses on the yield surface associated to any strain rates $\dot{\boldsymbol{\epsilon}}$ through the plasticity condition. Since the stress space described in Equation (4.5) is bounded in all directions, any strain rate is normal to its boundary and no constraints are introduced. Then the power of dissipation can be formulated as a function of strain rates as

$$\dot{D}_p(\boldsymbol{\sigma}_\epsilon, \boldsymbol{\epsilon}) = \sigma_0\sqrt{\dot{\boldsymbol{\epsilon}}^T\mathbf{Q}\dot{\boldsymbol{\epsilon}}} \tag{4.9}$$

where

$$\mathbf{Q} = \mathbf{P}^{-1} = \frac{1}{3}\begin{bmatrix} 4 & 2 & 0 \\ 2 & 4 & 0 \\ 0 & 0 & 1 \end{bmatrix} \tag{4.10}$$

The internal dissipation power of the two-dimensional plate domain Ω can be written as

$$\dot{W}_{int}(\dot{\boldsymbol{\kappa}}) = \int_{\Omega}\int_{-t/2}^{t/2} \dot{D}_p(\boldsymbol{\sigma}_\epsilon, \boldsymbol{\epsilon})\ \mathrm{dz}\ \mathrm{d}\Omega = m_p \int_{\Omega} \sqrt{\dot{\boldsymbol{\kappa}}^T \mathbf{Q}\ \dot{\boldsymbol{\kappa}}}\ \mathrm{d}\Omega \tag{4.11}$$

where $m_p = \sigma_0 t^2/4$ is the plastic moment of resistance per unit width of a plate of thickness t.

The upper bound limit analysis problem for plates can be expressed as

$$\lambda^+ = \min \dot{W}_{int}(\dot{\boldsymbol{\kappa}}) \tag{4.12}$$

subject to

$$\dot{\boldsymbol{\kappa}} = \nabla^2 \dot{u}^h \tag{4.13}$$

$$\dot{W}_{ext} = \int_{\Omega} q\dot{u}^h\ \mathrm{d}\Omega = 1 \tag{4.14}$$

where λ^+ is the load factor, q is the pressure load and where Equation (4.14) prescribes unitary external work and is accompanied by appropriate boundary conditions.

4.3 The EFG method

The moving least square technique is utilised to construct an approximation function $u^h(\mathbf{x})$ that fits a discrete set of data (Belytschko et al., 1994), so that

$$u^h(\mathbf{x}) = \sum_{I=1}^{n} \Phi_I(\mathbf{x}) u_I \tag{4.15}$$

$$\Phi_I(\mathbf{x}) = \mathbf{p}^T(\mathbf{x})\mathbf{A}^{-1}(\mathbf{x})\mathbf{B}_I(\mathbf{x}) \tag{4.16}$$

$$\mathbf{A}(\mathbf{x}) = \sum_{I=1}^{n} w_I(\mathbf{x})\mathbf{p}(\mathbf{x}_I)\mathbf{p}^T(\mathbf{x}_I) \tag{4.17}$$

$$\mathbf{B}_I(\mathbf{x}) = w_I(\mathbf{x})\mathbf{p}(\mathbf{x}_I) \tag{4.18}$$

where n is the number of nodes; $\mathbf{p}(\mathbf{x})$ is a set of basis functions; $w_I(\mathbf{x})$ is a weight function associated with node I. For the purpose of consistency of fourth-order problems, the polynomial basis function $\mathbf{p}(\mathbf{x})$ must be at least quadratic (Krysl & Belytschko, 1995). In this work, the quadratic polynomial for 2D bending problems is used, which is given by

$$\mathbf{p}^T(\mathbf{x}) = \left(1, x, y, xy, x^2, y^2\right) \tag{4.19}$$

Furthermore, for the weight functions an isotropic quartic spline function is used, i.e.

$$w_I(\mathbf{x}) = \begin{cases} 1 - 6s_I^2 + 8s_I^3 - 3s_I^4 & \text{if } s_I \leq 1 \\ 0 & \text{if } s_I > 1 \end{cases} \tag{4.20}$$

with $s_I = \frac{\|\mathbf{x}-\mathbf{x}_I\|}{R_I}$, where R_I is the support radius of node I. We will need first and second partial derivatives of the shape function with respect to $\mathbf{x}$, as described in Chapter 3. To avoid the loss of accuracy due to roundoff error the origin is shifted to the evaluation point (Belytschko et al., 1996a).

4.4 Stabilised conforming nodal integration

The integrals in Equations (4.11) and (4.14) are commonly evaluated by Gauss integration which requires the use of background integration cells. It is normal to use rectangular and triangle cells and high order quadratures. As an alternative, nodal integration which uses nodes as integration points is employed. This results in a truly meshless method due to the absence of integration cells. However, direct nodal integration is unstable because of under-integration and vanishing

derivatives of shape functions at the nodes (Beissel & Belytschko, 1996). A stabilised conforming nodal integration (SCNI) is proposed in Chen et al. (2001a) to eliminate spatial instability problems and to improve accuracy and convergence properties. The main idea of the method is that nodal strains are determined by spatially averaging strains using the divergence theorem. We will extend this idea here to plastic plate bending.

With the use of nodal integration and strain smoothing stabilisation, Equation (4.11) yields

$$\dot{W}_{int} = m_p \sum_{J=1}^{n} a_J \sqrt{\dot{\boldsymbol{\kappa}}^T(\mathbf{x}_J)\mathbf{Q}\,\dot{\boldsymbol{\kappa}}(\mathbf{x}_J)} \tag{4.21}$$

in which $\dot{\boldsymbol{\kappa}}(\mathbf{x}_J)$ follows from curvature smoothing at nodal point $\mathbf{x}_J$ (Sze et al., 2004; Wang & Chen, 2004)

$$\begin{aligned}\dot{\boldsymbol{\kappa}}^T(\mathbf{x}_J) &= -\int_{\Omega_J} \left[\dot{u}^h_{,xx},\ \ \dot{u}^h_{,yy},\ \ 2\dot{u}^h_{,xy}\right] \mathrm{d}\Omega \\ &= -\oint_{\Gamma_J} \left[\dot{u}^h_{,x}\, n_x,\ \ \dot{u}^h_{,y}\, n_y,\ \ (\dot{u}^h_{,x}\, n_y\ +\ \dot{u}^h_{,y}\, n_x)\right] \mathrm{d}\Gamma \end{aligned} \tag{4.22}$$

where Ω_J is the nodal representative domain that can be a Voronoi diagram; a_J and Γ_J are its area and boundary, respectively.

Introducing a moving least square approximation of the transverse displacement rate $\dot{u}^h(\mathbf{x})$, the smoothed curvature $\dot{\boldsymbol{\kappa}}(\mathbf{x}_J)$ is expressed as

$$\dot{\boldsymbol{\kappa}}(\mathbf{x}_J) = -\mathbf{G}\ \mathbf{v} \tag{4.23}$$

$$\mathbf{v}^T = [\dot{u}_1,\ \dot{u}_2,\ \ldots\ , \dot{u}_n] \tag{4.24}$$

$$\mathbf{G} = \begin{bmatrix} \tilde{\Phi}_{1,xx}(\mathbf{x}_J) & \tilde{\Phi}_{2,xx}(\mathbf{x}_J) & \ldots & \tilde{\Phi}_{n,xx}(\mathbf{x}_J) \\ \tilde{\Phi}_{1,yy}(\mathbf{x}_J) & \tilde{\Phi}_{2,yy}(\mathbf{x}_J) & \ldots & \tilde{\Phi}_{n,yy}(\mathbf{x}_J) \\ 2\tilde{\Phi}_{1,xy}(\mathbf{x}_J) & 2\tilde{\Phi}_{2,xy}(\mathbf{x}_J) & \ldots & 2\tilde{\Phi}_{n,xy}(\mathbf{x}_J) \end{bmatrix} \tag{4.25}$$

with

$$\begin{aligned}\tilde{\Phi}_{I,\alpha\beta}(\mathbf{x}_j) &= \frac{1}{2a_j}\int_{\Gamma_j}\left(\Phi_{I,\alpha}(\mathbf{x}_j)n_\beta(\mathbf{x})+\Phi_{I,\beta}(\mathbf{x}_j)n_\alpha(\mathbf{x})\right)\mathrm{d}\Gamma \\ &= \frac{1}{4a_j}\sum_{k=1}^{ns}\left(n_\beta^k\, l^k + n_\beta^{k+1}\, l^{k+1}\right)\Phi_{I,\alpha}(\mathbf{x}_j^{k+1}) \\ &+ \frac{1}{4a_j}\sum_{k=1}^{ns}\left(n_\alpha^k\, l^k + n_\alpha^{k+1}\, l^{k+1}\right)\Phi_{I,\beta}(\mathbf{x}_j^{k+1}) \qquad (4.26)\end{aligned}$$

where $\tilde{\Phi}$ is the smoothed version of Φ, ns is the number of segments of a Voronoi nodal domain, as shown in Figure 4.1, and $\mathbf{x}^k$ and $\mathbf{x}^{k+1}$ are coordinates the two end points of boundary segment k which has length l^k and outward surface normal n^k. Note that the Voronoi node numbers k are defined recursively, i.e. $k = ns+1 \rightarrow k = 1$.

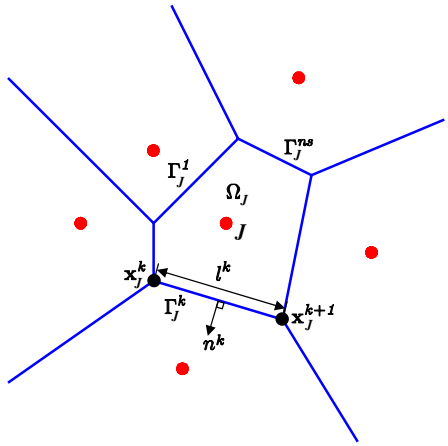

FIGURE 4.1: Geometry definition of a representative nodal domain

Similarly, the external energy can be determined using a nodal integration scheme and moving least square approximation of the transverse displacement rate $\dot{u}^h(\mathbf{x})$ as

$$\begin{aligned}\dot{W}_{ext} &= \int_\Omega q\dot{u}^h\,\mathrm{d}\Omega = \sum_{J=1}^{n} a_J q\dot{u}^h(\mathbf{x}_J) \\ &= \sum_{J=1}^{n}\sum_{I=1}^{n} a_J q\Phi_I(\mathbf{x}_J)\dot{u}_I \qquad (4.27)\end{aligned}$$

Hence the upper bound limit analysis problem for plates can be formulated as

$$\lambda^+ = \min \; m_p \sum_{J=1}^{n} a_J \sqrt{\dot{\boldsymbol{\kappa}}^T(\mathbf{x}_J)\mathbf{Q}\;\dot{\boldsymbol{\kappa}}(\mathbf{x}_J)}$$

$$\text{Subject to} \;\; \sum_{J=1}^{n}\sum_{I=1}^{n} a_J q \Phi_I(\mathbf{x}_J)\dot{u}_I = 1 \tag{4.28}$$

Considering boundary conditions, it is important to note that enforcement of $\dot{u}_I = \dot{\bar{u}}_I$ is not appropriate since the moving least squares approximation does not satisfy the Kronecker delta property and therefore $\dot{u}_I$ is not the velocity at node I. To overcome this difficulty, collocation at nodes (Zhu & Atluri, 1998) is used to enforce essential boundary conditions: $\dot{u}^h(\mathbf{x}_b) = \dot{\bar{u}}_I(\mathbf{x}_b)$, where $\mathbf{x}_b$ are nodes on essential boundaries. Since essential boundaries are fixed, the boundary conditions are given as

$$\dot{u}^h(\mathbf{x}_b) = \sum_{I=1}^{n} \Phi_I(\mathbf{x}_b)\dot{u}_I = 0 \tag{4.29}$$

$$\dot{\theta}_x = \dot{u}^h_{,x}(\mathbf{x}_b) = \sum_{I=1}^{n} \Phi_{I,x}(\mathbf{x}_b)\dot{u}_I = 0 \tag{4.30}$$

$$\dot{\theta}_y = \dot{u}^h_{,y}(\mathbf{x}_b) = \sum_{I=1}^{n} \Phi_{I,y}(\mathbf{x}_b)\dot{u}_I = 0 \tag{4.31}$$

Where Equations (4.29), (4.30) and (4.31) enforce the vertical displacement and x and y axis rotations respectively. Then the Equation (4.28) and boundary conditions can be written as a standard linear equality constraint

$$\mathbf{A}_{eq}\mathbf{v} = \mathbf{b}_{eq} \tag{4.32}$$

where the matrix $\mathbf{A}_{eq}$ and vector $\mathbf{b}_{eq}$ of Equation (4.32) are given by

$$\mathbf{A}_{eq} = \begin{bmatrix} \sum_{J=1}^{n} a_J \Phi_1(\mathbf{x}_J) & \sum_{J=1}^{n} a_J \Phi_2(\mathbf{x}_J) & \dots & \sum_{J=1}^{n} a_J \Phi_n(\mathbf{x}_J) \\ \Phi_1(\mathbf{x}_1^b) & \Phi_2(\mathbf{x}_1^b) & \dots & \Phi_n(\mathbf{x}_1^b) \\ \vdots & \vdots & \ddots & \vdots \\ \Phi_1(\mathbf{x}_d^b) & \Phi_2(\mathbf{x}_d^b) & \dots & \Phi_n(\mathbf{x}_d^b) \\ \Phi_{1,x}(\mathbf{x}_1^b) & \Phi_{2,x}(\mathbf{x}_1^b) & \dots & \Phi_{n,x}(\mathbf{x}_1^b) \\ \vdots & \vdots & \ddots & \vdots \\ \Phi_{1,x}(\mathbf{x}_{rx}^b) & \Phi_{2,x}(\mathbf{x}_{rx}^b) & \dots & \Phi_{n,x}(\mathbf{x}_{rx}^b) \\ \Phi_{1,y}(\mathbf{x}_1^b) & \Phi_{2,y}(\mathbf{x}_1^b) & \dots & \Phi_{n,y}(\mathbf{x}_1^b) \\ \vdots & \vdots & \ddots & \vdots \\ \Phi_{1,y}(\mathbf{x}_{ry}^b) & \Phi_{2,y}(\mathbf{x}_{ry}^b) & \dots & \Phi_{n,y}(\mathbf{x}_{ry}^b) \end{bmatrix} \tag{4.33}$$

$$\mathbf{b}_{eq}^T = \begin{bmatrix} 1 & \overbrace{0 \;\; 0 \;\; \dots \;\; 0}^{d} & \overbrace{0 \;\; 0 \;\; \dots \;\; 0}^{rx} & \overbrace{0 \;\; 0 \;\; \dots \;\; 0}^{ry} \end{bmatrix} \tag{4.34}$$

d is the number of boundary nodes having displacement conditions, while rx and ry are the number of boundary nodes having rotation conditions about x and y, respectively.

4.5 Second-order cone programming

The above limit analysis problem is a non-linear optimisation problem with equality constraints and it can be solved using a general non-linear optimisation solver, such as a sequential quadratic programming (SQP) algorithm (which is generalisation of Newton's method for unconstrained optimisation) or a direct iterative algorithm (Capsoni & Corradi, 1999). However, in Andersen et al. (1998) it is shown that the problem can be reduced to the problem of minimizing a sum of norms. In fact a problem of this sort can be cast as a SOCP problem, for which highly efficient solvers exist. Further details of SOCP and its applications can be found in Lobo et al. (1998); the general form of a SOCP problem with N_s sets of

constraints is as follows

$$\min \ \mathbf{f}^T\mathbf{x}$$

$$\text{Subject to } \ \|\mathbf{H}_i\mathbf{x}+\mathbf{v}_i\| \leq \mathbf{y}_i^T\mathbf{x}+z_i, \ i=1,2,\ldots,N_s \tag{4.35}$$

where $\mathbf{x} \in \mathbb{R}^n$ are the optimisation variables, and the problem coefficients are $\mathbf{f} \in \mathbb{R}^n$, $\mathbf{H}_i \in \mathbb{R}^{m\times n}$, $\mathbf{v}_i \in \mathbb{R}^m$, $\mathbf{y}_i \in \mathbb{R}^n$, and $z_i \in \mathbb{R}$. For optimisation problems in 2D or 3D Euclidean space, $m=2$ or $m=3$. When $m=1$ the SOCP problem reduces to a linear programming problem.

Since $\mathbf{Q}$ in Equation (4.21) is a positive definite matrix, this can be rewritten in a form involving a sum of norms as

$$\dot{W}_{int} = m_p \sum_{J=1}^{n} a_J \|\mathbf{C}^T \ \dot{\boldsymbol{\kappa}}(\mathbf{x}_J)\| = m_p \sum_{J=1}^{n} a_J \|\mathbf{C}^T\mathbf{G}\mathbf{v}\| \tag{4.36}$$

where $\mathbf{C}$ is the so-called Cholesky factor of $\mathbf{Q}$

$$\mathbf{C} = \frac{1}{\sqrt{3}} \begin{bmatrix} 2 & 0 & 0 \\ 1 & \sqrt{3} & 0 \\ 0 & 0 & 1 \end{bmatrix} \tag{4.37}$$

Note that $\mathbf{C}$ depends only on the yield condition; for one-dimensional problems $\mathbf{C}=1$.

The upper bound limit analysis of plates problem can be now written as one of minimizing a sum of norms subject to linear equality constraints

$$\lambda^+ = \min \ m_p \sum_{J=1}^{n} a_J \|\mathbf{C}^T\mathbf{G}\mathbf{v}\|$$

$$\text{Subject to } \ \mathbf{A}_{eq}\mathbf{v} = \mathbf{b}_{eq} \tag{4.38}$$

This is a convex programming problem in which the objective function is not differentiable at any point in the rigid domain where plastic strains do not develop ($\mathbf{C}^T\mathbf{G}\mathbf{v} = 0$). Of the several methods that have been developed to treat such a singularity, the primal-dual interior-point method proposed by Andersen et al.

(2003) has been found to be especially efficient. The traditional way of replacing a singular function by a differentiable one is to add a square of a fixed positive number μ_0 to the root, so that the function becomes $\sqrt{\|\mathbf{C}^T\mathbf{G}\mathbf{v}\|^2 + \mu_0^2}$. However, this may lead to slow convergence as $\mu_0 \to 0$. In Andersen et al. (2003), the quantity μ_0 is treated as an additional variable and can be determined by a duality estimate. With the use of this method, the optimisation problem is solved rapidly and accurately even if there are a large number of variables and/or zero terms in the objective function. Since the method is implemented in generally available second order cone programming software (e.g. Mosek (2008)), the limit analysis problem can be efficiently solved using such software.

Thus the present optimisation problem is cast as a standard SOCP problem by introducing auxiliary variables $t_1,\ t_2,\ \ldots,\ t_n$

$$\lambda^+ = \min\ m_p \sum_{j=1}^{n} a_j t_j$$

$$\text{Subject to}\ \ \mathbf{A}_{eq}\mathbf{v} = \mathbf{b}_{eq};\ \ \mathbf{C}^T\mathbf{G}\mathbf{v} = \mathbf{r}_i \tag{4.39}$$

$$\| \mathbf{r}_i \| \leq t_i,\ \ i = 1, 2, \ldots, n \tag{4.40}$$

in which Equation (4.40) expresses quadratic cones and $\mathbf{r}_i \in \mathbf{R}^n$ are additional variables defined by Equation (4.39), where every $\mathbf{r}_i$ is a 3×1 vector.

4.6 Numerical examples

To test the performance of the new numerical procedure it is appropriate to apply it to a number of two-dimensional examples of interest in engineering practice, e.g. plate problems. However, for most geometries analytical solutions do not exist for plate problems, which makes objective validation difficult. Therefore the procedure is first applied to a number of beam examples for which analytical solutions are available, thereby enabling objective validation.

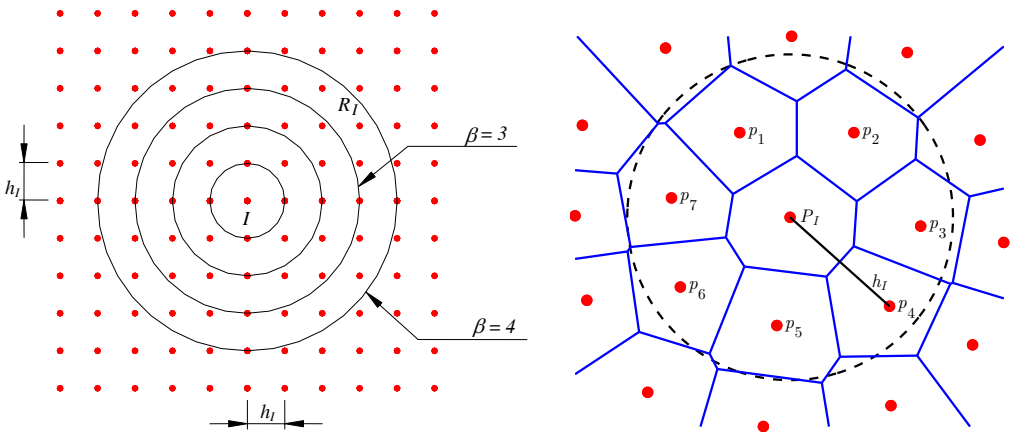

(a) Regular nodal layout (b) Irregular nodal layout

FIGURE 4.2: Sizes of influence domain

The radius of influence domain R_I at node I is determined by

$$R_I = \beta \cdot h_I \tag{4.41}$$

where β is the dimensionless size of influence domain and h_I is the nodal spacing when nodes were distributed regularly, or the maximum distance to neighbouring nodes when nodes were distributed irregularly (Figure 4.2). For the irregular nodal layout case, the size of the influence domain needs to be locally determined. Based on Voronoi cell information, the neighbouring nodes of node I can be identified and grouped as N_I as shown in Figure 4.2b.

$$\begin{aligned} N_I &= \{P_J : V(P_J) \cap V(P_I) \neq \oslash\} \\ &= \{p_1, p_2, p_3, p_4, p_5, p_6, p_7\} \end{aligned} \tag{4.42}$$

where $V(P_I)$ is the Voronoi cell of node P_I. The maximum distance is then determined by

$$h_I = \max\{d_J : d_J = \overline{P_I P_J}, \forall P_J \in N_I\} \tag{4.43}$$

4.6.1 Beam examples

Since the Euler beam is the one dimensional degeneration of the Kirchhoff plate, limit analysis of beams in bending can be considered to examine the effectiveness of the proposed method in a lower dimension. Beams of rectangular cross section ($b \times h$) are subjected to a uniform load and various boundary conditions at the ends, as shown in Figure 4.3. Analytical limit load factors for beams are given as

$$\lambda^+ = \frac{m_p}{qL^2} \begin{cases} 16.000 & \text{beam clamped at ends} \\ 11.657 & \text{clamped-simply supported beam} \\ 8.000 & \text{beam simply supported at ends} \end{cases} \tag{4.44}$$

where $m_p = \sigma_0 bh^2/4$ is the plastic moment of beams.

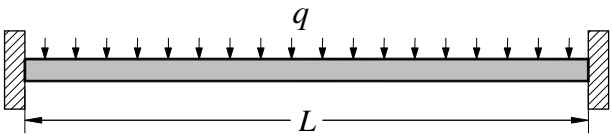

FIGURE 4.3: Clamped beam subjected to uniform load

The kinematic formulation of the beam problem is the reduced form of the kinematic plate limit analysis problem, in which the curvature component is $\dot{\boldsymbol{\kappa}}_x = -\dot{u}_{,xx}$ only and $\mathbf{C} = 1$. The smoothed curvature at node j^{th} on beam can be calculated as

$$\dot{\boldsymbol{\kappa}}(\mathbf{x}_j) = \frac{1}{\Delta \mathbf{x}_j} \left(\Phi_{I,x}(\mathbf{x}_{jR}) - \Phi_{,x}(\mathbf{x}_{jL}) \right) \tag{4.45}$$

where $\Delta \mathbf{x}_j = \mathbf{x}_{jR} - \mathbf{x}_{jL}$ is the length of representative length Ω_j, as shown in Figure 4.4.

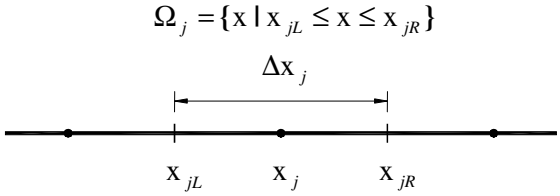

FIGURE 4.4: Degeneration of Voronoi diagram to one-dimension

The limit analysis of beams problem is one which can be solved by linear programming, or alternatively using a SOCP algorithm. Therefore, most of the techniques used in plate problems can be applied here for beams.

Half symmetry was used when possible, with 81 and 161 nodes used to discretise the simply supported and clamped beams respectively. The beam clamped at one end and simply supported at the other was modelled in full, using a total of 321 nodes.

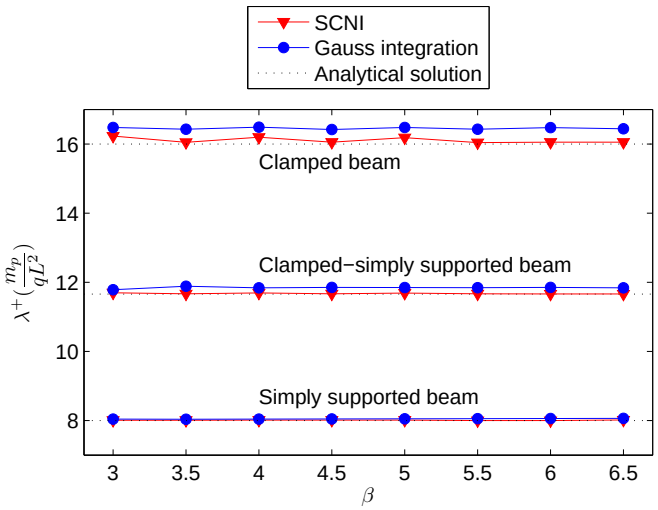

FIGURE 4.5: Comparison of Gauss integration (5×1) and SCNI for 1-D problems

As can be seen from Figure 4.5, taking $\beta = 3.5h_i$ appears to give the best results. Limit load factors are reported in Table 4.1 and it can be seen that the numerical results are in good agreement with analytical solutions. This demonstrates the efficiency and high accuracy of proposed numerical procedure when applied to one-dimensional problems.

The convergence rates are plotted in Figure 4.6. They range between the theoretically expected value of 1 : 1 for the clamped beam to 1 : 2 for the simply supported beam; see Figure 4.6.

TABLE 4.1: Collapse limit load of beams in comparison with analytical solutions

	Present method	Analytical solution	error (%)
Clamped	16.051	16.000	0.31
Simply supported (s.s)	8.001	8.000	~ 0.00
1 clamped, 1 s.s	11.666	11.657	0.08

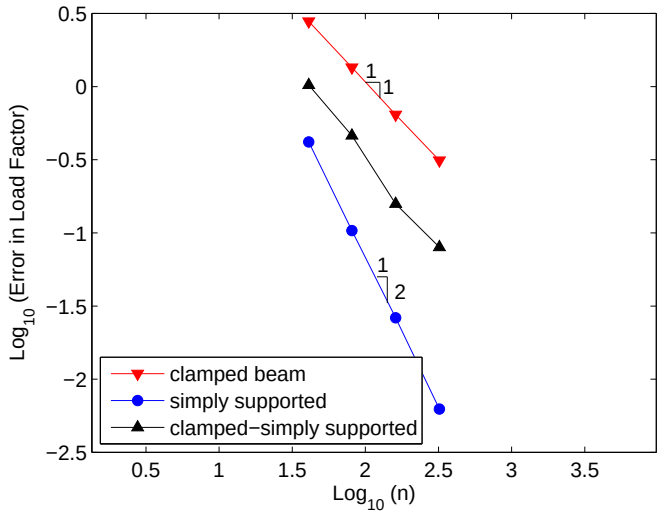

FIGURE 4.6: Rate of convergence for beam problems

4.6.2 Plate examples

A number of plate examples are then considered in the remainder of this section, with the main focus being on benchmark problems for which upper and lower bound solutions have previously been reported in the literature. For all the examples considered the following was assumed: length $L = 10$ m; plate thickness $t = 0.1$ m; yield stress $\sigma_0 = 250$ MPa. Quarter symmetry was assumed when appropriate (see Figure 4.7).

The example comprises a square plate with clamped supports and subjected to uniform out-of-plane pressure loading. A uniform discretisation $n = 15 \times 15$ nodes and various sizes of influence domain $\beta = 3 \sim 6.5$ were used. Matlab optimisation toolbox 3.0 and Mosek version 5.0 optimisation solvers were used to obtain solutions (using a 2.8 GHz Pentium 4 PC running Microsoft XP).

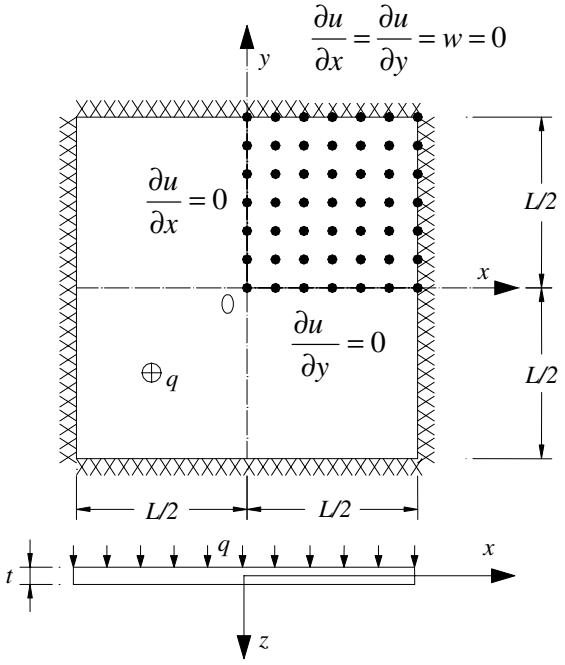

FIGURE 4.7: Square plate clamped along edges and loaded by a uniform pressure

Firstly, potential integration schemes were considered. In the formulation presented a quadratic basis function and an isotropic quartic spline weight function were used with a moving least squares approximation, which results in a high order of the approximated displacement field. Therefore, in order to evaluate accurately the integrals in the limit analysis problem, very large numbers of Gauss points would be needed. Here results are reported for the plate problem with 5×5 Gauss points per cell. It can be seen in Figure 4.8 that the solutions obtained using SCNI are lower, and hence likely to be more accurate, than when using 5×5 Gauss points (except for the extreme case of $\beta = 3$), i.e. SCNI appears to increase the accuracy of solutions as long as the radius of the influence domain is sufficiently large. If nonlinear programming is employed both SCNI and Gauss integration schemes give rise to problems with an identical number of variables (equal to the number of discretisation nodes, $n = 225$ in this case). However, less CPU time is required to evaluate integrals when using the SCNI scheme. The difference in CPU time is even more marked when either linear programming or SOCP are used to solve the underlying optimisation problem. This is because 5 times as many additional

variables need to be added for each spatial dimension when Gauss integration is used, compared with when SCNI is used. In summary, SCNI appears to offer a good combination of accuracy and computational efficiency, not only for elastic analysis problems (Chen et al., 2001a) but now also for plastic analysis problems.

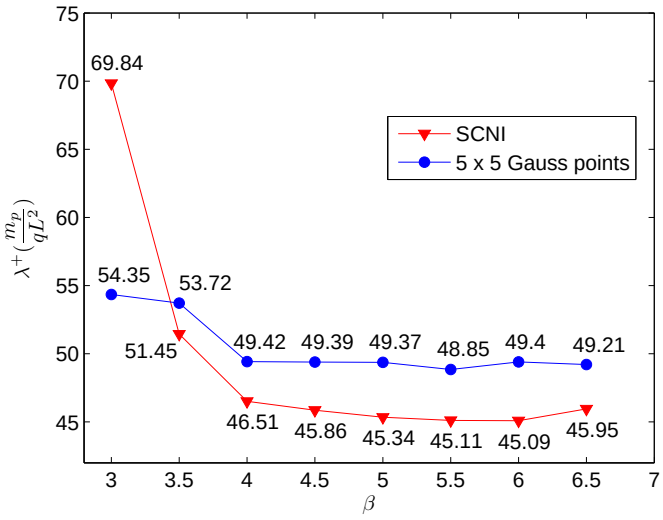

FIGURE 4.8: Limit load factor for various influence domain sizes

Next, the efficacy of various optimisation algorithms was considered (using SCNI). Figure 4.9 shows that SQP and SOCP algorithms produced very similar solutions for the square plate problem. However, the SOCP algorithm produced solutions very much more quickly, even though the number of variables involved was much greater ($5n$ cf. n when using SQP). The SOCP algorithm typically took only $2 \sim 5$ seconds to compute a solution, compared with $300 \sim 600$ seconds when using SQP. Moreover, the SOCP algorithm can be guaranteed to identify globally optimal solutions, whereas SQP cannot.

It is advantageous to choose a size of influence domain that meets both accuracy and computation cost requirements. With this in mind, the radius of influence domain was set to be equal to $6h_i$ for all plate problems considered hereafter (even though use of a higher radius value may sometimes lead to a better upper-bound solution).

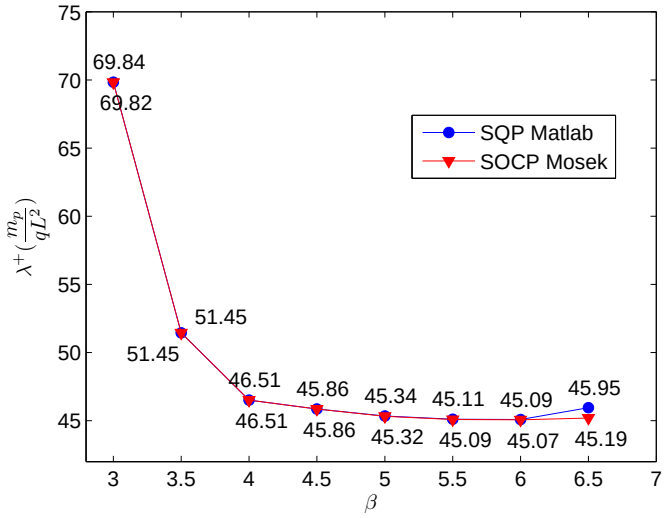

FIGURE 4.9: Comparison between SQP and SOCP using SCNI

Table 4.2 compares solutions obtained using the present method with previously obtained solutions obtained using FEM simulations. Considering previously obtained upper bound solutions, the present method provides lower solutions than in Lubliner (1990), Hodge & Belytschko (1968) and Capsoni & Corradi (1999), by 13.34%, 8.49% and 0.49% respectively. If a comparison is made in terms of the number of variables in the optimisation problem, the present method using EFG has a significantly smaller number than mesh-based approaches; in the EFG method there is only one variable at each node while in the FE method at least 3 nodal degrees of freedom (displacement and 2 rotation components) are required to accommodate the C^1 continuity needed to discretise the problem according to thin plate theory (Capsoni & Corradi, 1999). The only obvious drawback is that the high order shape functions used in EFG make *a priori* proof of the strict upper bound status of the solutions difficult (though this can potentially be checked *a posteriori*).

Further illustration of the method can be made by examining the same square plate with different boundary conditions. Table 4.3 provides solutions in the case of a uniformly loaded square plate with simply supported edges. The limit load factor obtained by the proposed method is the lowest. Figure 4.10 shows the associated collapse mechanisms for both clamped and simply supported plates.

TABLE 4.2: Limit load factor of clamped plate in comparison with other solutions

Authors	upper bound	lower bound
Present method	45.07^{+}	–
Hodge & Belytschko (1968)	49.25	42.86
Lubliner (1990)	52.01	–
Capsoni & Corradi (1999)	45.29	–
Andersen et al. (1998) (mixed element)	44.13	

$^{+}$Approximate rather than rigorous upper bound due to the high order EFG shape functions used

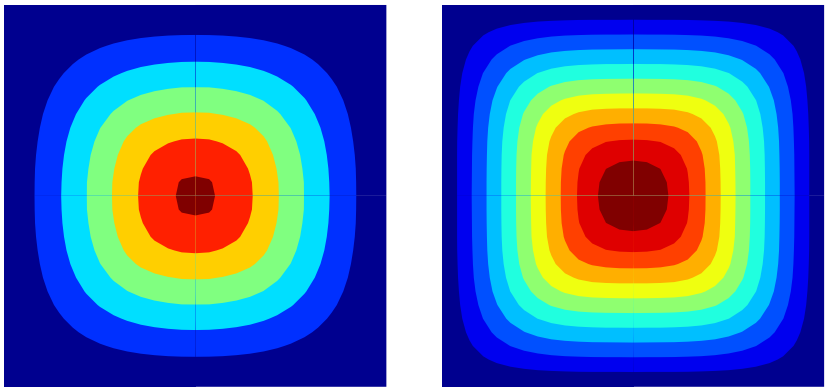

(a) Clamped (b) Simply supported

FIGURE 4.10: Iso-displacement contours at collapse for uniformly loaded plates

TABLE 4.3: Limit load factor of simply supported plate in comparison with other solutions

Authors	upper bound	lower bound
Present method	25.01^{+}	–
Hodge & Belytschko (1968)	26.54	24.86
Lubliner (1990)	27.71	23.81
Capsoni & Corradi (1999)	25.02	–
Andersen et al. (1998) (mixed element)	25.00	

$^{+}$Approximate rather than rigorous upper bound due to the high order EFG shape functions used

Rectangular plates (dimensions $a \times b$) with different boundary conditions under uniform pressure were also considered. Collapse mechanisms and limit loads are shown in Figure 4.11 and Table 4.4, with $a \div b = 2$. The plate with 3 clamped

and 1 free edge was solved using 60×15 nodes using half symmetry whilst in the remaining cases quarter symmetry was used with 30×15 nodes. It is evident from Table 4.4 that the present solution for the simply supported case is in excellent agreement to the solution obtained in Capsoni & Corradi (1999). It should also be noted that plates having simply supported boundaries converge faster than those with clamped boundaries (see Figure 4.12).

TABLE 4.4: Collapse limit load of rectangular plates with various boundary conditions

Models	clamped	supported	3 clamped, 1 free	2 clamped, 2 free
Present results	54.61	29.88	43.86	9.49
Capsoni & Corradi (1999)	–	29.88	–	–

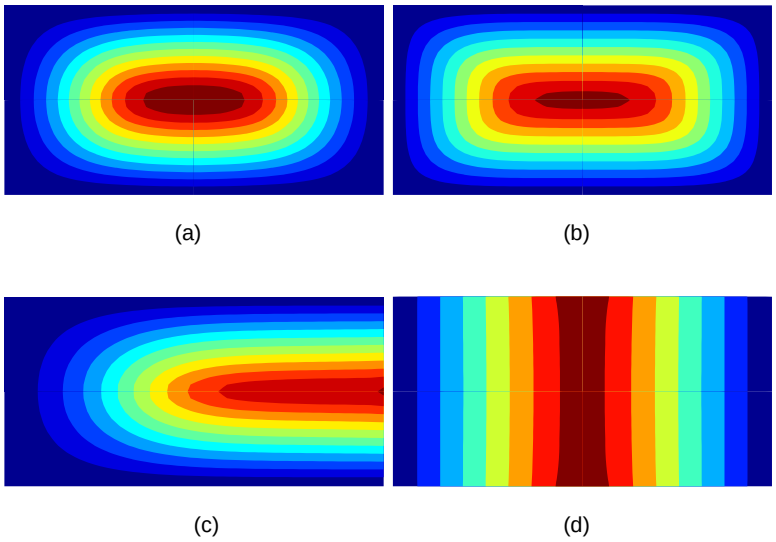

FIGURE 4.11: Iso-displacement contours at collapse for uniformly loaded rectangular plates: (a) clamped plate (b) simply supported (c) 3 clamped edges, 1 free (d) 2 clamped, 2 free edges

The advantages of the proposed method can be further demonstrated by considering a clamped circular plate with central concentrated load P. This problem exhibits a logarithmic singularity in the displacement field near the point load and has a known exact solution (Hopkins & Wang, 1954), $\lambda = \frac{4\pi m_p}{\sqrt{3}P} = 7.255\ \frac{m_p}{P}$. Here a numerical solution was obtained by using an irregular layout of nodes comprising 225 nodes laid out over a quarter of the slab, Figure 4.13. The optimal

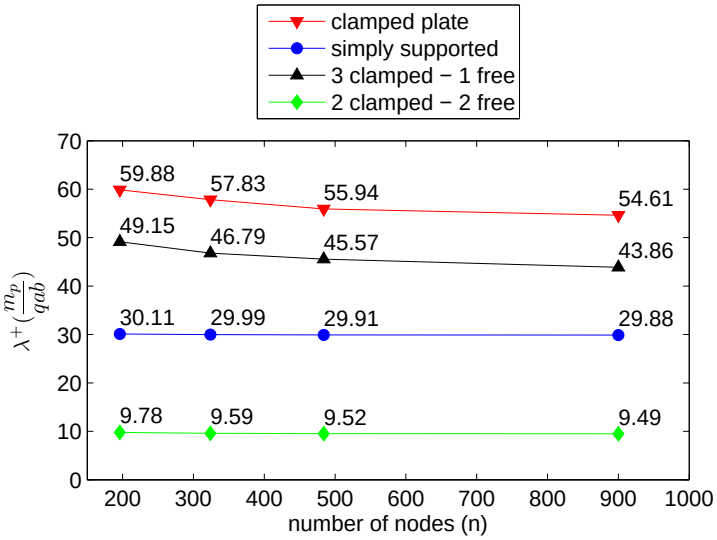

FIGURE 4.12: Collapse multipliers for rectangular plates

size of the domain of influence β was found to be equal to 4.5 and a computed collapse multiplier of 7.385 was obtained, which is just 1.8% higher than the exact solution. The corresponding collapse mechanism is shown in Figure 4.14. When a concentrated load is applied the collapse multiplier does not depend on the shape of the plate (Capsoni & Corradi, 1999; Christiansen & Pedersen, 2001), so the present result can also be compared with previously obtained numerical solutions for square plates. It can be observed that the present solution is much lower than solutions given by Hodge & Belytschko (1968), and Capsoni & Corradi (1999) (7.831 and 9.122, respectively).

Finally, an L-shape plate subject to a uniform load was considered. The plate geometry is shown in Figure 4.15. Collapse load factors for various numbers of nodes are reported in Table 4.5 and the collapse mechanism when 3816 nodes were used is plotted in Figure 4.16.

TABLE 4.5: Collapse limit load of L-shape plate λ^+

number of nodes	341	645	1045	1825	2640	3008	3400	3816
CPU time (s)*	6	38	92	171	340	381	460	789
Computed values	6.79	6.58	6.47	6.38	6.33	6.31	6.30	6.298

*Time taken to solve on a 2.8GHz Pentium 4 PC

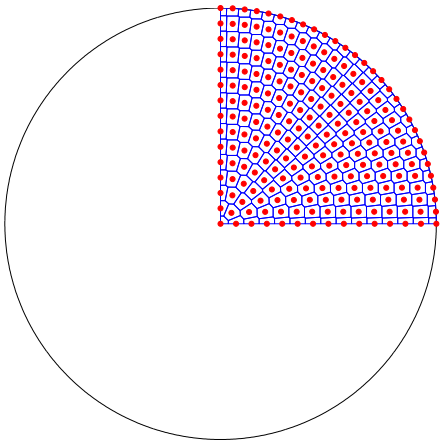

FIGURE 4.13: Irregular nodal layout and Voronoi diagram

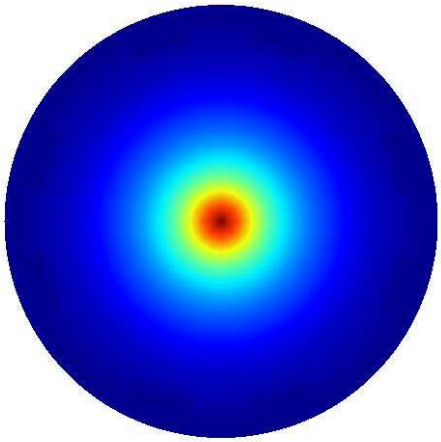

FIGURE 4.14: Clamped circular plate with central point load: collapse mechanism

4.7 Conclusions

The implementation of a numerical limit analysis procedure which uses the Element-Free Galerkin (EFG) method and mathematical programming has been investigated. The numerical procedure demonstrates that the EFG method can be applied successfully not only to lower-bound limit analysis problems (Chen et al., 2008) but also to upper-bound limit analysis problems. The solutions obtained show good agreement with results available in the literature. Advantages of applying EFG to limit analysis problems are that problem size is reduced, and accurate

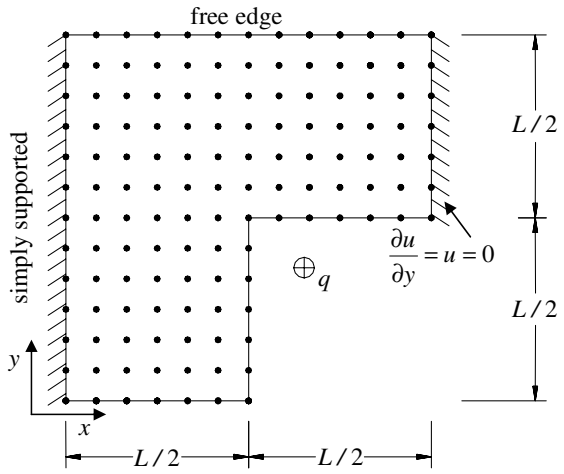

FIGURE 4.15: L-shaped geometry

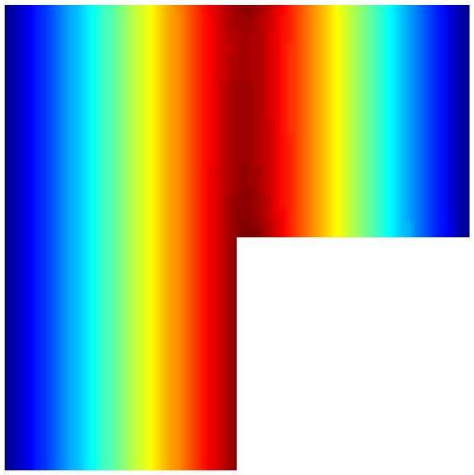

FIGURE 4.16: Iso-displacement contours at collapse for uniformly loaded L-shaped plate

solutions can be obtained using a relatively small number of nodes. The combination of the stabilised conforming nodal integration technique (SCNI) and second order cone programming (SOCP) optimisation algorithm leads to an efficient and robust method. The main features of the method can be summarised as:

1. Since the displacement field is approximated using the moving least squares technique, the problem field and its derivatives are smooth across the whole domain. Due to the use of only one nodal parameter (displacement only

rather than displacement and two rotations) the number of variables in the optimisation problem is small compared with the number required in finite element method formulations.

2. The SCNI scheme has been applied successfully to the kinematic limit analysis of plates problem. The SCNI scheme results in a truly meshless method and stable solutions. This nodal integration scheme produces more accurate results than when Gauss integration is used. Furthermore, the size of optimisation problem reduces significantly when this smoothing technique is used in conjunction with the Element-Free Galerkin method.

3. A primal-dual interior-point SOCP algorithm can efficiently solve problems involving linear or conic constraints. This algorithm is of particular interest in the field of limit analysis since most plasticity problems can be formulated as conic programming problems (Krabbenhoft et al., 2007).

Finally, although a kinematic limit analysis formulation for plates is presented here, the numerical procedure can be extended to tackle more complex structural configurations, subject to a variety of loading regimes. It would for example be interesting to extend the proposed method to treat plane strain problems, 3D problems and also problems involving shakedown.

Chapter 5

Adaptive Element-Free Galerkin method applied to the limit analysis of plates[1]

The implementation of an h-adaptive Element-Free Galerkin (EFG) method in the framework of limit analysis is described. The naturally conforming property of meshfree approximations (with no nodal connectivity required) facilitates the implementation of h-adaptivity. Nodes may be moved, discarded or introduced without the need for complex manipulation of the data structures involved. With the use of the Taylor expansion technique, the error in the computed displacement field and its derivatives can be estimated throughout the problem domain with high accuracy. A stabilised conforming nodal integration scheme is extended to error estimators and results in an efficient and truly meshfree adaptive method. To demonstrate its effectiveness the procedure is then applied to plates with various boundary conditions.

[1]based on C.V. Le, H. Askes and M. Gilbert, Adaptive Element-Free Galerkin method applied to the limit analysis of plates, Computer Methods in Applied Mechanics and Engineering, revising, 2009.

5.1 Introduction

Limit analysis makes use of the fundamental theorems of plastic analysis to provide a powerful means of estimating the maximum load sustainable by a solid or structure. Mathematical programming techniques can often be applied to permit the collapse load to be determined directly. However, the accuracy of numerical limit analysis solutions is highly affected by local singularities arising from localised plastic deformations (Borges et al., 2001). In order to achieve accurate solutions automatic h-refinement is often performed, so that the resolution of the spatial discretisation is refined in plastic zones. Automatic finite element mesh refinement based on both stress and strain fields has been previously proposed (Christiansen & Pedersen, 2001), where elements are candidates for refinement if the strain tensor is non-zero. Alternatively, adaptive procedures based on *a posteriori* error estimates to measure the local and global errors associated with the interpolation have been developed for limit analysis problems. A directional error estimate using recovery gradients and/or the Hessian of mixed finite element solutions was proposed in Borges et al. (2001). The scheme was then adapted to lower bound limit analysis by using quasi-velocities and plastic multipliers from the dual solution (Lyamin et al., 2005). Using solutions of the lower and upper bound problem in combination, another effective error estimate was proposed in Ciria et al. (2008) and Munoz et al. (2009). These techniques have been used successfully for various 2D problems.

Meshfree methods are very attractive computational techniques due to their flexibility, e.g. no nodal connectivity is required. The naturally conforming property of meshfree approximations offers considerable advantages in adaptive analysis. Nodes can easily be added and removed without the need for complex manipulation of the data structures involved. Since error estimates for finite elements are not always directly transferable to meshfree methods, various approaches have been proposed (Chung & Belytschko, 1998; Liu & Tu, 2002; Haussler-Combe & Korn, 1998; Rabczuk & Belytschko, 2005; You et al., 2003; Yvonnet et al., 2006). Effective approaches to estimate the interpolation/approximation error were proposed in Liu et al. (1997); Krongauz & Belytschko (1997); Haussler-Combe & Korn

(1998) and Rabczuk & Belytschko (2005). The approximation error in the computed displacement field and its derivatives can be evaluated with high accuracy using a Taylor expansion of the relevant field variable. It is also shown in Rabczuk & Belytschko (2005) that this estimate is generally suitable for problems with high stress and strain gradients and singularities. While these approaches have been developed for structured meshfree particle methods using Gauss integration, it is also desirable to develop an efficient method for general irregular nodal layouts. In this paper the error density in a representative nodal cell can be determined using smoothed values of the displacement derivatives. This not only results in a truly meshfree method but also reduces the effort required to calculate displacement derivatives in the error estimate. Furthermore, since the Voronoi diagram for a set of nodes is unique, properties of Voronoi cells can be conveniently used as a reference for refinement strategies and for determining locally the size of the domain of influence.

The objective of this paper is to develop a meshfree h-adaptivity procedure for limit analysis problems. The layout of the paper is as follows: Section 5.2 briefly describes a kinematic upper bound limit analysis formulation for plates using the Element-Free Galerkin (EFG) method and stabilised conforming nodal integration (SCNI). A cell-based error estimate for the displacement field and its derivatives is presented in Section 5.3. Based on the error estimate discussed in Section 5.3, error indicators and refinement strategies are introduced in Section 5.4. Numerical examples are provided in Section 5.5 to illustrate the performance of the proposed procedure.

5.2 Limit analysis of plates - discrete kinematic formulation

In this section the kinematic formulation for the plate limit analysis problem is outlined, together with details of the EFG method and the second-order cone

programming (SOCP) problem formulation. More details can be found in Le et al. (2009).

Consider a rigid-perfectly plastic plate governed by the von Mises yield criterion, subjected to a distributed load $\lambda^+ q$ and with a constrained boundary Γ_u. The upper bound limit analysis problem for plates can be written as

$$\lambda^+ = \min \int_\Omega m_p \, \|\mathbf{C}^T \, \dot{\boldsymbol{\kappa}}\|_{L^2(\Omega)} \, \mathrm{d}\Omega \tag{5.1a}$$

s.t

$$\dot{\boldsymbol{\kappa}} = -\left\{ \begin{array}{ccc} \dfrac{\partial^2 \dot{u}^h}{\partial x^2} & \dfrac{\partial^2 \dot{u}^h}{\partial y^2} & 2\dfrac{\partial^2 \dot{u}^h}{\partial x \partial y} \end{array} \right\}^T \tag{5.1b}$$

$$\int_\Omega q u^h \, \mathrm{d}\Omega = 1 \tag{5.1c}$$

accompanied by appropriate boundary conditions, where q is unit load per area, λ^+ is a scalar collapse load multiplier, $m_p = \sigma_0 t^2/4$ is the plastic moment of resistance per unit width of a plate of thickness t and $\mathbf{C}$ is a matrix that depends on the yield criterion involved. For the von Mises criterion,

$$\mathbf{C} = \frac{1}{\sqrt{3}} \begin{bmatrix} 2 & 0 & 0 \\ 1 & \sqrt{3} & 0 \\ 0 & 0 & 1 \end{bmatrix} \tag{5.2}$$

The approximated transverse displacement $u^h(\mathbf{x})$ is computed using a Moving Least Squares (MLS) technique and is expressed as

$$u^h(\mathbf{x}) = \sum_{I=1}^{n} \Phi_I(\mathbf{x}) u_I \tag{5.3}$$

The MLS shape functions $\Phi_I(\mathbf{x})$ are given as (Belytschko et al., 1994)

$$\Phi_I(\mathbf{x}) = \mathbf{p}^T(\mathbf{x}) \mathbf{A}^{-1}(\mathbf{x}) \mathbf{B}_I(\mathbf{x}) \tag{5.4}$$

with

$$\mathbf{A}(\mathbf{x}) = \sum_{I=1}^{n} w_I(\mathbf{x}) \mathbf{p}(\mathbf{x}_I) \mathbf{p}^T(\mathbf{x}_I) \tag{5.5}$$

$$\mathbf{B}_I(\mathbf{x}) = w_I(\mathbf{x})\mathbf{p}(\mathbf{x}_I) \tag{5.6}$$

where n is the number of nodes; $\mathbf{p}(\mathbf{x}) = [1, x, y, xy, x^2, y^2]^T$ is a quadratic basis function and $w_I(\mathbf{x})$ is an isotropic quartic spline weight function associated with node I.

Introducing stabilised conforming nodal integration (Chen et al., 2001a), smoothed curvature rates $\dot{\boldsymbol{\kappa}}(\mathbf{x}_J)$ at nodal point $\mathbf{x}_J$ are written as

$$\dot{\boldsymbol{\kappa}}(\mathbf{x}_J) = -\mathbf{G}\ \mathbf{v} \tag{5.7}$$

where

$$\mathbf{v}^T = [\dot{u}_1,\ \dot{u}_2,\ \ldots\ , \dot{u}_n] \tag{5.8}$$

$$\mathbf{G} = \begin{bmatrix} \tilde{\Phi}_{1,xx}(\mathbf{x}_J) & \tilde{\Phi}_{2,xx}(\mathbf{x}_J) & \ldots & \tilde{\Phi}_{n,xx}(\mathbf{x}_J) \\ \tilde{\Phi}_{1,yy}(\mathbf{x}_J) & \tilde{\Phi}_{2,yy}(\mathbf{x}_J) & \ldots & \tilde{\Phi}_{n,yy}(\mathbf{x}_J) \\ 2\tilde{\Phi}_{1,xy}(\mathbf{x}_J) & 2\tilde{\Phi}_{2,xy}(\mathbf{x}_J) & \ldots & 2\tilde{\Phi}_{n,xy}(\mathbf{x}_J) \end{bmatrix} \tag{5.9}$$

with

$$\begin{aligned} \tilde{\Phi}_{I,\alpha\beta}(\mathbf{x}_j) &= \frac{1}{2a_j}\int_{\Gamma_j} \left(\Phi_{I,\alpha}(\mathbf{x}_j)n_\beta(\mathbf{x}) + \Phi_{I,\beta}(\mathbf{x}_j)n_\alpha(\mathbf{x})\right) \mathrm{d}\Gamma \\ &= \frac{1}{4a_j}\sum_{k=1}^{ns} \left(n_\beta^k\ l^k + n_\beta^{k+1}\ l^{k+1}\right) \Phi_{I,\alpha}(\mathbf{x}_j^{k+1}) \\ &+ \frac{1}{4a_j}\sum_{k=1}^{ns} \left(n_\alpha^k\ l^k + n_\alpha^{k+1}\ l^{k+1}\right) \Phi_{I,\beta}(\mathbf{x}_j^{k+1}) \end{aligned} \tag{5.10}$$

where $\tilde{\Phi}$ is the smoothed version of Φ; a_J, Γ_J and ns are respectively the area, boundary and the number of segments of a Voronoi nodal domain Ω_J as shown in the Figure 5.1; $\mathbf{x}_J^k$ and $\mathbf{x}_J^{k+1}$ are the coordinates of the two end points of boundary segment Γ_J^k which has length l^k and outward surface normal n^k.

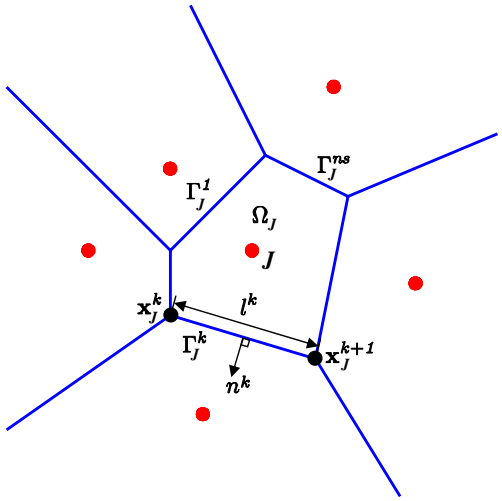

FIGURE 5.1: Geometry of a representative nodal domain

The kinematic limit analysis problem for plates can now be written in the form of a SOCP problem as follows:

$$\lambda^+ = \min \; m_p \sum_{j=1}^{n} a_j t_j \tag{5.11a}$$

s.t

$$\mathbf{A}_{eq}\mathbf{v} = \mathbf{b}_{eq} \tag{5.11b}$$

$$\mathbf{C}^T\mathbf{G}\mathbf{v} = \mathbf{r}_i \tag{5.11c}$$

$$\| \mathbf{r}_i \| \leq t_i, \quad i = 1, 2, \ldots, n \tag{5.11d}$$

in which Equation (5.11d) expresses quadratic cones and $\mathbf{r}_i \in \mathbb{R}^3$ are additional variables defined by Equation (5.11c), where every $\mathbf{r}_i$ is a 3×1 vector. Matrix $\mathbf{A}_{eq}$ and vector $\mathbf{b}_{eq}$ are obtained from unitary external work Equation (5.1c) and

boundary conditions, and they are given by

$$\mathbf{A}_{eq} = \begin{bmatrix} \sum_{J=1}^{n} a_J \Phi_1(\mathbf{x}_J) & \sum_{J=1}^{n} a_J \Phi_2(\mathbf{x}_J) & \dots & \sum_{J=1}^{n} a_J \Phi_n(\mathbf{x}_J) \\ \Phi_1(\mathbf{x}_1^b) & \Phi_2(\mathbf{x}_1^b) & \dots & \Phi_n(\mathbf{x}_1^b) \\ \vdots & \vdots & \ddots & \vdots \\ \Phi_1(\mathbf{x}_d^b) & \Phi_2(\mathbf{x}_d^b) & \dots & \Phi_n(\mathbf{x}_d^b) \\ \Phi_{1,x}(\mathbf{x}_1^b) & \Phi_{2,x}(\mathbf{x}_1^b) & \dots & \Phi_{n,x}(\mathbf{x}_1^b) \\ \vdots & \vdots & \ddots & \vdots \\ \Phi_{1,x}(\mathbf{x}_{rx}^b) & \Phi_{2,x}(\mathbf{x}_{rx}^b) & \dots & \Phi_{n,x}(\mathbf{x}_{rx}^b) \\ \Phi_{1,y}(\mathbf{x}_1^b) & \Phi_{2,y}(\mathbf{x}_1^b) & \dots & \Phi_{n,y}(\mathbf{x}_1^b) \\ \vdots & \vdots & \ddots & \vdots \\ \Phi_{1,y}(\mathbf{x}_{ry}^b) & \Phi_{2,y}(\mathbf{x}_{ry}^b) & \dots & \Phi_{n,y}(\mathbf{x}_{ry}^b) \end{bmatrix} \tag{5.12}$$

$$\mathbf{b}_{eq}^T = \begin{bmatrix} 1 & \overbrace{0 \;\; 0 \;\; \dots \;\; 0}^{d} & \overbrace{0 \;\; 0 \;\; \dots \;\; 0}^{rx} & \overbrace{0 \;\; 0 \;\; \dots \;\; 0}^{ry} \end{bmatrix} \tag{5.13}$$

Here d is the number of boundary nodes having displacement conditions and rx and ry are the number of boundary nodes having rotation conditions about x and y, respectively. It is noted that tangential rotations along the boundary are also enforced as this has been found to increase the accuracy of the solutions.

5.3 Estimation of approximation errors

A key ingredient of any adaptive analysis procedure is the formulation of an error estimate which determines which parts of the domain are most in need of refinement. Here we will use the error estimate approach given in Liu et al. (1997); Krongauz & Belytschko (1997); Haussler-Combe & Korn (1998) and Rabczuk & Belytschko (2005). The estimated error for general approximations of s^{th} order completeness is presented first, from which the error for linear and quadratic cases in 2D can be retrieved. An approximation is complete to order s if any polynomial

up to order s is exactly reproduced as

$$\sum_{I=1}^{n} x^p \Phi_I(\mathbf{x}) = x^p \quad \text{for} \quad 0 \leq p \leq s \tag{5.14}$$

The error can be written as

$$u^h(\mathbf{x}) - u(\mathbf{x}) = \sum_{I=1}^{n} \Phi_I(\mathbf{x}) u_I - u(\mathbf{x}) \tag{5.15}$$

Expanding $u(\mathbf{x})$ by a Taylor series, the nodal values of the exact solution are indicated as $u(\mathbf{x}_I)$ and can be expressed as

$$u(\mathbf{x}_I) = \sum_{m=0}^{s} \frac{1}{m!} \left((x_I - x)\frac{\partial}{\partial x} + (y_I - y)\frac{\partial}{\partial y} + (z_I - z)\frac{\partial}{\partial z} \right)^m u(\mathbf{x}) + \mathscr{R}_{s+1} + O(h^{s+2}) \tag{5.16}$$

with

$$\mathscr{R}_{s+1} = \frac{1}{(s+1)!} \left((x_I - x)\frac{\partial}{\partial x} + (y_I - y)\frac{\partial}{\partial y} + (z_I - z)\frac{\partial}{\partial z} \right)^{s+1} u(\mathbf{x}) \tag{5.17}$$

Combining the conditions of an approximation of s^{th} order completeness with Equations (5.15, 5.16) and ignoring higher order terms, the approximation error reads

$$u^h(\mathbf{x}) - u(\mathbf{x}) = \frac{1}{(s+1)!} \left((x_I - x)\frac{\partial}{\partial x} + (y_I - y)\frac{\partial}{\partial y} + (z_I - z)\frac{\partial}{\partial z} \right)^{s+1} u(\mathbf{x}) \tag{5.18}$$

The shape functions are bounded, that is $|\Phi(\mathbf{x})| \leq c$ where c is a bounded constant, and have compact support ($|x_I - x| \leq R_I$, $|y_I - y| \leq R_I$ and $|z_I - z| \leq R_I$, R_I is the radius of the domain of influence). Defining

$$D = \left(\frac{\partial}{\partial x} + \frac{\partial}{\partial y} + \frac{\partial}{\partial z} \right) \tag{5.19}$$

and taking the L^2-norm of the error estimate, Equation (5.18) becomes

$$\|u^h(\mathbf{x}) - u(\mathbf{x})\|_{L^2(\Omega)} = cR_I^{s+1} \left|\left| \frac{1}{(s+1)!} D^{s+1} u \right|\right|_{L^2(\Omega)} \tag{5.20}$$

Similarly, the approximation error associated with the derivatives can be estimated. The error in the first derivative is expressed as

$$\left|\left| \frac{\partial u^h(\mathbf{x})}{\partial \mathbf{x}} - \frac{\partial u(\mathbf{x})}{\partial \mathbf{x}} \right|\right|_{L^2(\Omega)} = cR_I^{s} \left|\left| \frac{1}{(s+1)!} D^{s+1} u \right|\right|_{L^2(\Omega)} \tag{5.21}$$

For 2D problems, the approximation error of the first derivative is

$$\left|\left| \frac{\partial u^h(\mathbf{x})}{\partial \mathbf{x}} - \frac{\partial u(\mathbf{x})}{\partial \mathbf{x}} \right|\right|_{L^2(\Omega)} = cR_I \left|\left| \frac{1}{2} \left(u_{,xx} + u_{,yy} + 2u_{,xy}\right) \right|\right|_{L^2(\Omega)} \tag{5.22}$$

for a linear basis function, and it is

$$\left|\left| \frac{\partial u^h(\mathbf{x})}{\partial \mathbf{x}} - \frac{\partial u(\mathbf{x})}{\partial \mathbf{x}} \right|\right|_{L^2(\Omega)} = cR_I^2 \left|\left| \frac{1}{6} \left(u_{,xxx} + u_{,yyy} + 3\left(u_{,xxy} + u_{,yyx}\right)\right) \right|\right|_{L^2(\Omega)} \tag{5.23}$$

for a quadratic basis function.

5.4 Adaptive procedure

5.4.1 Updating the shape functions

In meshfree adaptive analysis, new nodes are added in those parts of the domain where the error exceeds a predefined tolerance. These new nodes locally impact on the shape functions of neighbouring nodes. In order to reduce computational cost and to ensure consistency of the MLS approximation, matrix $\mathbf{A}$ in the shape

functions of existing nodes are reconstructed locally as (You et al., 2003):

$$\begin{aligned}\mathbf{A}(\mathbf{x}) &= \sum_{I=1}^{n_{old}} w_I(\mathbf{x})\mathbf{p}(\mathbf{x}_I)\mathbf{p}^T(\mathbf{x}_I) + \sum_{I=1}^{n_{new}} w_I(\mathbf{x})\mathbf{p}(\mathbf{x}_I)\mathbf{p}^T(\mathbf{x}_I) \\ &= \mathbf{A}_{old}(\mathbf{x}) + \sum_{I=1}^{n_{new}} w_I(\mathbf{x})\mathbf{p}(\mathbf{x}_I)\mathbf{p}^T(\mathbf{x}_I) \end{aligned} \tag{5.24}$$

This is illustrated with a one-dimensional example in Figure 5.2, where an added node 12 can be seen to affect the shape functions of nodes 6 and 7.

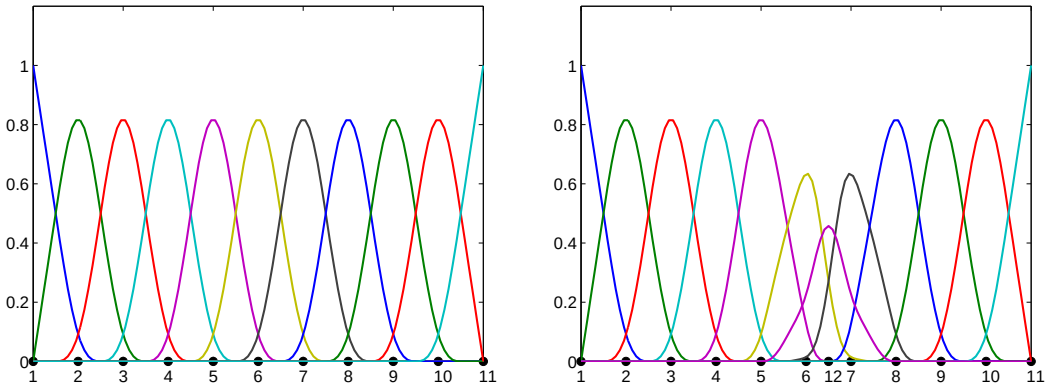

(a) Before adaptivity (b) After adaptivity

FIGURE 5.2: Nodal refinement strategies based on Voronoi cells

Note that in an adaptive refinement procedure nodes will often be distributed irregularly. Therefore the size of the domain of influence needs to be determined locally. The Voronoi diagram for a set of nodes is unique, and from the Voronoi cell information, the neighbours of node I can be identified and grouped as N_I, as shown in Figure 5.3

$$\begin{aligned} N_I &= \{P_J : V(P_J) \cap V(P_I) \neq \oslash\} \\ &= \{p_1, p_2, p_3, p_4, p_5, p_6, p_7\} \end{aligned} \tag{5.25}$$

where $V(P_I)$ is the Voronoi cell of particle P_I.

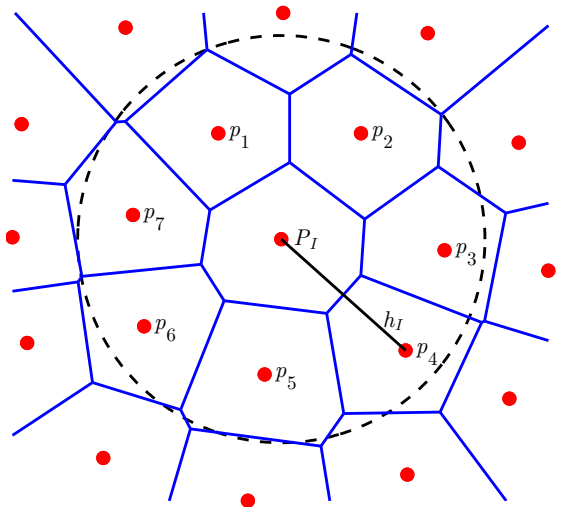

FIGURE 5.3: Determination of shape function support size

The size of the domain of influence of node I is then determined as

$$R_I = \beta \cdot h_I = \beta \cdot \max\{d_J : d_J = \overline{P_I P_J},\ \forall P_J \in N_I\} \tag{5.26}$$

5.4.2 Refinement criteria

Based on the error estimate discussed in Section 5.3, the local error is computed for each integration cell from the displacement fields obtained by solving the optimisation problem. This local error is controlled as follows

$$R_I^s \left|\left| \frac{1}{(s+1)!} D^{s+1} u \right|\right|_{L^2(\Omega)} \leq \delta \tag{5.27}$$

where δ is a dimensionless user-defined error tolerance value which will be discussed in more detail in Section 5.5.

It is important to note that it is often computationally expensive to calculate the terms $D^{s+1}u$ in Equation (5.27), especially for problems using second, or higher, order basis functions. Furthermore, in order to evaluate accurately the LHS term in Equation (5.27) a large number of Gauss points would be needed (Rabczuk & Belytschko, 2005). The smoothing technique proposed in Chen et al. (2001a) can

be extended to overcome this difficulty. Introducing smoothing of $D^{s+1}u(\mathbf{x})$ at a representative nodal domain Ω_j, we have

$$D^{s+1}\tilde{u}(\mathbf{x}_j) = \frac{1}{a_j}\int_{\Omega_j} D^{s+1}u(\mathbf{x})\mathrm{d}\Omega \tag{5.28}$$

Introducing now the MLS approximation of the displacement field, we obtain

$$D^{s+1}\tilde{u}(\mathbf{x}_j) = \sum_{I=1}^{n} D^{s+1}\tilde{\Phi}_I(\mathbf{x}_j)u_I \tag{5.29}$$

where

$$D^{s+1}\tilde{\Phi}_I(\mathbf{x}_j) = \frac{1}{a_j}\int_{\Omega_j} D^{s+1}\Phi_I(\mathbf{x})\mathrm{d}\Omega \tag{5.30}$$

With the use of this smoothing technique, the cell-based error tolerance can be rewritten as

$$a_j R_j^s \left|\left|\frac{1}{(s+1)!}D^{s+1}\tilde{u}(\mathbf{x}_j)\right|\right|_{L^2(\Omega_j)} \leq \delta \tag{5.31}$$

The global error estimator is the sum of the local errors of all cells and is given by

$$||e||_{L^2(\Omega)} = \left(\sum_{j=1}^{n}\left(a_j R_j^s \left|\left|\frac{1}{(s+1)!}D^{s+1}\tilde{u}(\mathbf{x}_j)\right|\right|_{L^2(\Omega_j)}\right)^2\right)^{1/2} \tag{5.32}$$

For plate problems, quadratic basis functions must be used (Krysl & Belytschko, 1995). The local cell-based error estimator then reads

$$a_j R_j^2 \left|\left|\frac{\tilde{u}_{,xxx}(\mathbf{x}_j) + \tilde{u}_{,yyy}(\mathbf{x}_j) + 3\left(\tilde{u}_{,xxy}(\mathbf{x}_j) + \tilde{u}_{,yyx}(\mathbf{x}_j)\right)}{6}\right|\right|_{L^2(\Omega_j)} \leq \delta \tag{5.33}$$

in which

$$\tilde{u}_{,\alpha\alpha\beta}(\mathbf{x}_j) = \sum_{I=1}^{n}\tilde{\Phi}_{I,\alpha\alpha\beta}(\mathbf{x}_j)u_I \tag{5.34}$$

$$\tilde{\Phi}_{I,\alpha\alpha\beta}(\mathbf{x}_j) = \frac{1}{2a_j}\oint_{\Gamma_j}\left(\Phi_{I,\alpha\alpha}(\mathbf{x}_j)n_\beta(\mathbf{x}) + \Phi_{I,\alpha\beta}(\mathbf{x}_j)n_\alpha(\mathbf{x})\right)\mathrm{d}\Gamma \tag{5.35}$$

The technique used to determine the boundary integral in Equation (5.10) can be applied here to evaluate the term on the RHS of Equation (5.35).

5.4.3 Refinement strategy

The problem domain is subdivided into nodes and an associated Voronoi diagram is constructed. If the local error in a Voronoi cell exceeds the predefined value δ, new nodes are added as shown in Figure 5.4 (You et al., 2003; Yvonnet et al., 2006). It can be seen from the figure that the cells in the Voronoi diagram resulting from strategy (I) are more uniformly sized than those resulting from strategy (II), and also that the number of nodes added in the two cases is identical.

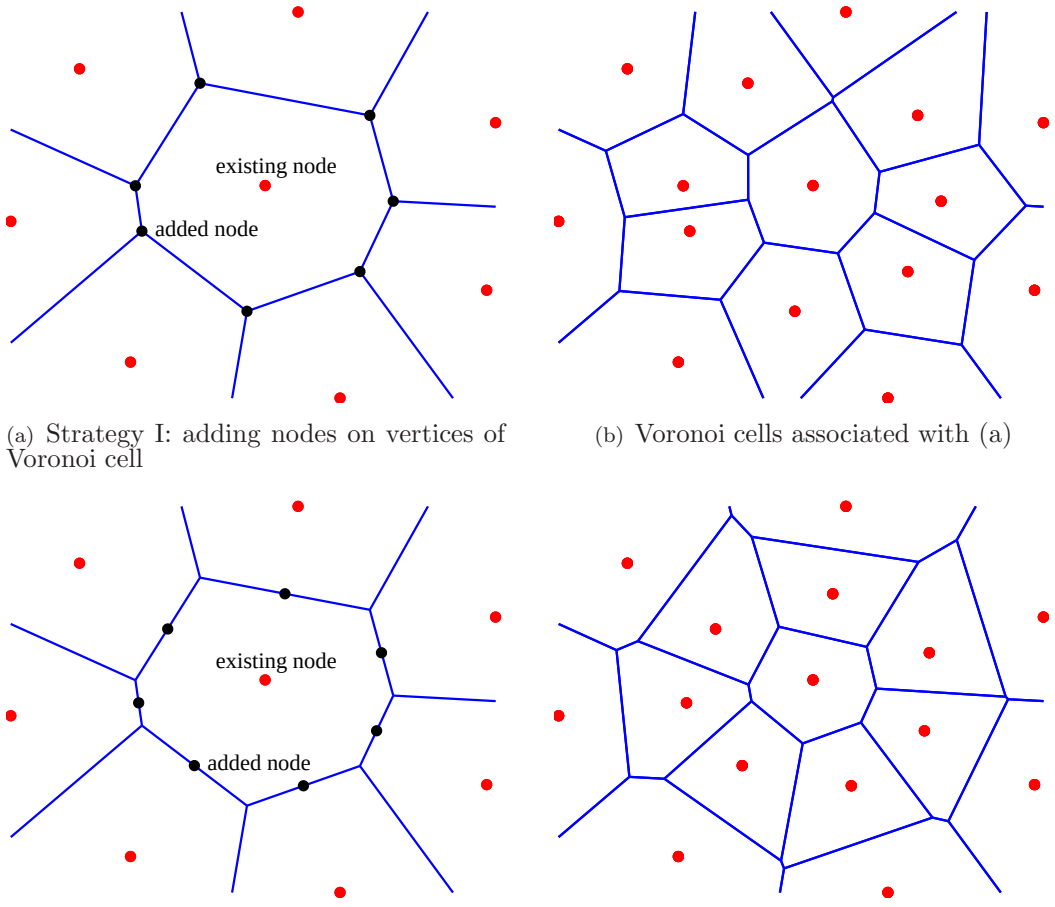

(a) Strategy I: adding nodes on vertices of Voronoi cell

(b) Voronoi cells associated with (a)

(c) Strategy II: adding midpoint nodes on edges of Voronoi cell

(d) Voronoi cells associated with (c)

FIGURE 5.4: Nodal refinement strategies based on Voronoi cells

The efficiency of these refinement strategies will be discussed in the next section. The adaptive procedure can be summarised as follows:

1. Construct Voronoi diagram from an initial set of nodes.
2. Construct shape functions, derivatives and smoothed values.
3. Build matrices and vectors for the optimisation problem.
4. Solve the optimisation problem to obtain a collapse load multiplier and displacement field data.
5. Calculate the local error for each Voronoi cell or node.
6. Calculate the global error (= sum of local errors).
7. If all local errors are smaller than the user-defined error tolerance δ then terminate as no further refinement is necessary.
8. Otherwise refine cells with a large local error and add new nodes.
9. Repeat from step 1.

5.5 Numerical examples

The efficacy of the proposed adaptive meshfree procedure for limit analysis problems will now be demonstrated by applying it to plate problems of various geometries and loaded by either a uniform pressure or concentrated forces. For all the examples considered the following parameters were assumed: plate thickness $t = 0.1$ m; yield stress $\sigma_0 = 250$ MPa and the parameter β in Equation (5.26) was taken to be 3.0 (Rabczuk & Belytschko, 2005). Quarter symmetry was assumed where appropriate. The commercial interior point solver (Mosek, 2008), which is capable of rapidly solving large-scale mathematical optimisation problems, was used to solve all optimisation problems. Note that the high order shape functions used in the EFG method make *a priori* proof of the strict upper bound status of the solutions difficult. However, as the discretisation is progressively refined using the adaptive procedure, increasingly close approximations of the true plastic collapse load multiplier can be expected to be obtained.

5.5.1 Rectangular plate

The first example considered comprises a rectangular plate, simply supported at two opposite edges and subjected to uniform out-of-plane pressure loading, as shown on Figure 5.5. The plate dimensions were set as $a = b/2 = 5$ m. In all cases

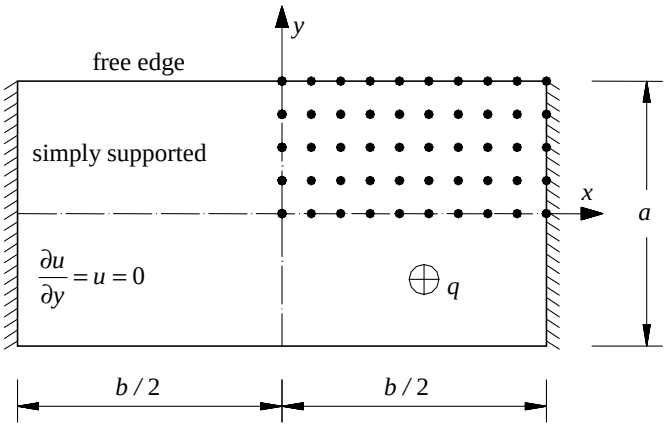

FIGURE 5.5: Rectangular plate simply supported along 2 edges and subject to uniform pressure: geometry and initial nodal discretisation (50 nodes over quarter of plate)

a total of 10×5 nodes were initially used to discretise a quarter of the plate, as shown in Figure 5.5.

Firstly the threshold error tolerance δ was taken as 0.001 and the efficacy of the two refinement strategies illustrated in Figure 5.4 was investigated. Figure 5.6 shows the improvement in the computed collapse load as the problem is refined. It can be seen that adaptive strategy (I), which adds vertex nodes in Voronoi cells, results in a much better computed collapse load multiplier than strategy (II). This can be explained by the fact that the Voronoi cells are more regular with strategy (I) than with strategy (II); strategy (I) was therefore used in all subsequent computations described herein. The best solution found was 4.52 with 480 nodes, compared with 4.55 obtained using 648 nodes when using a uniform layout of nodes.

The progress of the adaptive refinement procedure using strategy (I) is also shown graphically in Figure 5.7. What is clear is that the majority of nodes must be positioned in zones of plastic yielding in order to ensure that an accurate collapse load multiplier is obtained.

Secondly the influence of the local error tolerance, in the range $0.0002 \leq \delta \leq 0.001$, was investigated. Numerical collapse load multipliers and global error estimator values for various error tolerance values δ are shown in Figure 5.8 (where strategy

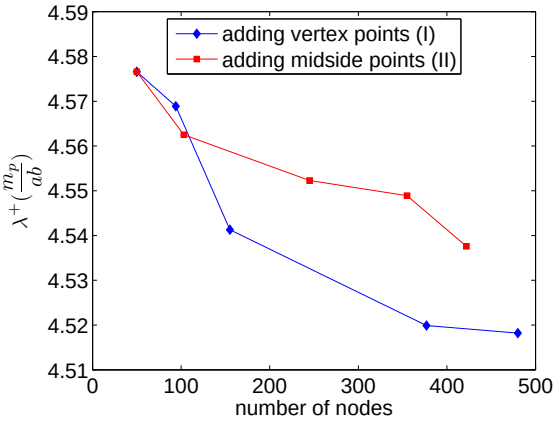

FIGURE 5.6: Influence of adaptive strategy (I) and (II) on the computed load multiplier

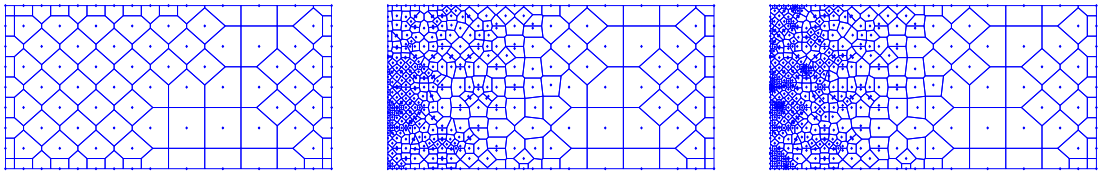

(a) Step 2, $\|e\| = 0.0109$ (b) Step 4, $\|e\| = 0.0097$ (c) Step 5, $\|e\| = 0.0044$

FIGURE 5.7: Adaptive refinement using strategy (I) and $\delta = 0.001$ (rectangular plate)

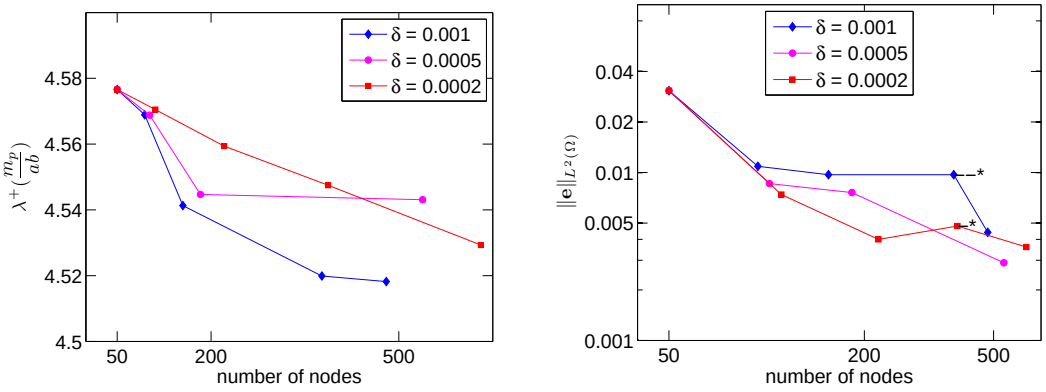

(a) Collapse load multiplier vs number of nodes (b) Global error estimator vs number of nodes

FIGURE 5.8: Influence of the error tolerance value δ (rectangular plate)

(*) - MOSEK solution status reported as either *Near-optimal* or *Unknown*

(I) was used in all cases). It can be seen that the use of smaller tolerance values δ results in a higher computational cost, but does not always provide an improved computed collapse load multiplier.

5.5.2 L-shaped plate

The next example comprises an L-shape plate subjected to a uniform load and with geometry and kinematic boundary conditions as shown in Figure 5.9. In all computations L was taken as 10 m and a total of 133 nodes were initially used to discretise the plate.

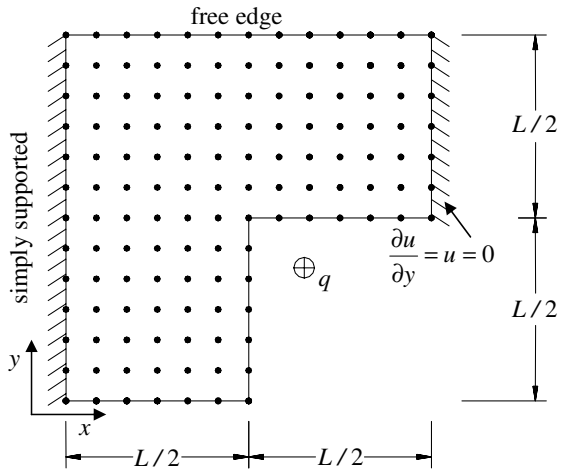

FIGURE 5.9: L-shaped plate geometry and initial nodal discretisation

This problem was found to exhibit a singularity at the re-entrant corner, with a predicted yield line passing parallel to the supports from the re-entrant corner to the uppermost free edge. Computed collapse load multipliers and global error estimators for various different error tolerance values δ are plotted in Figure 5.10. It is evident from the two examples that a good estimate of the load multiplier could be obtained even when δ was taken as 0.001, despite the fact that the maximum number of nodes was in this case much smaller than when δ was taken as a lower value. This may be explained by the fact that in plastic regions error tolerance values greater than 0.001 are encountered, and nodes should be added in these zones. When δ is set to be smaller, a more *uniform* refinement is favoured,

which affects efficiency. It is also shown in Haussler-Combe & Korn (1998) that in some cases when δ is set close or equal to zero the global error estimator is surprisingly greater than when $\delta = 0.001$. The progress of the refinement is shown graphically in Figure 5.11. It is evident that errors are large in the zones near the re-entrant corner and emerging yield line, and consequently these areas are refined in each step of the adaptive scheme. The best upper-bound load multiplier was found to be 6.15 when a total of 453 nodes were present, which is considerably lower than the value of 6.298 obtained previously (Le et al., 2009), when using up to 3816 nodes distributed uniformly across the plate.

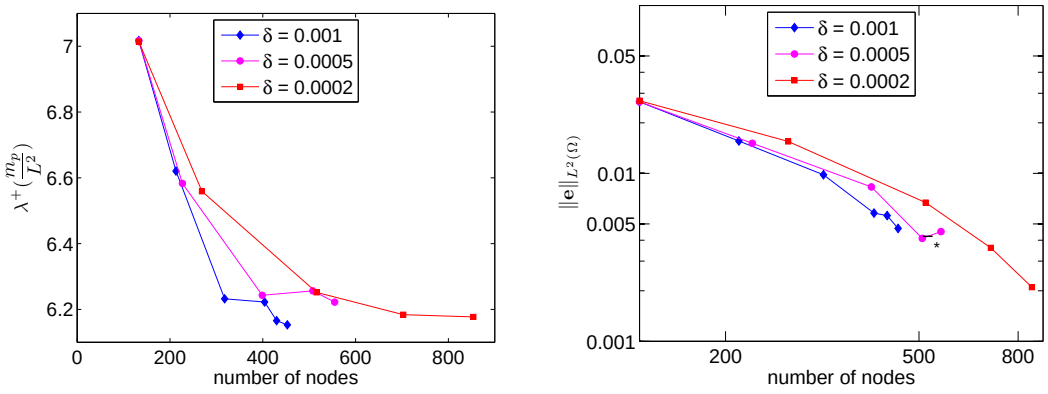

(a) Collapse load multiplier vs number of nodes

(b) Global error estimator vs number of nodes

FIGURE 5.10: Influence of the error tolerance value δ (L-shape plate)

(*) - MOSEK solution status reported as *Near-optimal*

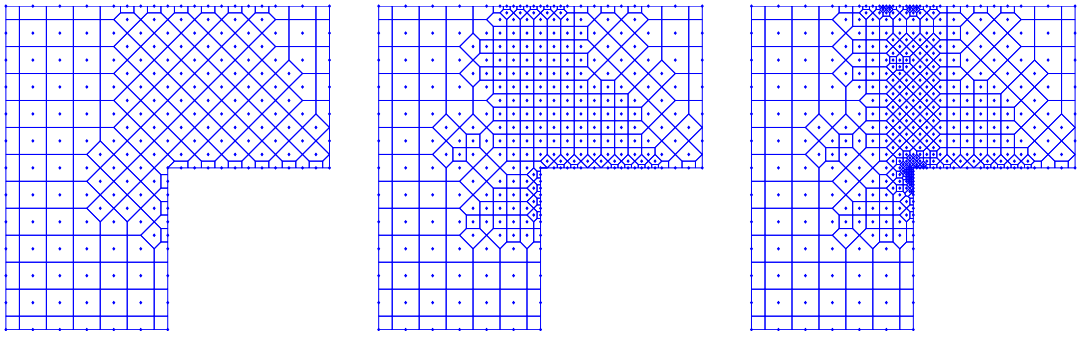

(a) Step 2 $\|e\| = 0.0156$

(b) Step 3 $\|e\| = 0.0058$

(c) Step 5 $\|e\| = 0.0047$

FIGURE 5.11: Adaptive refinement with $\delta = 0.001$ (L-shape plate)

5.5.3 Clamped circular plate

The third example involves a clamped circular plate with central concentrated load P. This problem exhibits a logarithmic singularity in the displacement field near the point load and has a known exact solution (Hopkins & Wang, 1954), $\lambda^+ = \frac{4\pi m_p}{\sqrt{3}P} = 7.255\ \frac{m_p}{P}$. The effectiveness of the proposed adaptive EFG method is demonstrated by comparing errors in the computed collapse load multiplier with and without nodal refinement; see Figure 5.12. In the adaptive analysis, δ was taken as 0.001 and strategy (I) was once again used. The best computed kinematic collapse load multiplier obtained was 7.27, which is just 0.2% higher than the exact solution. In the adaptive scheme the majority of the nodes were found to be concentrated in the zone around the singular point, as shown on Figure 5.13.

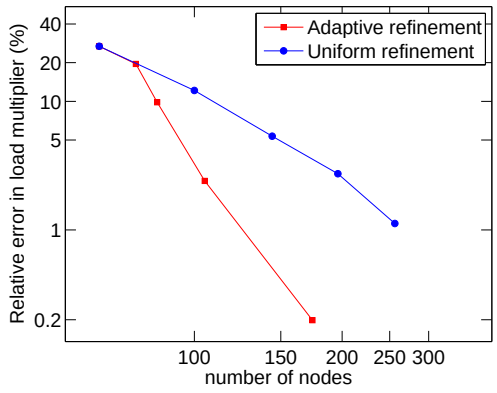

FIGURE 5.12: Performance of uniform vs adaptive refinement schemes (circular plate)

5.5.4 Rectangular plate with eccentric square cutout

The last example involves a rectangular plate with an eccentric square cutout, of the same geometry as examined previously using an elasto-plastic model (Askes et al., 1999a). All external and internal edges are simply supported and the dimensions are shown in Figure 5.14. Figure 5.15b shows a plot of the plastic dissipation for this problem. The implied yield line pattern shows good qualitative agreement

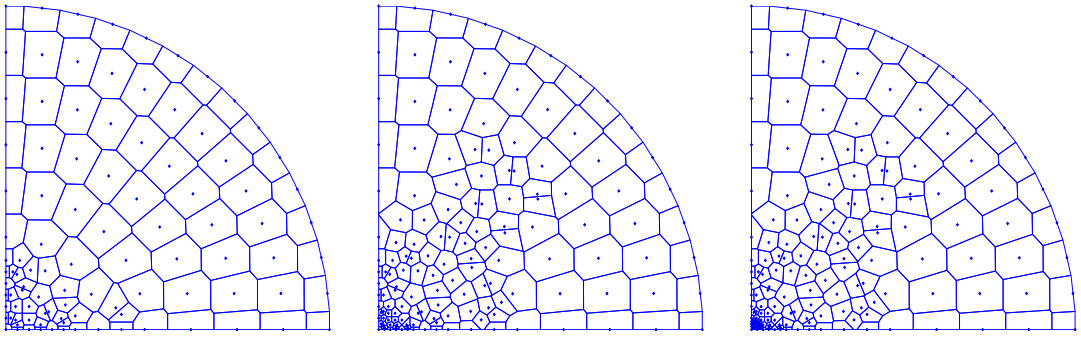

(a) Step 2 (b) Step 4 (c) Step 5

FIGURE 5.13: Adaptive refinement (clamped circular plate)

with the result in Askes et al. (1999a). Due to the dominance of the yield lines in the left part of the plate, most nodes were added in this area, as shown on Figure 5.15a. The best estimate of the collapse load multiplier was found to be 51.45 $\frac{m_p}{ab}$.

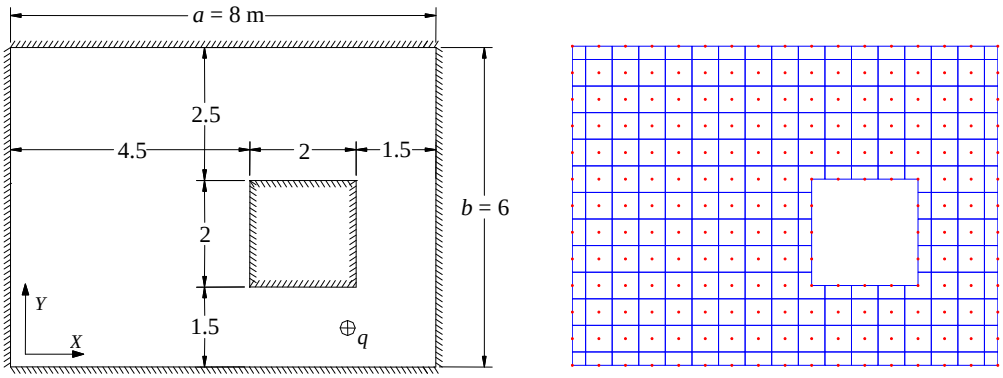

(a) Geometry and boundary conditions (b) Initial nodal discretisation

FIGURE 5.14: Details of rectangular plate with eccentric square cutout

5.6 Conclusions

An efficient adaptive meshless limit analysis procedure for plates has been described. h-refinement is used and the smoothing technique used for nodal integration has been extended to allow error estimation at representative nodal cells,

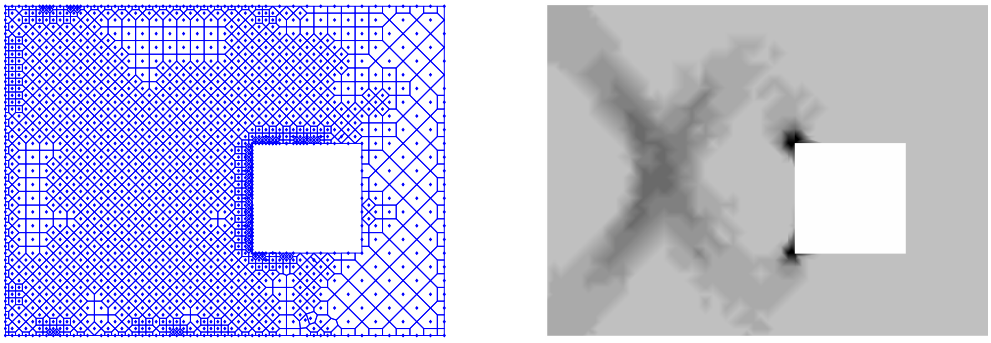

(a) Step 4: 1459 nodes (b) Plastic dissipation distribution

FIGURE 5.15: Adaptive refinement (rectangular plate with eccentric square cutout)

resulting in an efficient adaptive EFG method. Due to the naturally conforming properties of the meshfree approximation, the proposed adaptive scheme is conveniently performed without the need for complex manipulation of the data structures involved. Since properties of Voronoi cells are used as a reference for nodal addition strategies, irregular nodal layouts can be treated efficiently by the method. The adaptive scheme is able to capture yield line patterns arising from localised plastic deformations for problems of arbitrary geometry. It is found that the majority of nodes are concentrated in these plastic zones and that accurate estimates of the collapse load multiplier can be obtained using a relatively small number of nodes.

Chapter 6

Limit analysis of plates and slabs using a meshless equilibrium formulation[1]

A meshless Element-Free Galerkin (EFG) equilibrium formulation is proposed to compute the limit loads which can be sustained by plates and slabs. In the formulation pure moment fields are approximated using a moving least squares technique, which means that the resulting fields are smooth over the entire problem domain. There is therefore no need to enforce continuity conditions at interfaces within the problem domain, which would be a key part of a comparable finite element formulation. The collocation method is used to enforce the strong form of the equilibrium equations and a stabilised conforming nodal integration scheme is introduced to eliminate numerical instability problems. The combination of the collocation method and the smoothing technique means that equilibrium only needs to be enforced at the nodes, and stable and accurate solutions can be obtained with minimal computational effort. The von Mises and Nielsen yield criteria

[1]based on C.V. Le, M. Gilbert and H. Askes, Limit analysis of plates and slabs using a meshless equilibrium formulation, International Journal for Numerical Methods in Engineering, accepted subject to minor revisions, 2009.

which are used in the analysis of plates and slabs respectively are enforced by introducing second-order cone constraints, ensuring that the resulting optimisation problem can be solved using efficient interior-point solvers. Finally, the efficacy of the procedure is demonstrated by applying it to various benchmark plate and slab problems.

6.1 Introduction

The fundamental theorems of limit analysis can be used to provide upper and lower bound estimates of the load required to cause collapse of a body or structure. If a suitable approximation for the displacement field is used, and the kinematic theorem is applied, an upper bound on the exact limit load can be obtained. Alternatively, if a suitable approximation for the stress field is used, and the static theorem is applied, a lower bound can be obtained. Applying these theorems and using a finite element discretisation, numerical procedures have been developed to perform the limit analysis of perfectly plastic plates and slabs, e.g. Hodge & Belytschko (1968); Chan (1972); Anderheggen & Knopfel (1972); Faccioli & Vitiello (1973); Munro & Fonseca (1978); Lubliner (1990) and Capsoni & Corradi (1999). These procedures can provide good bounds on the exact collapse load (or 'load multiplier'), with the results in Hodge & Belytschko (1968) remarkably providing the best lower-bounds available for plate problems for many years (Save et al., 1997). However, solutions obtained from nite element based computational limit analysis procedures can be very sensitive to mesh geometry, particularly for problems which contain strong singularities in the stress and/or displacement elds. It is therefore worthwhile to explore a range of alternative methods. Recently Le et al. (2009) proposed a numerical kinematic formulation using the Element-Free Galerkin (EFG) method and second-order cone programming (SOCP) to furnish good (approximate) upper-bound solutions for Kirchhoff plate problems governed by the von Mises failure criterion. It has also been demonstrated (Chen et al., 2008; Le et al., 2009) that the EFG method is in general well suited for limit analysis problems, allowing accurate solutions to be obtained with relatively few nodes.

Following this line of research, the main objective of this paper is to develop an equilibrium formulation which combines the EFG method with SOCP to obtain accurate solutions for both plate and slab problems.

In a static equilibrium formulation, the stress/moment fields are generally chosen so that the equilibrium equations, boundary conditions and continuity requirements are met for all feasible values of the problem variables. In Chen et al. (2008), a self-equilibrium stress basis vector at each Gaussian point is calculated by solving the equivalent weak form of the equilibrium equations. The self-equilibrium stress field is then obtained by a linear combination of several self-equilibrium stress basis vectors which are generated by considering the differences between intermediate stresses during the elasto-plastic equilibrium iteration. However, the stress field obtained is not guaranteed to be statically admissible as it is derived from an approximated virtual displacement field by solving the weak form of the equilibrium equation. In contrast, in this paper the stress/moment fields will be constructed by using a moving least squares approximation. It is well-known that the field obtained when using this technique is smooth over the entire problem domain. There is therefore no need to enforce continuity conditions at interfaces within the problem domain (which would be a key part of a comparable finite element formulation).

In the framework of meshfree methods, it is advantageous if the problem under consideration can be solved be evaluating quantities at the nodes only. For problems involving integration, a stabilised conforming nodal integration (SCNI) scheme proposed in Chen et al. (2001a) is an effective option. The main idea of the scheme is that nodal values are determined by spatially averaging field values using the divergence theorem. The scheme has been applied successfully to various analysis problems (Sze et al., 2004; Wang & Chen, 2004; Yoo et al., 2004; Le et al., 2009). It is shown that, when the SCNI scheme is applied, the solutions obtained are accurate and stable, and the computational cost is much lower than when using Gauss integration. Due to these advantages the scheme will be used here to stabilise the moment derivatives. Using smoothed second derivatives of the moment field at nodes, the equilibrium equations only need to be fulfilled at the

nodes. Furthermore, properties of Voronoi cells (which are representative nodal domains used in the smoothing scheme) can be used as a reference when enforcing the yield criteria.

The aim of this paper is to present an EFG based equilibrium limit analysis formulation for application to rigid-perfectly plastic plates and slabs, governed by the von Mises and Nielsen yield criteria respectively. The Kirchhoff moment field is approximated by using the moving least squares technique and nodal collocation is used to impose boundary conditions. The yield criteria are cast in terms of conic constraints, allowing the limit analysis problem to be posed as a standard second-order cone programming problem which can be solved using highly efficient solvers (Mosek, 2008). Finally, in order to test the performance of the method, several benchmark plate and slab examples from the literature are investigated.

6.2 Limit analysis of plates - equilibrium formulation

A lower-bound solution to the problem involving a rigid-perfectly plastic plate or slab can be obtained by using the static theorem of plasticity, which states that a moment field is statically and plastically admissible if (i) equilibrium and boundary conditions are fully satisfied, and (ii) the yield condition is not violated anywhere. The exact plastic collapse load multiplier, λ_p, is the largest value among a set of lower bound multipliers, λ^-, corresponding to any statically and plastically admissible moment distribution (Hodge & Belytschko, 1968; Chan, 1972). The moment field is denoted as $\mathbf{m} = [m_{xx} \;\; m_{yy} \;\; m_{xy}]^T$ and is constrained to belong to the domain

$$\mathcal{B} = \{\mathbf{m} \,|\, \psi(\mathbf{m}) \leq 0\}\,, \tag{6.1}$$

in which the so-called yield function $\psi(\mathbf{m})$ is convex.

In this study, the yield criterion proposed by Nielsen (1964); Wolfensberger (1964) and Nielsen (1998) is used for the analysis of reinforced concrete slabs. The criterion is expressed as

$$\begin{aligned}(m_{px}^{+} - m_{xx})(m_{py}^{+} - m_{yy}) &\geq m_{xy}^{2} \\ (m_{px}^{-} + m_{xx})(m_{py}^{-} + m_{yy}) &\geq m_{xy}^{2} \\ -m_{px}^{-} \leq m_{xx} &\leq m_{px}^{+} \\ -m_{py}^{-} \leq m_{yy} &\leq m_{py}^{+}\end{aligned} \tag{6.2}$$

where m_{px}^{-} and m_{py}^{-} are the negative yield moments in the x and y directions, respectively, and similarly m_{px}^{+} and m_{py}^{+} are the positive yield moments in the two directions. The constraints in (6.2) represent a bi-conical yield surface, as shown in Figure 6.1.

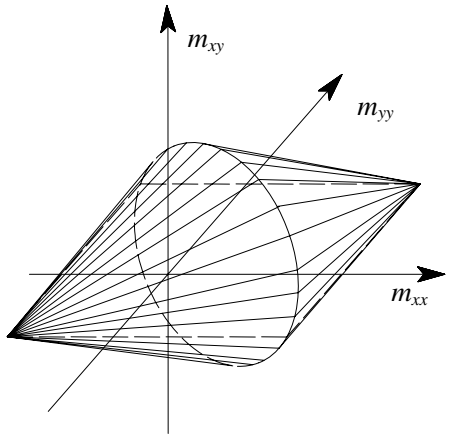

FIGURE 6.1: Yield criterion for reinforced concrete slabs (Nielsen (1964); Wolfensberger (1964) and Nielsen (1998))

For steel plates, the von Mises failure criterion is often used, and can be expressed as

$$\psi(\mathbf{m}) = \sqrt{\mathbf{m}^{T}\ \mathbf{P}\ \mathbf{m}} - m_{p} \tag{6.3}$$

where $m_p = \sigma_0 t^2/4$ is the plastic moment of resistance per unit width of a plate of thickness t and yield stress σ_0, and where

$$\mathbf{P} = \frac{1}{2}\begin{bmatrix} 2 & -1 & 0 \\ -1 & 2 & 0 \\ 0 & 0 & 6 \end{bmatrix} \tag{6.4}$$

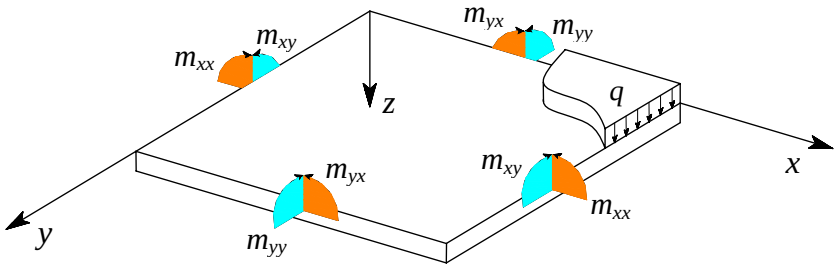

FIGURE 6.2: Plate sign conventions

Following the sign convention given in Figure 6.2, the lower-bound limit analysis of plate/slab problems can be expressed in the form of a mathematical programming problem, as

$$\lambda^- = \max\ \lambda \tag{6.5a}$$

$$\text{s.t} \quad \nabla^2 \mathbf{m} + \lambda q = 0 \tag{6.5b}$$

$$\mathbf{m} \in \mathcal{B} \tag{6.5c}$$

where λ^- is the numerically computed load multiplier, q is the pressure load, $\nabla^2 = \left\{ \frac{\partial^2}{\partial x^2} \quad \frac{\partial^2}{\partial y^2} \quad 2\frac{\partial^2}{\partial x \partial y} \right\}$, and the moment field $\mathbf{m}$ must also satisfy appropriate boundary conditions.

6.3 The EFG equilibrium model

6.3.1 Moving least squares approximation

Whereas in the kinematic formulation the displacement field is approximated, here the moment field needs to be approximated. By using the moving least squares technique (Belytschko et al., 1994), which is the most frequently used approximation in meshless methods, approximations of these moment fields can be expressed as

$$\mathbf{m}^h(\mathbf{x}) = \begin{bmatrix} m^h_{xx} \\ m^h_{yy} \\ m^h_{xy} \end{bmatrix} = \sum_{I=1}^{n} \Phi_I(\mathbf{x}) \begin{bmatrix} m_{xxI} \\ m_{yyI} \\ m_{xyI} \end{bmatrix} \tag{6.6}$$

in which

$$\Phi_I(\mathbf{x}) = \mathbf{p}^T(\mathbf{x})\mathbf{A}^{-1}(\mathbf{x})\mathbf{B}_I(\mathbf{x}) \tag{6.7}$$

$$\mathbf{A}(\mathbf{x}) = \sum_{I=1}^{n} w_I(\mathbf{x})\mathbf{p}(\mathbf{x}_I)\mathbf{p}^T(\mathbf{x}_I) \tag{6.8}$$

$$\mathbf{B}_I(\mathbf{x}) = w_I(\mathbf{x})\mathbf{p}(\mathbf{x}_I) \tag{6.9}$$

where n is the number of nodes; $\mathbf{p}(\mathbf{x})$ is a set of basis functions; $w_I(\mathbf{x})$ is a weight function associated with node I. In this work, an isotropic quartic spline function is used, which is given by

$$w_I(\mathbf{x}) = \begin{cases} 1 - 6s_I^2 + 8s_I^3 - 3s_I^4 & \text{if } s_I \leq 1 \\ 0 & \text{if } s_I > 1 \end{cases} \tag{6.10}$$

with $s_I = \frac{\|\mathbf{x}-\mathbf{x}_I\|}{R_I}$, where R_I is the support radius of node I and determined by

$$R_I = \beta \cdot h_I \tag{6.11}$$

where β is the dimensionless size of influence domain and h_I is the nodal spacing when nodes were distributed regularly, or the maximum distance to neighbouring nodes when nodes were distributed irregularly (Figure 6.3). The maximum

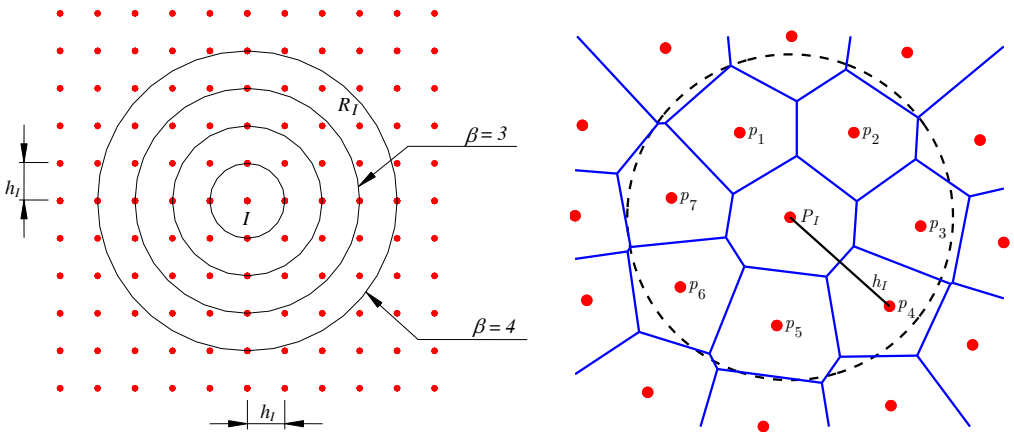

(a) Regular nodal layout (b) Irregular nodal layout

FIGURE 6.3: Sizes of influence domain

distance is determined by

$$h_I = \max\{d_J : d_J = \overline{P_I P_J},\ \forall P_J \in N_I\} \tag{6.12}$$

where

$$\begin{aligned} N_I &= \{P_J : V(P_J) \cap V(P_I) \neq \oslash\} \\ &= \{p_1, p_2, p_3, p_4, p_5, p_6, p_7\} \end{aligned} \tag{6.13}$$

in which $V(P_I)$ is the Voronoi cell of particle P_I.

6.3.2 Stabilised equilibrium equation

The equilibrium equations are frequently treated in one of two ways in numerical procedures: (i) equilibrium is enforced at nodes in the problem domain and also at boundaries (using the 'collocation' method), or (ii) the equilibrium equations are transformed into the equivalent weak-form (involving integrals), using the so-called 'weighted residual method' (Zienkiewicz & Taylor, 2000; Liu & Gu, 2005). The former method is simple and fast, but it has been reported to suffer from numerical stability problems (Liu & Gu, 2005; Chen et al., 2006). In contrast, formulations

which use the weak-form can usually produce a stable set of discretised system equations, in turn leading to accurate solutions. Finite element based formulations have been developed by several authors (Fraeijs de Veubeke & Zienkiewicz, 1967; Fraeijs de Veubeke, 2001). Considering meshless methods, an equilibrium model for elastostatic problems was first introduced in Duflot & Nguyen-Dang (2002), where stress fields were expressed by means of an Airy stress function, approximated using the moving least squares method. Alternatively the self-equilibrium stress field can be calculated by using an assumed displacement field and solving the weak form of the equilibrium equations (Chen et al., 2008). However, here an alternative EFG equilibrium formulation in which the collocation method is used in combination with a smoothing technique is proposed.

A strain smoothing method was firstly presented in Chen et al. (2000) for the regularisation of material instabilities. The strain smoothing method was then modified to allow stabilisation in nodal integration schemes, leading to the so-called stabilised conforming nodal integration (SCNI) scheme Chen et al. (2001a). The SCNI scheme was then successfully applied to both elastic analysis (Sze et al., 2004; Wang & Chen, 2004) and plastic analysis (Le et al., 2009) problems. It has been shown that the SCNI scheme results in an efficient and truly mesh-free method, and also to numerically stable solutions. This smoothing technique will now be adapted in order to stabilise problems involving bending moment derivatives as follows

$$\tilde{m}^h_{\alpha\beta,\alpha\beta}(\mathbf{x}_J) = \int_{\Omega_J} m^h_{\alpha\beta,\alpha\beta}(\mathbf{x})\varphi(\mathbf{x}, \mathbf{x}-\mathbf{x}_J)\,\mathrm{d}\Omega \tag{6.14}$$

where $\tilde{m}^h_{\alpha\beta,\alpha\beta}$ is the smoothed value of the second-derivative of moment $m^h_{\alpha\beta,\alpha\beta}$ at node J, and φ is a distribution (or 'smoothing') function that has to satisfy the following properties (Chen et al., 2000; Yoo et al., 2004)

$$\varphi \geq 0 \quad \text{and} \quad \int_{\Omega_J} \varphi\,\mathrm{d}\Omega = 1 \tag{6.15}$$

For simplicity, the function φ is assumed to be a piecewise constant function and is given by

$$\varphi(\mathbf{x}, \mathbf{x}-\mathbf{x}_J) = \begin{cases} 1/a_J, & \mathbf{x} \in \Omega_J \\ 0, & \mathbf{x} \notin \Omega_J \end{cases} \tag{6.16}$$

where a_J is the area of the representative domain of node J, as shown in Figure 6.4.

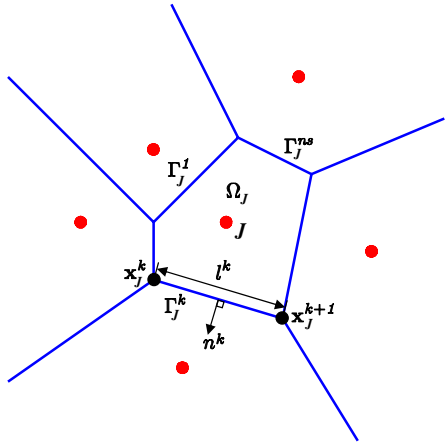

FIGURE 6.4: Geometry of a representative nodal domain

Substituting Equation (6.16) into Equation (6.14), and applying the divergence theorem, the following expressions can be derived

$$\begin{aligned} \tilde{m}^h_{\alpha\beta,\alpha\beta}(\mathbf{x}_J) &= \frac{1}{a_J}\int_{\Omega_J} m^h_{\alpha\beta,\alpha\beta}(\mathbf{x})\,\mathrm{d}\Omega \\ &= \frac{1}{2a_J}\int_{\Gamma_J} \left(m^h_{\alpha\beta,\alpha}(\mathbf{x})n_\beta(\mathbf{x}) + m^h_{\alpha\beta,\beta}(\mathbf{x})n_\alpha(\mathbf{x})\right)\,\mathrm{d}\Gamma \end{aligned} \tag{6.17}$$

where Γ_J is the boundary of the representative domain Ω_J.

Now introducing a moving least squares approximation of the moment fields, the smooth version of the moment second-derivative can be expressed as

$$\tilde{m}^h_{\alpha\beta,\alpha\beta}(\mathbf{x}_J) = \sum_{I=1}^{n} \tilde{\Phi}_{I,\alpha\beta}(\mathbf{x}_J) m_{\alpha\beta I} \tag{6.18}$$

with

$$\begin{aligned}\tilde{\Phi}_{I,\alpha\beta}(\mathbf{x}_j) &= \frac{1}{2a_j}\int_{\Gamma_j}\left(\Phi_{I,\alpha}(\mathbf{x}_j)n_\beta(\mathbf{x}) + \Phi_{I,\beta}(\mathbf{x}_j)n_\alpha(\mathbf{x})\right)\mathrm{d}\Gamma \\ &= \frac{1}{4a_j}\sum_{k=1}^{ns}\left(n_\beta^k\, l^k + n_\beta^{k+1}\, l^{k+1}\right)\Phi_{I,\alpha}(\mathbf{x}_j^{k+1}) \\ &+ \frac{1}{4a_j}\sum_{k=1}^{ns}\left(n_\alpha^k\, l^k + n_\alpha^{k+1}\, l^{k+1}\right)\Phi_{I,\beta}(\mathbf{x}_j^{k+1}) \qquad (6.19)\end{aligned}$$

where $\tilde{\Phi}$ is the smoothed version of Φ; ns is the number of segments of a Voronoi nodal domain Ω_J as shown in the Figure 6.4; $\mathbf{x}_J^k$ and $\mathbf{x}_J^{k+1}$ are the coordinates of the two end points of boundary segment Γ_J^k which has length l^k and outward surface normal n^k.

With the use of the smoothed value $\tilde{m}^h_{\alpha\beta,\alpha\beta}$ the equilibrium equation can be enforced at n nodes, and Equation (6.5b) can be rewritten as

$$\mathbf{A}_1\mathbf{m}_1 + \mathbf{A}_2\mathbf{m}_2 + \mathbf{A}_3\mathbf{m}_3 + \lambda q\mathbf{I} = \mathbf{0} \qquad (6.20)$$

where

$$\mathbf{I}^T = \begin{bmatrix} 1 & 1 & \dots & 1 \end{bmatrix}_{1\times n} \qquad (6.21)$$

$$\mathbf{A}_1 = \begin{bmatrix} \dots & \dots & \dots & \dots \\ \tilde{\Phi}_{1,xx}(\mathbf{x}_J) & \tilde{\Phi}_{2,xx}(\mathbf{x}_J) & \dots & \tilde{\Phi}_{n,xx}(\mathbf{x}_J) \\ \dots & \dots & \dots & \dots \end{bmatrix}_{n\times n} \qquad (6.22)$$

$$\mathbf{A}_2 = \begin{bmatrix} \dots & \dots & \dots & \dots \\ \tilde{\Phi}_{1,yy}(\mathbf{x}_J) & \tilde{\Phi}_{2,yy}(\mathbf{x}_J) & \dots & \tilde{\Phi}_{n,yy}(\mathbf{x}_J) \\ \dots & \dots & \dots & \dots \end{bmatrix}_{n\times n} \qquad (6.23)$$

$$\mathbf{A}_3 = \begin{bmatrix} \dots & \dots & \dots & \dots \\ 2\tilde{\Phi}_{1,xy}(\mathbf{x}_J) & 2\tilde{\Phi}_{2,xy}(\mathbf{x}_J) & \dots & 2\tilde{\Phi}_{n,xy}(\mathbf{x}_J) \\ \dots & \dots & \dots & \dots \end{bmatrix}_{n\times n} \qquad (6.24)$$

$$\mathbf{m}_1 = \begin{bmatrix} m_{xx1} & \dots & m_{xxn} \end{bmatrix}^T \tag{6.25}$$

$$\mathbf{m}_2 = \begin{bmatrix} m_{yy1} & \dots & m_{yyn} \end{bmatrix}^T \tag{6.26}$$

$$\mathbf{m}_3 = \begin{bmatrix} m_{xy1} & \dots & m_{xyn} \end{bmatrix}^T \tag{6.27}$$

It is important to note that when the smoothing technique is used, the equilibrium equation is fulfilled at nodes only (unlike in Chen et al. (2008) where the equilibrium is transformed into the equivalent weak form and enforced at Gauss points).

6.3.3 Enforcement of boundary conditions

It should be borne in mind that the quantities m_{xxI}, m_{yyI} and m_{xyI} in Equation (6.6) are fictitious nodal values, rather than actual moments acting at the nodes. This unfortunately complicates matters when seeking to enforce boundary conditions. One way of addressing this is to use the collocation method proposed in Zhu & Atluri (1998). Let M_n, M_{nt} and Q_n denote the normal bending moment, twisting moment and transverse shear force at node $\mathbf{x}_b$ on a free unloaded edge, where its normal vector $\mathbf{n}$ forms an angle α_a with the x-axis. Conditions for this boundary can be expressed as

$$\begin{aligned} M_n &\equiv m^h_{xx} c^2_{\alpha_a} + m^h_{yy} s^2_{\alpha_a} + 2m^h_{xy} c_{\alpha_a} s_{\alpha_a} = 0 \\ M_{nt} &\equiv (m^h_{yy} - m^h_{xx}) c_{\alpha_a} s_{\alpha_a} + 2m^h_{xy}(c^2_{\alpha_a} - s^2_{\alpha_a}) = 0 \\ Q_n &\equiv Q_x c_{\alpha_a} + Q_y s_{\alpha_a} = 0 \end{aligned} \tag{6.28}$$

where $c_{\alpha_a} = \cos\alpha_a$ and $s_{\alpha_a} = \sin\alpha_a$. It is important to note that smoothed moment derivatives are used in the equilibrium equation (6.20). Consequently, the shear forces Q_x and Q_y must also be calculated from these smoothed moment

derivatives as follows

$$Q_x = \frac{\partial \tilde{m}_{xx}}{\partial x} + \frac{\partial \tilde{m}_{xy}}{\partial y} \tag{6.29}$$

$$Q_y = \frac{\partial \tilde{m}_{xy}}{\partial x} + \frac{\partial \tilde{m}_{yy}}{\partial y} \tag{6.30}$$

Introducing a moving least squares approximation of the moment field, Equation (6.28) can be rewritten as

$$\mathbf{B}_1\mathbf{m}_1 + \mathbf{B}_2\mathbf{m}_2 + \mathbf{B}_3\mathbf{m}_3 = \mathbf{0} \tag{6.31}$$

where

$$\mathbf{B}_1 = \begin{bmatrix} \dots & \dots & \dots & \dots \\ c^2_{\alpha_a}\Phi_1(\mathbf{x}_i) & c^2_{\alpha_a}\Phi_2(\mathbf{x}_i) & \dots & c^2_{\alpha_a}\Phi_n(\mathbf{x}_i) \\ \dots & \dots & \dots & \dots \\ -c_{\alpha_a}s_{\alpha_a}\Phi_1(\mathbf{x}_i) & -c_{\alpha_a}s_{\alpha_a}\Phi_2(\mathbf{x}_i) & \dots & -c_{\alpha_a}s_{\alpha_a}\Phi_n(\mathbf{x}_i) \\ \dots & \dots & \dots & \dots \\ c_{\alpha_a}\tilde{\Phi}_{1,x}(\mathbf{x}_i) & c_{\alpha_a}\tilde{\Phi}_{2,x}(\mathbf{x}_i) & \dots & c_{\alpha_a}\tilde{\Phi}_{n,x}(\mathbf{x}_i) \\ \dots & \dots & \dots & \dots \end{bmatrix} \tag{6.32}$$

$$\mathbf{B}_2 = \begin{bmatrix} \dots & \dots & \dots & \dots \\ s^2_{\alpha_a}\Phi_1(\mathbf{x}_i) & s^2_{\alpha_a}\Phi_2(\mathbf{x}_i) & \dots & s^2_{\alpha_a}\Phi_n(\mathbf{x}_i) \\ \dots & \dots & \dots & \dots \\ c_{\alpha_a}s_{\alpha_a}\Phi_1(\mathbf{x}_i) & c_{\alpha_a}s_{\alpha_a}\Phi_2(\mathbf{x}_i) & \dots & c_{\alpha_a}s_{\alpha_a}\Phi_n(\mathbf{x}_i) \\ \dots & \dots & \dots & \dots \\ s_{\alpha_a}\tilde{\Phi}_{1,y}(\mathbf{x}_i) & s_{\alpha_a}\tilde{\Phi}_{2,y}(\mathbf{x}_i) & \dots & s_{\alpha_a}\tilde{\Phi}_{n,y}(\mathbf{x}_i) \\ \dots & \dots & \dots & \dots \end{bmatrix} \tag{6.33}$$

$$\mathbf{B}_3 = \begin{bmatrix} \cdots & \cdots & \cdots & \cdots \\ 2c_{\alpha_a}s_{\alpha_a}\Phi_1(\mathbf{x}_i) & 2c_{\alpha_a}s_{\alpha_a}\Phi_2(\mathbf{x}_i) & \cdots & 2c_{\alpha_a}s_{\alpha_a}\Phi_n(\mathbf{x}_i) \\ \cdots & \cdots & \cdots & \cdots \\ 2(c^2_{\alpha_a} - s^2_{\alpha_a})\Phi_1(\mathbf{x}_i) & 2(c^2_{\alpha_a} - s^2_{\alpha_a})\Phi_2(\mathbf{x}_i) & \cdots & 2(c^2_{\alpha_a} - s^2_{\alpha_a})\Phi_n(\mathbf{x}_i) \\ \cdots & \cdots & \cdots & \cdots \\ |s_{\alpha_a}\tilde{\Phi}_{1,x} + c_{\alpha_a}\tilde{\Phi}_{1,y}|_{\mathbf{x}_i} & |s_{\alpha_a}\tilde{\Phi}_{1,x} + c_{\alpha_a}\tilde{\Phi}_{2,y}|_{\mathbf{x}_i} & \cdots & |s_{\alpha_a}\tilde{\Phi}_{1,x} + c_{\alpha_a}\tilde{\Phi}_{n,y}|_{\mathbf{x}_i} \\ \cdots & \cdots & \cdots & \cdots \end{bmatrix} \tag{6.34}$$

where $i = 1, 2, \ldots, n_b$, and where n_b is the number of nodes with boundary conditions.

6.4 Second-order cone programming (SOCP)

It was recognised in Krabbenhoft et al. (2007) that most commonly used yield criteria can be cast in the form of conic constraints, and optimisation problems involving such constraints can be solved using highly efficient solvers (Mosek, 2008). Consequently, several numerical limit analysis procedures which involve the use of cone programming techniques have been reported recently (Makrodimopoulos & Martin, 2006b; Ciria et al., 2008; Le et al., 2009). This paper continues this trend by combining SOCP with the presented EFG equilibrium model.

There are two types of second-order cone (also known as 'Lorentz' or 'ice cream' cones) in general use. The first is the standard quadratic cone, defined as

$$\mathscr{L}_q = \left\{ \mathbf{x} \in \mathbb{R}^m \mid x_1 \geq \sqrt{\sum_{j=2}^{m} x_j^2} = \|\mathbf{x}_{2\to m}\|_{L^2} \right\} \tag{6.35}$$

and the second is the rotated quadratic cone, defined as

$$\mathscr{L}_r = \left\{ \mathbf{x} \in \mathbb{R}^{m+2} \mid x_1 x_2 \geq \sum_{j=3}^{m+2} x_j^2 = \|\mathbf{x}_{3\to m+2}\|^2_{L^2},\ x_1,\, x_2 \geq 0 \right\} \tag{6.36}$$

In the following sections, the Nielsen and von Mises yield criteria will be formulated using rotated and standard quadratic cones respectively.

6.4.1 The Nielsen yield criterion

Introducing additional problem variables as follows

$$\boldsymbol{\rho}^{+} = \begin{bmatrix} \rho_1^{+} \\ \rho_2^{+} \\ \rho_3^{+} \end{bmatrix} = \begin{bmatrix} m_{px}^{+} - m_{xx}^{h} \\ m_{py}^{+} - m_{yy}^{h} \\ \sqrt{2}\, m_{xy}^{h} \end{bmatrix} = \mathbf{D}^{+}\mathbf{m} + \mathbf{d}^{+} \tag{6.37}$$

$$\boldsymbol{\rho}^{-} = \begin{bmatrix} \rho_1^{-} \\ \rho_2^{-} \\ \rho_3^{-} \end{bmatrix} = \begin{bmatrix} m_{px}^{-} + m_{xx}^{h} \\ m_{py}^{-} + m_{yy}^{h} \\ \sqrt{2}\, m_{xy}^{h} \end{bmatrix} = \mathbf{D}^{-}\mathbf{m} + \mathbf{d}^{-} \tag{6.38}$$

where

$$\mathbf{D}^{+} = \begin{bmatrix} -1 & 0 & 0 \\ 0 & -1 & 0 \\ 0 & 0 & \sqrt{2} \end{bmatrix};\ \mathbf{d}^{+} = \begin{bmatrix} m_{px}^{+} \\ m_{py}^{+} \\ 0 \end{bmatrix};\ \mathbf{D}^{-} = \begin{bmatrix} 1 & 0 & 0 \\ 0 & 1 & 0 \\ 0 & 0 & \sqrt{2} \end{bmatrix};\ \mathbf{d}^{-} = \begin{bmatrix} m_{px}^{-} \\ m_{py}^{-} \\ 0 \end{bmatrix} \tag{6.39}$$

the relations in Equation (6.2) are the intersection of two rotated cones and are expressed as

$$\boldsymbol{\rho}^{+} \in \mathscr{L}_r^{+},\ \ \mathscr{L}_r^{+} = \left\{ \boldsymbol{\rho}^{+} \in \mathbb{R}^3 \mid 2\rho_1^{+}\rho_2^{+} \geq (\rho_3^{+})^2,\ \rho_1^{+},\ \rho_2^{+} \geq 0 \right\} \tag{6.40}$$

$$\boldsymbol{\rho}^{-} \in \mathscr{L}_r^{-},\ \ \mathscr{L}_r^{-} = \left\{ \boldsymbol{\rho}^{-} \in \mathbb{R}^3 \mid 2\rho_1^{-}\rho_2^{-} \geq (\rho_3^{-})^2,\ \rho_1^{-},\ \rho_2^{-} \geq 0 \right\} \tag{6.41}$$

6.4.2 The von Mises yield criterion

In order to represent the von Mises criterion as a second-order cone constraint, Equation (6.3) is first rewritten in terms of the L^2 norm as

$$\psi(\mathbf{m}) = \|\mathbf{J}^T\ \mathbf{m}\|_{L^2} - m_p \tag{6.42}$$

where $\mathbf{J}$ is the so-called Cholesky factor of $\mathbf{P}$

$$\mathbf{J} = \frac{1}{2}\begin{bmatrix} 2 & 0 & 0 \\ -1 & \sqrt{3} & 0 \\ 0 & 0 & 2\sqrt{3} \end{bmatrix} \tag{6.43}$$

By applying the following transformation of the moment variables $\mathbf{m}$

$$\boldsymbol{\rho}_{2\to 4} = \begin{bmatrix} \rho_2 \\ \rho_3 \\ \rho_4 \end{bmatrix} = \mathbf{J}^T\ \mathbf{m} = \begin{bmatrix} m^h_{xx} - \dfrac{1}{2}\, m^h_{yy} \\ \dfrac{\sqrt{3}}{2}\, m^h_{yy} \\ \sqrt{3}\, m^h_{xy} \end{bmatrix} \tag{6.44}$$

and defining $\rho_1 = m_p$, constraint (6.1) can be cast in terms of a second-order cone constraint as follows

$$\mathcal{B} \equiv \mathscr{L}_q = \left\{ \boldsymbol{\rho} \in \mathbb{R}^4 \mid \rho_1 \geq \|\boldsymbol{\rho}_{2\to 4}\|_{L^2} = \sqrt{\rho_2^2 + \rho_3^2 + \rho_4^2},\ \rho_1 = m_p \right\} \tag{6.45}$$

where $\mathscr{L}_q$ is the four-dimensional quadratic cone and $\boldsymbol{\rho}^T = \{\rho_1\ \rho_2\ \rho_3\ \rho_4\}$.

Using a moving least squares approximation of the moment fields, the vector $\boldsymbol{\rho}_{2\to 4}$ is evaluated at point $\mathbf{x}_k$ and expressed as

$$\boldsymbol{\rho}^k_{2\to 4} = \mathbf{C}_k\mathbf{M} \tag{6.46}$$

where $\mathbf{M} = [\ \mathbf{m}_1\ \ \mathbf{m}_2\ \ \mathbf{m}_3\ ]^T$ and

$$\mathbf{C}_k = \begin{bmatrix} \mathbf{C}_{1k}^T & -\frac{1}{2}\,\mathbf{C}_{2k}^T & \mathbf{0} \\ \mathbf{0} & \frac{\sqrt{3}}{2}\,\mathbf{C}_{2k}^T & \mathbf{0} \\ \mathbf{0} & \mathbf{0} & \sqrt{3}\,\mathbf{C}_{3k}^T \end{bmatrix} \tag{6.47}$$

with

$$\begin{aligned} \mathbf{C}_{1k}^T &= \begin{bmatrix} \Phi_{1,xx}(\mathbf{x}_k) & \Phi_{2,xx}(\mathbf{x}_k) & \dots & \Phi_{n,xx}(\mathbf{x}_k) \end{bmatrix} \\ \mathbf{C}_{2k}^T &= \begin{bmatrix} \Phi_{1,yy}(\mathbf{x}_k) & \Phi_{2,yy}(\mathbf{x}_k) & \dots & \Phi_{n,yy}(\mathbf{x}_k) \end{bmatrix} \\ \mathbf{C}_{3k}^T &= \begin{bmatrix} \Phi_{1,xy}(\mathbf{x}_k) & \Phi_{2,xy}(\mathbf{x}_k) & \dots & \Phi_{n,xy}(\mathbf{x}_k) \end{bmatrix} \end{aligned} \tag{6.48}$$

Consequently, the quadratic cone at point $\mathbf{x}_k$ is

$$\mathscr{L}_q^k = \left\{ \boldsymbol{\rho}^k \in \mathbb{R}^4 \mid \rho_1 \geq \|\boldsymbol{\rho}_{2\to 4}^k\|_{L^2},\ \rho_1 = m_p \right\} \tag{6.49}$$

6.4.3 Limit analysis formulation

The limit analysis formulation can now be expressed in the form of a standard second-order cone programming problem as

$$\begin{aligned} \lambda^- \;=\; & \max\ \lambda \\ & \text{s.t} \begin{cases} \mathbf{A}_1\mathbf{m}_1 + \mathbf{A}_2\mathbf{m}_2 + \mathbf{A}_3\mathbf{m}_3 + \lambda q\mathbf{I} = \mathbf{0} \\ \mathbf{B}_1\mathbf{m}_1 + \mathbf{B}_2\mathbf{m}_2 + \mathbf{B}_3\mathbf{m}_3 = \mathbf{0} \\ \boldsymbol{\rho}^k \in \mathscr{L}^k,\ k = 1,\ 2,\ \dots,\ np \end{cases} \end{aligned} \tag{6.50}$$

where np is the number of yield points and $\boldsymbol{\rho}$ is defined by Equations 6.37, 6.38 or 6.46 (depends on the use of yield criteria). Using the existing Voronoi cell geometry, the yield condition can conveniently be enforced at vertex points within Voronoi cells, as well as at nodes, as indicated in Figure 6.5.

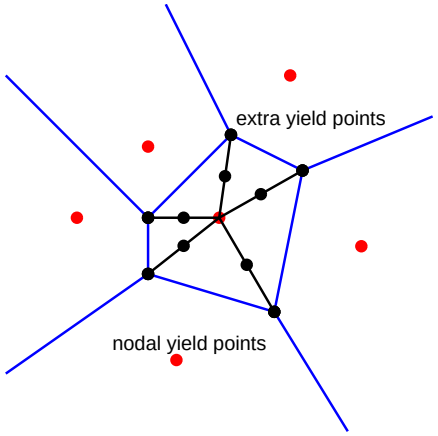

FIGURE 6.5: Locations of yield points (at nodes and elsewhere within Voronoi cells)

It should be emphasised that the collapse multiplier λ^- determined using the described procedure is not guaranteed to represent a strict lower-bound on the exact value. This is because the smoothed moment derivative field may not fully satisfy equilibrium conditions everywhere in the domain, and because the yield condition is only enforced at a limited number of points. However, as the numerical discretisation becomes increasingly fine one can expect to achieve an increasingly reliable approximation of the actual collapse load multiplier.

6.5 Numerical examples

The performance of the limit analysis procedure described will now be tested by examining a number of benchmark plate and slab problems for which upper and/or lower bound solutions have previously been reported in the literature. For all the examples considered uniform out-of-plane pressure loading was applied and the reference length L was taken as 10 m in the numerical simulations. Problems were setup using MATLAB and the Mosek version 5.0 optimisation solver was used to obtain all solutions. Note that for convenience in each case the whole plate or slab problem has been solved, obviating the need to consider symmetry boundary conditions.

6.5.1 Reinforced concrete slab examples

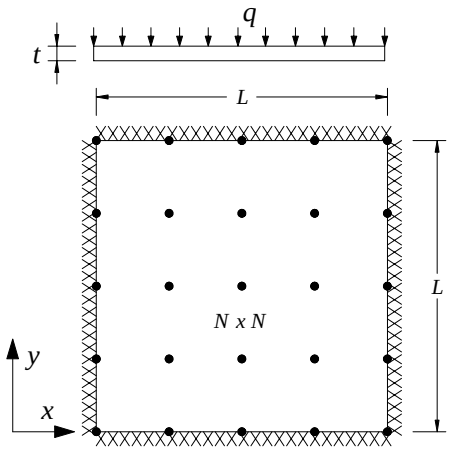

FIGURE 6.6: Clamped square slab subject to a uniform pressure load

The first example comprises a clamped square slab, as shown in Figure 6.6, which has been investigated numerically by Chan (1972), Krenk et al. (1994); Krabbenhoft & Damkilde (2002) and Krabbenhoft & Damkilde (2003). It is assumed that the slab is isotropic with positive and negative yield moments m_p in both directions (constant reinforcement). For this case, the yield criterion (6.2) may be represented as a square yield locus in the plane of the principal moments (Krabbenhoft et al., 2007; Braestrup, 2008), and the exact solution has been identified by Fox (1974) as

$$\lambda_p = 42.851 \frac{m_p}{qL^2} \tag{6.51}$$

The problem has been solved using a $N \times N$ nodes uniformly distributed across the whole slab. The solutions obtained with the size of the domain of influence, β, taken as 3 for various values of N are shown in Table 6.1.

TABLE 6.1: Clamped square slab: variation of collapse load multiplier with level of nodal refinement, N

$N \times N$	10×10	15×15	20×20	30×30	40×40
Collapse multiplier $\lambda^- \left(\frac{m_p}{qL^2}\right)$	42.33	42.67	42.73	42.80	42.83
Errors (%)	1.22	0.42	0.28	0.12	0.05

It can be observed from Table 6.1 that close estimates of the exact solution can be obtained even when only a moderate number of nodes are used. For the finest nodal discretisation used (40×40 nodes), the solution obtained is very close (within 0.05%) of the exact solution. Furthermore, although it has been pointed out that the procedure cannot be guaranteed to provide strict lower bound solutions, it is clear that all the solutions obtained are below the exact value.

The relationship between the computed collapse load multiplier and the size of the influence domain, governed by the parameter β, are illustrated in Figure 6.7. It can be observed that, when β is taken to be larger than 3, a higher (i.e. improved) computed load multiplier can sometimes be obtained. However, since the computational cost increases with the size of the influence domain, a reasonable compromise between accuracy and computational cost can be achieved when β is taken as 3, as will be the case for all problems considered henceforth.

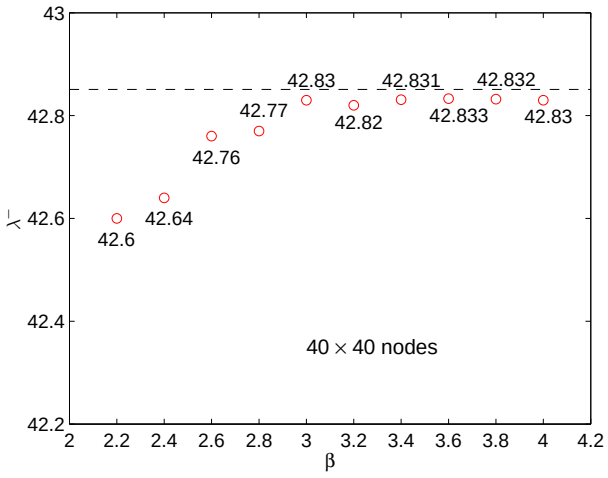

FIGURE 6.7: Clamped square slab: normalised collapse load multiplier vs size of the influence domain, β (dotted line represents exact solution of Equation (6.51))

Compared to results obtained by previous workers, the best solution obtained using the present procedure is significantly higher than that obtained in Krenk et al. (1994) and Chan (1972) (41.78 and 42.32 respectively), and slightly higher than the solution obtained in Krabbenhoft & Damkilde (2003) (42.82), despite the fact that the number of nodes used here is significant smaller than in Krabbenhoft

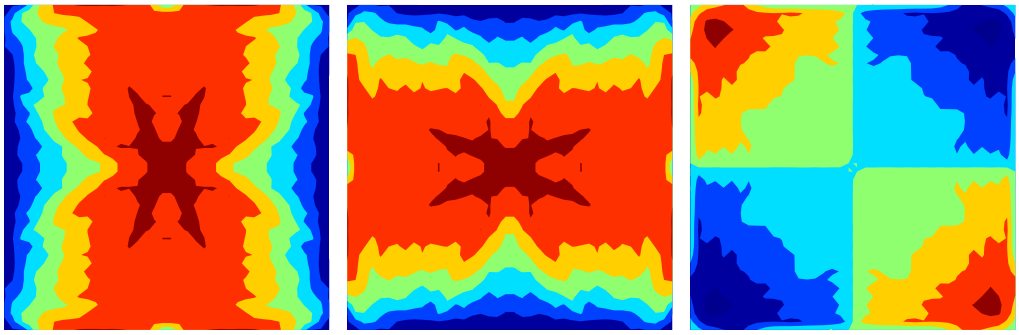

(a) m_{xx}/m_p (b) m_{yy}/m_p (c) m_{xy}/m_p

FIGURE 6.8: Clamped square slab: moment distributions

& Damkilde (2003) (40×40 nodes compared to 101×101 nodes for the whole slab). The moment distributions at collapse are shown in Figure 6.8.

A simply supported isotropic square slab will be considered next. For this case the exact collapse load multiplier was given in Save et al. (1997) as $\lambda_p = 24\frac{m_p}{qL^2}$. When 20×20 nodes were used to model the slab, the corresponding normalised collapse multiplier was found to be 23.996, which is clearly in excellent agreement with the exact solution.

The method will next be applied to a clamped isotropic circular slab subjected to a uniform pressure loading. The exact collapse multiplier was given in Save et al. (1997) as $\lambda_p = 12\frac{m_p}{qR^2}$, where R is the slab radius. The problem was solved using 49 nodes laid out radially across the slab, as shown on Figure 6.9. A normalised solution of 11.89 was obtained, which is just 0.9% lower than the exact collapse multiplier.

6.5.2 Metal plate examples

Square steel plates with either clamped or simply supports on all edges will now be considered; these have also been investigated by Hodge & Belytschko (1968), Andersen et al. (1998), Capsoni & Corradi (1999), and more recently by Le et al. (2009). The problems were solved using $N \times N$ nodes uniformly distributed across the whole plate and in all numerical simulations the plate thickness was taken as

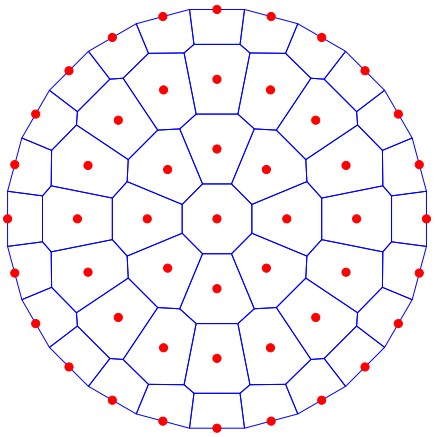

FIGURE 6.9: Clamped circular slab: nodal discretisation and Voronoi cells

$t = 0.1$ m. The solutions and CPU times are shown in Table 6.2 for various levels of nodal refinement.

TABLE 6.2: Clamped & simply supported square plates: results for different level of nodal refinement, N

	clamped		simply supported	
$N \times N$	$\lambda^-(\frac{m_p}{qL^2})$	CPU time (s)†	$\lambda^-(\frac{m_p}{qL^2})$	CPU time (s)†
14×14	43.2467	30	24.8554	42
18×18	43.5364	107	24.9175	97
22×22	43.6961	304	24.9462	226
30×30	43.8562	952	24.9766	882

†Time taken to solve on a 2.8GHz Pentium 4 PC running Microsoft XP (Mosek time only)

Table 6.3 compares normalised solutions obtained using the present method with upper and lower bound solutions that have previously been reported in the literature. It can be observed that the solutions obtained using the present method are in good agreement with previous results. For both clamped and simply supported plate problems, the solutions obtained here are higher than the best lower-bounds obtained in Hodge & Belytschko (1968) (2.33% in the case of the clamped plate and 0.48% in the case of the simply supported plate). Together with Le et al. (2009), this indicates that numerical limit analysis procedures which use the EFG method are capable of producing good results. Note that in the case of the simply

supported square plate, the mean value of the lower-bound obtained here and the upper-bound obtained in Le et al. (2009) is 24.995, which is evidently in excellent agreement with the solution obtained by Andersen et al. (1998). Moment distributions at collapse for these plates are shown in Figures 6.10 and 6.11.

TABLE 6.3: Clamped & simply supported square plates: comparison with literature results

Authors	clamped		simply supported	
	lower-bound (LB)	upper-bound (UB)	lower-bound (LB)	upper-bound (UB)
Present method	43.86*	–	24.98*	–
Le et al. (2009) (EFGM)	–	45.07*	–	25.01*
Hodge & Belytschko (1968)	42.86	49.25	24.86	26.54
Lubliner (1990)	–	52.01	23.81	27.71
Capsoni & Corradi (1999)	–	45.29	–	25.02
Andersen et al. (1998)	44.13‡		25.00‡	

* methods produce approximate rather than rigorous lower or upper bound solutions
‡ mixed elements were used

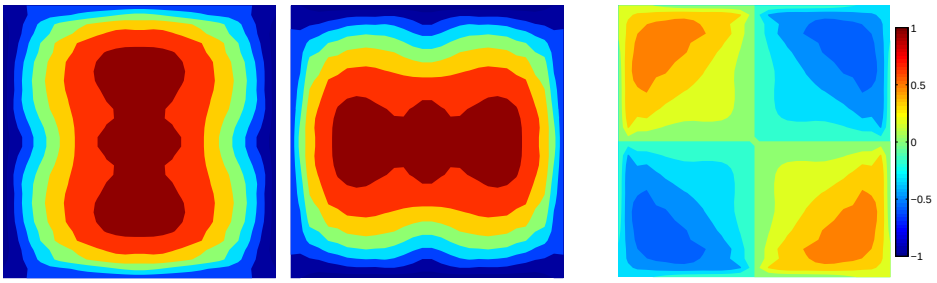

(a) m_{xx}/m_p (b) m_{yy}/m_p (c) m_{xy}/m_p

FIGURE 6.10: Clamped square plate: moment distributions

Rectangular plates (dimensions $a \times b$) with different boundary conditions will now be considered. All problems here were solved using 60×30 nodes with $a = 2b = 10$ m. In case of the plate with 3 clamped boundaries and 1 free edge, note that the free edge has length b. Collapse load multipliers are shown in Table 6.4. It can be observed from the table that the gaps between the (approximate) lower-bounds

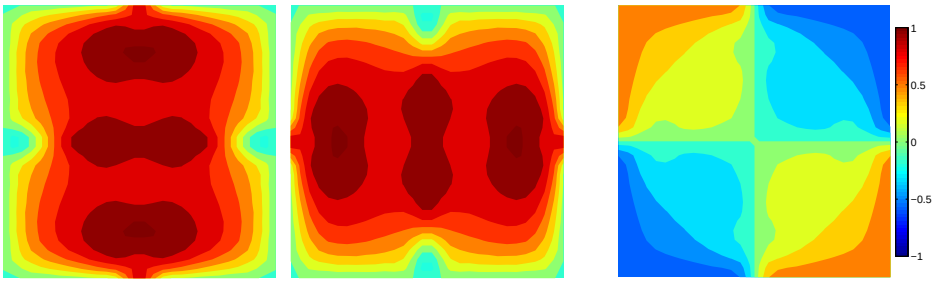

(a) m_{xx}/m_p (b) m_{yy}/m_p (c) m_{xy}/m_p

FIGURE 6.11: Simply supported square plate: moment distributions

found in this paper and (approximate) upper-bounds in Le et al. (2009) are narrow, particularly for the case of a rectangular plate with simply supported boundaries.

TABLE 6.4: Rectangular plates: collapse loads multipliers with various boundary conditions ($\frac{m_p}{qab}$)

Models	clamped	simply supported	3 clamped, 1 free
Present results	53.43	29.85	43.11
Le et al. (2009) (UB)	54.61	29.88	43.86
Capsoni & Corradi (1999)	–	29.88	–

Moment distributions at collapse are shown in Figure 6.12. In plates containing free boundaries it can be observed that the moments oscillate slightly close to a free edge, as shown in Figure 6.12c. This may be explained by the fact that average values of the shear forces were used to enforce the shear boundary condition. However, if the shear forces are computed using the actual values of the moment derivatives (rather than the smoothed values given in Equations (6.29) and (6.30)), larger oscillations result.

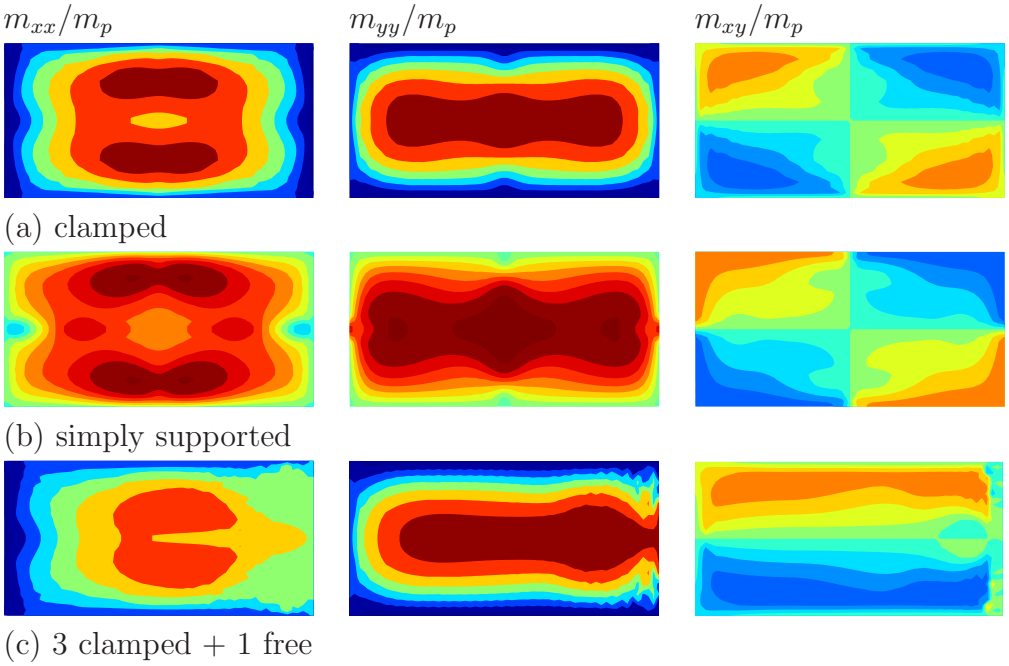

FIGURE 6.12: Rectangular plates: moment distributions

6.6 Conclusions

An Element-Free Galerkin (EFG) based equilibrium limit analysis formulation has been proposed. This uses a moving least squares approximation of the moment field, which means that the resulting field is smooth over the entire problem domain. The collocation method is used in combination with the stabilised conforming nodal integration (SCNI) scheme to ensure that equilibrium needs only to be enforced at nodes. The Nielsen and von Mises yield criteria are formulated as second-order cones so that the underlying limit analysis problem becomes a standard second-order cone programming problem, which can be solved efficiently using primal-dual interior point solvers. Although the procedure cannot be guaranteed to produce strict lower bound solutions, for the plate and slab problems investigated solutions were in practice always lower than known exact solutions, and higher than (improved cf.) existing lower bound numerical solutions in the literature.

Chapter 7

Discussion

In chapters 4, 5 and 6, details of novel numerical procedures developed were presented. In this chapter, a number of key issues which have arisen during the course of the work will be discussed. In the course of the discussion results from a convergence study will be presented, and the status of the solutions obtained will be considered in the context of the formal plasticity theorems. Additionally collapse mechanisms will be presented and advantages and disadvantages of the EFG method compared with the finite element (FE) method will be discussed in the context of limit analysis.

7.1 Convergence study

Numerical procedures based on the EFG formulation and second-order cone programming for upper and lower limit analysis problems have been presented in the previous chapters (4, 5 and 6). Theoretically, when increasing the number of nodes the numerical solution must converge to the exact solution. While lower bound solutions converge to the actual collapse multiplier from below, upper bound solutions converge from above. For most commonly encountered practical engineering problems, the analytical solution will not be available; however a reliable estimation of the exact solution can be obtained numerically using upper and lower

bound limit analysis (dual model limit analysis). Note that dual model limit analysis means that solutions are obtained independently by using either displacement or equilibrium models, not by using the dual form of the optimisation problem as discussed in Section 3.1.3, which provides quasi-upper or quasi-lower bounds, as illustrated in Figure 7.1. In this section, a convergence analysis of solutions obtained using both displacement and equilibrium models is shown, and the actual collapse load multiplier of problems investigated in previous chapters can then be estimated.

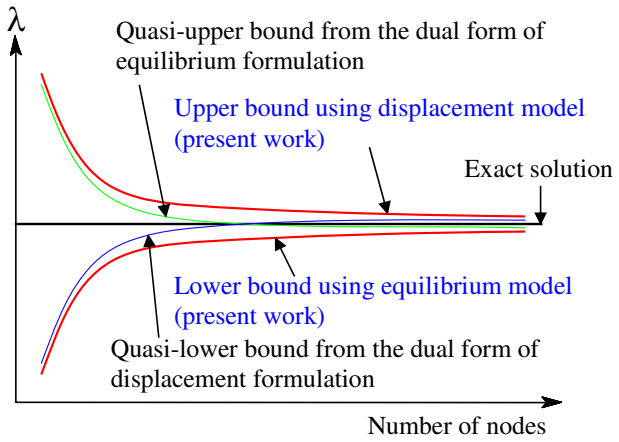

FIGURE 7.1: Illustration of limit analysis solutions

Convergence analysis for the simply supported square plate is shown in Figure 7.2. It can be observed that for the discretisations using 22×22 and 30×30 nodes, the mean value of the lower-bound obtained using the EFG equilibrium model and the upper-bound obtained using the EFG displacement model is 24.99, which is evidently in excellent agreement with the solution obtained by Andersen et al. (1998) and also by Owen & Hinton (1980). This value can be considered as the actual collapse load multiplier for practical engineering purposes.

For the clamped square plate, the gap between the upper bound and lower bound is larger than in the simply supported case, see Figure 7.3. Considering the solution of 44.13 obtained by Andersen et al. (1998), where mixed finite elements and up to 801×801 nodes were used, as the reference value, it can be seen from Figure 7.3 that the EFG equilibrium model has a smaller error than the EFG displacement

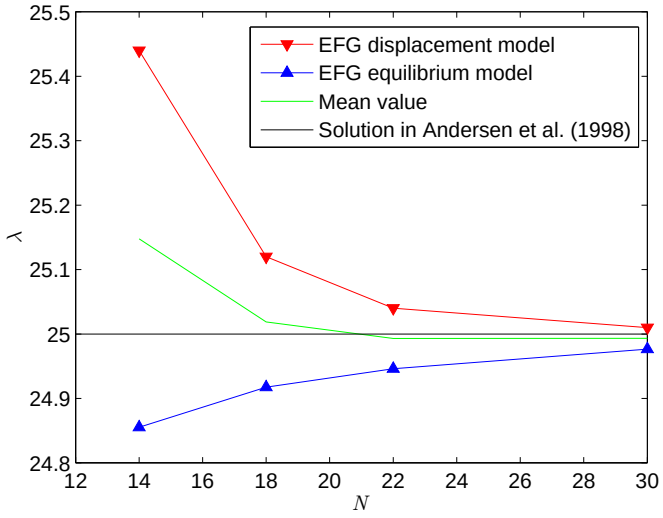

FIGURE 7.2: Convergence analysis for simply supported square plate under uniform pressure

model. This is quantified further in Figure 7.4 where the *rates* of convergence of the two methods are shown. This can be explained by the fact that the singularities in the form of so-called hinges along the boundary may affect convergence of the upper bound solution.

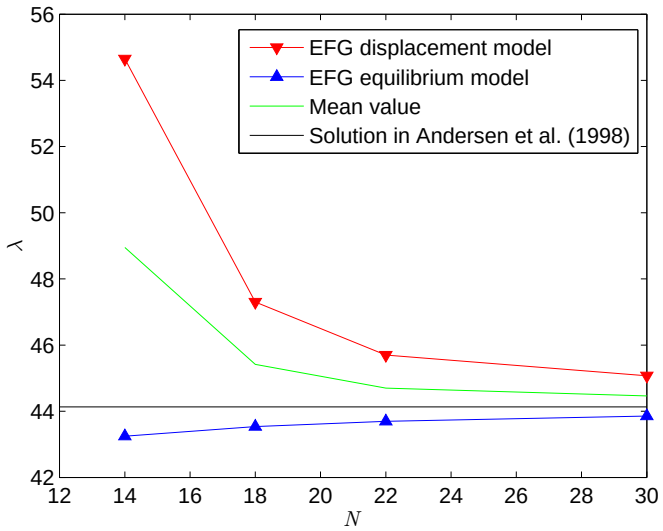

FIGURE 7.3: Convergence analysis for clamped square plate under uniform pressure

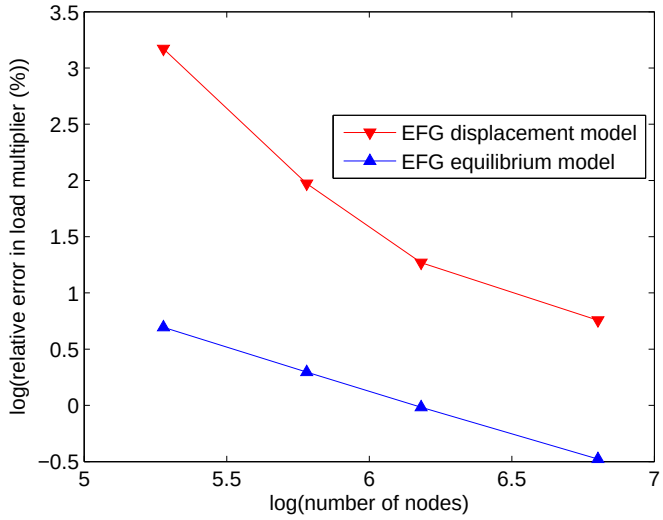

FIGURE 7.4: Convergence rates of the EFG models

In order to obtain a more accurate upper bound solution, a discretisation with 50×50 nodes ($N = 50$) was used, and the solution found was 44.80. The mean value of this upper bound result and the best lower bound obtained using the EFG equilibrium model is 44.33, which is slightly higher than the solution obtained by Andersen et al. (1998), by 0.5 %. Therefore, the value of 44.33 ± 0.5 % can be recommended for use in engineering practice.

TABLE 7.1: Rectangular plates: suggestion of the actual collapse load multipliers ($\frac{m_p}{qab}$)

Models	clamped	simply supported	3 clamped, 1 free
EFG displacement	54.61	29.88	43.86
EFG equilibrium	53.43	29.85	43.11
Mean values	**54.02**	**29.865**	**43.485**

For rectangular plates (dimensions $a \times b$) with different boundary conditions, the inferred actual collapse load multipliers are shown in Table 7.1.

7.2 Solution status

An upper bound which is always higher than the exact solution is a strict upper bound solution, whereas a strict lower bound solution is one which is always lower than the exact solution. In this section, we will discuss the status of the solutions obtained using the presented numerical procedures.

7.2.1 Upper bound solutions

In order to obtain a strict upper bound solution, the flow rule constraint in the associated kinematic formulation is required to hold throughout the problem domain. This results in a difficulty in the kinematic numerical procedure because the condition can only be enforced at a finite number of points. The obvious solution is to use constant strain elements where the condition only needs to be fulfilled at one point in the element. However standard linear displacement finite elements exhibit volumetric locking phenomena in the kinematic formulations associated with the von Mises or Tresca yield criteria (Tin-Loi & Ngo, 2003; Vicente da Silva & Antao, 2007). In the context of limit analysis, the most commonly used approach which both overcomes volumetric locking and guarantees true upper bound solutions for plane problems is to combine constant strain elements with discontinuities in the displacement field (Bottero et al., 1980; Sloan & Kleeman, 1995; Lyamin & Sloan, 2002b). For Kirchhoff plate and slab problems, if second-order shape functions are used (Hodge & Belytschko, 1968), the resulting curvatures are constant over an element. Therefore, the flow rule can be satisfied everywhere provided it is enforced at a given point in the element. However, this model does not satisfy the C^1 continuity condition, which requires at least 3 nodal degrees of freedom (displacement and 2 rotation components). Consequently, cubic shape functions (linear curvature elements) are frequently used in numerical limit analysis procedures for plate and slab problems. If the element sides are straight such that the curvature field varies as a simplex, the flow rule can be guaranteed to be satisfied everywhere in the element by enforcing it at the three vertices (Makrodimopoulos & Martin, 2006b). Nevertheless, this method of enforcing the yield condition has

not been applied to plate limit analysis problems and therefore no strict upper bounds obtained using continuous approximation methods have been reported in the literature, according to the author's knowledge.

In the present kinematic procedure, a quadratic basis function and an isotropic quartic spline weight function were used with a moving least-squares approximation, which results in a high-order of the approximated displacement field. This makes a proof of the strict bound status of the solutions difficult and challenging. Fortunately, when a stabilised conforming nodal integration is applied, the smoothed curvatures obtained are constant over a Voronoi cell. Therefore, the flow rule only needs to be enforced at a point in each smoothing cell, and it is guaranteed to be satisfied everywhere in the problem domain. Although the assumed curvatures using the strain smoothing technique relax the compatibility constraints somewhat, the computed collapse load obtained using the proposed method can still reasonably be considered as an upper bound on the actual value, albeit not a strict one.

7.2.2 Lower bound solutions

In the static formulation, the yield condition is required to be satisfied everywhere in the problem domain to ensure that a strict lower bound can be obtained. This requirement can be easily satisfied using constant or linear stress/moment equilibrium elements (Makrodimopoulos & Martin, 2006a). Various equilibrium triangular elements of this sort have been developed and applied to plate limit analysis problems by Krenk et al. (1994) and Krabbenhoft & Damkilde (2002). However, when a uniform pressure is applied to plates, these models do not exactly enforce the equilibrium relation. This is because the equation $\nabla^2\mathbf{m} + \lambda q = 0$ does not hold with the use of the constant or linear moment fields. Therefore quadratic moment fields must be employed to ensure equilibrium is fully enforced. In fact, a strict solution can be obtained with the use of quadratic equilibrium elements, see Hodge & Belytschko (1968). However, the scheme proposed in their paper is

time-consuming and complicated, and the relative maxima points may not exist or may be located outside the element.

In the present static procedure, it seems impossible to satisfy the yield condition throughout the problem domain since high-order EFG shape functions were used. It is, therefore, no longer possible to guarantee that the solution obtained will represent a strict lower bound on the collapse multiplier of the original, continuous problem. However, the proposed static formulation has two major advantages. First, the moment fields obtained when using a moving least squares technique are smooth over the entire problem domain. There is therefore no need to enforce continuity conditions at interfaces within the problem domain (which would be a key part of a comparable finite element formulation), and also there is no need to perform post-processing to obtain smooth fields. Second, using smoothed second derivatives of the moment field at nodes, the equilibrium equations only need to be fulfilled at the nodes. As shown in the numerical section of chapter 6, solutions obtained using the presented static procedure were always lower than known exact solutions, and higher than existing lower bound numerical solutions in the literature.

7.3 Collapse mechanism

Since the collapse mechanism is not unique, limit analysis problems can be solved using continuous (Capsoni & Corradi, 1997; Andersen et al., 1998; Vicente da Silva & Antao, 2007), semi-continuous (Sloan & Kleeman, 1995) or truly discontinuous (Chan, 1972; Munro & Fonseca, 1978; Smith & Gilbert, 2007) representations of the velocity field. The present method does not involve discontinuities, similar to the methods used in Capsoni & Corradi (1997) and Andersen et al. (1998). The collapse mechanism for the simply supported square plate under a uniform pressure is shown in Figure 7.5. As shown in chapter 5, the proposed adaptive scheme is capable of capturing yield line patterns arising from localised plastic deformations with improved accuracy, see Figure 7.6.

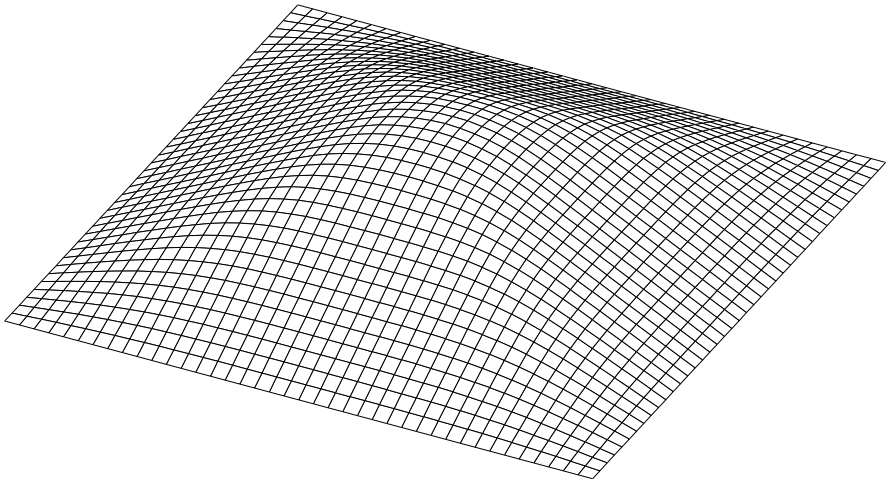

FIGURE 7.5: Simply supported square plate: collapse mechanism with 41×41 nodes obtained using the present method

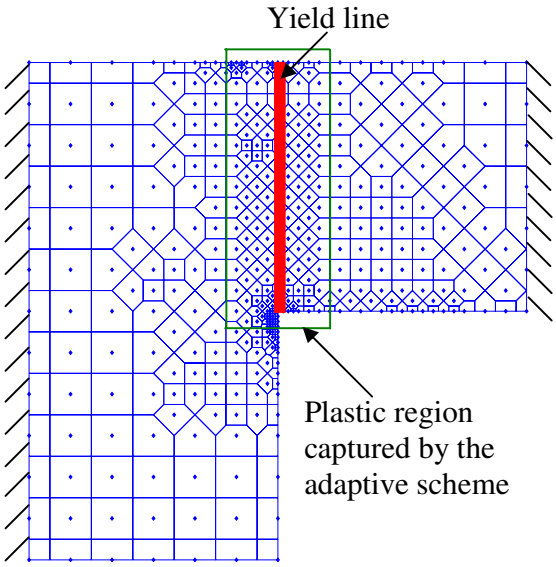

FIGURE 7.6: L-shape plate: yield line capturing

Note that the well-known yield line method can provide a mechanism in which discontinuities in the form of yield lines are clearly identified (Johansen, 1962; Wood, 1961). However, this hand-based analysis method encounters difficulties in problems of arbitrary geometry, especially in problems involving columns or holes.

As has been mentioned in chapter 2, the Discontinuity Layout Optimisation (DLO) procedure is another promising method for undertaking limit analysis of reinforced

concrete slabs. One of the advantages of DLO is that the method is capable of clearly displaying the collapse mechanism. Figures 7.7 and 7.8 illustrate yield line patterns of slabs with arbitrary geometries under uniform pressure obtained using DLO.

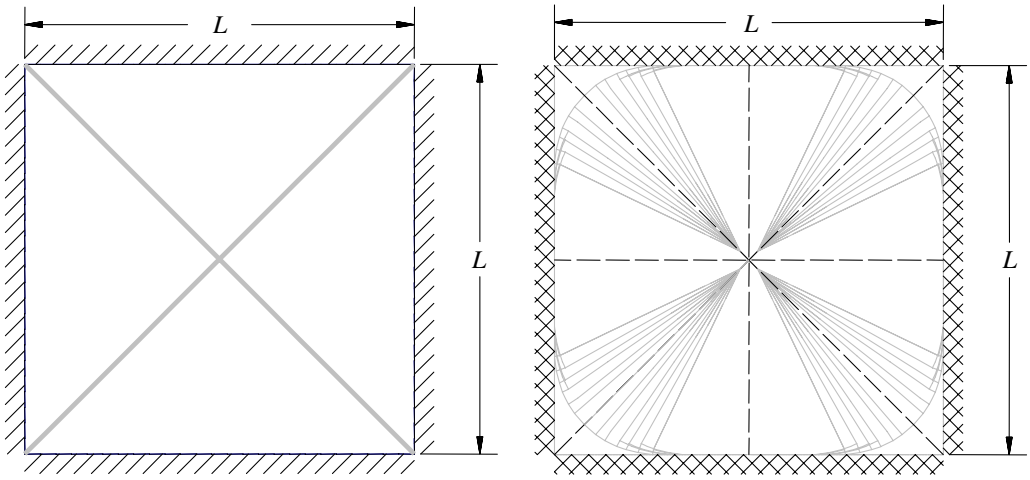

(a) Simply supported slab: $\lambda^+ = 24.00$ (b) Clamped slab: $\lambda^+ = 42.89$

FIGURE 7.7: Yield-line patterns obtained using DLO for square slabs supported on all edges

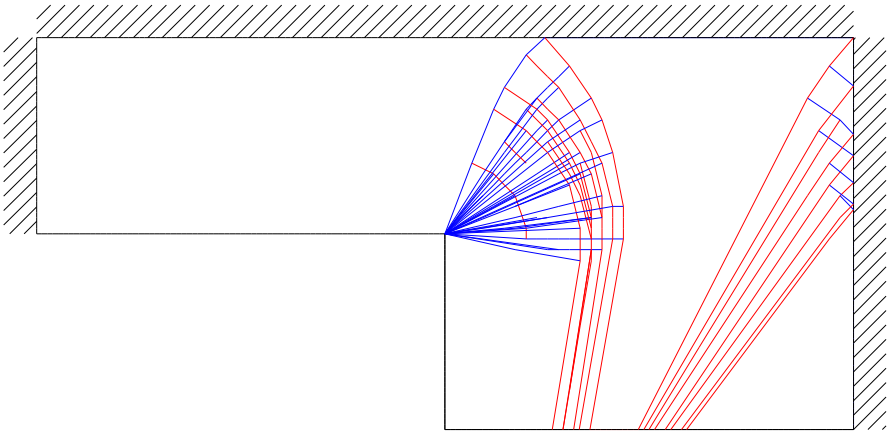

FIGURE 7.8: Yield-line patterns obtained using DLO for L-shaped slab simply-supported on three sides with one column (hogging yield lines in blue and sagging yield lines in red)

Although the DLO method can display clear collapse mechanisms, there is a need to subsequently identify rigid regions which lie between yield-lines in order to

show the deformed shape. On the other hand, the presented procedures can treat various problems governed by different yield criteria, such as the von Mises and Nielsen criteria. Furthermore, the present method can provide accurate solutions for problems of arbitrary geometries using a small number of nodes.

7.4 Advantages and disadvantages of the EFG method compared with the FE method

The fundamental difference between the EFG method and the FE method is the way in which shape functions are constructed. In the FE method, the shape functions are defined for each element as polynomials that satisfy the Kronecker delta property. This means that the shape function of a node follows a polynomial function inside all elements that are attached to that node. On the other hand, the EFG shape functions are constructed in a more flexible way, with no nodal connectivity required. This key difference leads to the advantages and disadvantages of the methods. FE shape functions are robust and computationally inexpensive, but in general have a low order of continuity which can result in locking problems. On the other hand, EFG shape functions require more computational time than the FE shape functions to construct, and do not satisfy the Kronecker delta property. Therefore, care must be taken when enforcing boundary conditions in the EFG method. However, EFG shape functions can easily be constructed to have any desired order of continuity. These high-order shape functions, in general, can result in better convergence rates compared to mesh-based FEM approximations with an equivalent basis. Moreover, the EFG method facilitates the implementation of h-adaptivity as no nodal connectivity is required in the moving least squares approximation.

In the upper bound plate limit analysis problem, if the FE method is used to approximate the displacement field, at least 3 nodal degrees of freedom (displacement and 2 rotation components) are required to fulfill the C^1 continuity condition needed to discretise the problem according to thin plate theory. Therefore, the FE

method has a significantly larger number of variables in the resulting optimisation problem than the EFG method, which requires only one variable for each node.

The advantages of the EFG method are even more marked in the lower bound limit analysis procedure. For Kirchhoff's plates, at least second-order moment fields are required to ensure equilibrium is fully enforced, as discussed previously. This requirement makes the performance of continuity conditions at element interfaces difficult. To the author's knowledge, no plate elements which satisfy these conditions (second-order field and interface continuity) have been proposed. However, when using the EFG method the moment fields are high-order and smooth over the entire problem domain, and there is therefore no need to enforce continuity conditions.

In summary, the EFG method is in general well suited for limit analysis problems, allowing accurate solutions to be obtained with relatively few nodes. The only obvious drawback is that the high order shape functions used in the EFG method make *a priori* proof of the strict bound status of the solutions difficult, as discussed previously.

7.5 A truly meshfree method

In the standard EFG method, a background mesh must be employed in the quadrature scheme, and therefore this partly loses the meshless character of the method. Direct nodal integration, wherein the integrals of the weak form are evaluated at the nodes only, can result in a truly meshless method. However, it is shown that direct nodal integration suffers from spurious singular/zero-energy modes (also known as hourglass modes in the context of finite element analysis). Beissel & Belytschko (1996) proposed a scheme to modify the potential energy functional by adding to it the square of the residual of the equilibrium equation, so that singular modes are eliminated. A similar but somewhat simplified technique was adopted in the SPH method by Bonet & Kulasegaram (2000). Since limit analysis does not involve solving linear equilibrium equations, these methods cannot be applied.

Another effective nodal integration method was proposed by Chen et al. (2001a), referred to as the stabilised conforming nodal integration (SCNI) scheme. In the SCNI scheme, nodal (smoothed) strains are computed by a divergence counterpart of a spatial averaging of strains.

In this research, the SCNI scheme was extended to (i) plastic limit analysis problems (ii) error estimation and (iii) stabilised equilibrium equations in the static formulation. In chapters 4, 5 and 6, it has been shown that the SCNI scheme both results in stable and accurate solutions and also keeps the size of the optimisation problem small. It can been seen from optimisation problem (4.38) that the number of terms in the objective function is equal to the number of integration points, n. When Gauss integration is used, a large number of integration points would be needed in order to obtain accurate solutions. This results in an increased number of additional variables t_j and cones $\|\mathbf{r}_i\| \leq t_i$; see Equation (4.40). Furthermore, in the static formulation Gauss integration also results in a larger number of equilibrium equations than the SCNI scheme; see Section 6.3.2. In short, the Gauss integration method increases optimisation cost.

In chapter 5, the SCNI scheme was extended to error estimators and results in an efficient and truly meshfree adaptive method. The smoothing stabilisation allows reduction of the required order of differentiation by one. This means that the SCNI scheme requires less computational time than Gauss integration which requires the calculation of higher order derivatives. Moreover, in the SCNI scheme Voronoi diagrams can help determine the sizes of the local domains of influence, whereas special measures must be taken to create a smoothed transition of the size of the domain of influence in Gauss integration schemes. This is because a poor moving least squares approximation may occur as a result of abrupt changes in the support size (Rabczuk & Belytschko, 2005).

Chapter 8

Conclusions and future work

In this chapter, firstly, the key contributions of this thesis are summarised, and secondly, directions for future research are recommended.

8.1 Conclusions

The primary aim of the thesis, which is to develop novel numerical limit analysis tools which are sufficiently efficient and robust to be of use to engineers working in practice, has been achieved through the development of a number of procedures presented in the thesis. The key ingredients of these procedures are: (i) the EFG discretisation strategy and (ii) use of the primal-dual interior-point SOCP optimisation algorithm. Specific and detailed conclusions on the performance of these novel numerical procedures were drawn at the end of chapters 4, 5 and 6. The most prominent points are outlined below.

- The EFG method was extended to allow computation of the limit load of plates and slabs. The problem fields were approximated using a moving least squares technique, which results in a high-order of the approximated field. In the kinematic formulation, only one displacement variable is required for each EFG node, ensuring that the total number of variables in the resulting

optimisation problem is kept to a minimum, with far fewer variables being required compared to finite element formulations. Moreover, the moment fields obtained by using this technique are smooth over the entire problem domain, and therefore there is no need to enforce continuity conditions at interfaces within the problem domain. Numerical results show that the EFG based procedures allow accurate solutions to be obtained using a relatively small number of nodes.

- Since the accuracy of numerical limit analysis solutions is highly affected by local singularities arising from localised plastic deformations, an efficient h-adaptive EFG scheme was developed to increase the accuracy of the solutions and to speed-up the computational process. Due to the naturally conforming properties of the meshfree approximation, the proposed adaptive scheme is conveniently performed without the need for complex manipulation of the data structures involved. Various numerical examples were presented to show that the adaptive scheme is able to capture yield line patterns arising from localised plastic deformations for problems of arbitrary geometry, and that the adaptive scheme does indeed produce better solutions than can be obtained using uniform refinement, despite the fact that a relatively small number of nodes were used.

- A stabilised conforming nodal integration (SCNI) scheme was extended to (i) plastic limit analysis problems, allowing integrals to be evaluated at nodes only, (ii) error estimation, allowing errors to be estimated at representative nodal cells, and (iii) stabilised equilibrium equations in the static formulation, allowing equilibrium to be enforced at nodes only. It was shown in several numerical examples that, when the SCNI scheme is applied, the solutions obtained are accurate and stable, and the SCNI scheme also results in an efficient and truly mesh-free method since the computational cost associated with using the SCNI scheme is much lower than that associated with using Gauss integration.

- The discretised formulations were cast in the form of a standard second-order cone programming problem, ensuring that the resulting optimisation problem could be solved using highly efficient primal-dual interior-point solvers. It is well-known that the objective function in the kinematic formulation is not differentiable at any point in the rigid domain where plastic strains do not develop. With the use of the primal-dual interior-point algorithm, such singularities can be treated efficiently. Moreover, the von Mises and Nielsen yield criteria which are used in the static plate and slab limit analysis problem respectively were also enforced by introducing second-order cone constraints. Numerical examples show that when an optimisation problem was formulated as a second-order cone programming problem, the proposed solution procedure can solve real-world problems in engineering practice, which require up to hundreds of thousands variables or more.

In short, the combination of the EFG method, stabilised conforming nodal integration and second-order cone programming results in an efficient and robust numerical limit analysis tool for practical engineering problems.

8.2 Suggestions for future work

Although the original aim has been largely met, there are still a number of aspects of this work which require further investigation, and there are also some other methods which can potentially be applied to limit analysis problems. The following tasks may be recommended as possible avenues for future research.

- The proposed numerical procedures (kinematic formulation, static formulation and adaptivity) can be extended to tackle more complex structural configurations, subject to a variety of loading regimes. It would for example be interesting to extend the proposed method to treat plane strain problems, 3D problems which exhibit volumetric locking, and also problems involving shakedown.

- Investigate the performance of *a posteriori* schemes to check the status of the solutions.

- The strain smoothing technique was recently extended to the standard finite element method by Liu et al. (2007a), who named it the smoothed finite element method (SFEM). It was shown that the SFEM retains most properties of the strain smoothing technique and also advantages of the FEM, and hence yields solutions that are accurate, free from locking and computationally inexpensive (Liu et al., 2007b; Nguyen-Xuan et al., 2008). It is, therefore, relevant to investigate the performance of SFEM in combination with second-order cone programming for kinematic limit analysis problems.

- The standard finite element method does not allow discontinuities within elements. As a result, in most finite element based semi-continuous procedures, discontinuities are located at the edges of elements of fixed topology (Sloan & Kleeman, 1995; Lyamin & Sloan, 2002b; Makrodimopoulos & Martin, 2008). Recently, Belytschko & Black (1999) and Moes et al. (1999) proposed the so-called the eXtended Finite Element Method (XFEM), which was originally used to treat crack problems. In this method, discontinuities are permitted to cross elements, and are often realised by the level-set method. Therefore, it may also be appropriate to apply the XFEM to limit analysis problems.

References

Anderheggen, E. 1976 Finite element analysis assuming rigid-ideal-plastic material behaviour. *Limit analysis using finite elements, ASME* .

Anderheggen, E. & Knopfel, H. 1972 Finite element limit analysis using linear programming. *International Journal of Solids and Structures* **8**, 1413–1431.

Andersen, E. D., Roos, C. & Terlaky, T. 2003 On implementing a primal-dual interior-point method for conic quadratic programming. *Mathematical Programming* **95**, 249–277.

Andersen, K. D. 1996 An efficient Newton barrier method for minimizing a sum of Euclidean norms. *SIAM Journal on Optimization* **6**, 74–95.

Andersen, K. D. & Christiansen, E. 1995 Limit analysis with the dual affine scaling algorithm. *Journal of Computational and Applied Mathematics* **59**, 233–243.

Andersen, K. D., Christiansen, E. & Overton, M. L. 1998 Computing limit loads by minimizing a sum of norms. *SIAM Journal on Scientific Computing* **19**, 1046–1062.

Argyris, J. H. 1967 Elasto-plastic matrix displacement analysis of three-dimensional stress systems by finite element method. *International Journal of Mechanical Sciences* **9**, 143–155.

Askes, H. 2000 *Advanced spatial discretisation strategies for localised failure: mesh adaptivity and meshless methods*, PhD thesis, Technical University Delft.

Askes, H., de Borst, R. & Heeres, O. 1999 Condition for locking-free elasto-plastic analyses in the Element-Free Galerkin method. *Computer Methods in Applied Mechanics and Engineering* **173**, 99–109.

Askes, H. & Pannachet, T. 2005 Negative penalty functions in the element-free Galerkin method. *Communications in Numerical Methods in Engineering* **21**, 97–98.

Askes, H., Rodríguez-Ferran, A. & Huerta, A. 1999a Adaptive analysis of yield line patterns in plates with the arbitrary Lagrangian-Eulerian method. *Computers and Structures* **70**, 257–271.

Atluri, S. N. & Zhu, T. 2000 New concepts in meshless methods. *International Journal for Numerical Methods in Engineering* **47**, 537–556.

Babuska, I. & Rheinboldt, W. 1978 Error estimates for adaptive finite element computations. *SIAM Journal on Numerical Analysis* **15**, 736–754.

Beissel, S. & Belytschko, T. 1996 Nodal integration of the element-free Galerkin method. *Computer Methods in Applied Mechanics and Engineering* **139**, 49–74.

Belinha, J. & Dinis, L. M. J. S. 2006 Analysis of plates and laminates using the element-free Galerkin method. *Computers and Structures* **84**, 1547–1559.

Belinha, J. & Dinis, L. M. J. S. 2007 Nonlinear analysis of plates and laminates using the element free Galerkin method. *Composite Structures* **78**, 337–350.

Belytschko, T. & Black, T. 1999 Elastic crack growth in finite elements with minimal remeshing. *International Journal for Numerical Methods in Engineering* **45**, 601–620.

Belytschko, T., Krongauz, Y., Dolbow, J. & Gerlach, C. 1998 On the completeness of meshfree particle methods. *International Journal for Numerical Methods in Engineering* **43**, 785–819.

Belytschko, T., Krongauz, Y., Organ, D., Fleming, M. & Krysl, P. 1996a Meshless methods: An overview and recent developments. *Computer Methods in Applied Mechanics and Engineering* **139**, 3–47.

Belytschko, T., Lu, Y. Y. & Gu, L. 1994 Element-Free Galerkin methods. *International Journal for Numerical Methods in Engineering* **37**, 229–256.

Belytschko, T., Lu, Y. Y., Gu, L. & Tabbara, M. 1996 Element-free Galerkin methods for static and dynamic fracture. *International Journal of Solids and Structures* **32**, 2547–2570.

Belytschko, T., Organ, D. & Gerlach, C. 2000 Element-free Galerkin methods for dynamic fracture in concrete. *Computer Methods in Applied Mechanics and Engineering* **187**, 385–399.

Belytschko, T. & Tabbara, M. 1996 Dynamic fracture using Element-Free Galerkin methods. *International Journal for Numerical Methods in Engineering* **39**, 923–938.

Ben-Tal, A. & Nemirovski, A. 2001 *Lectures on Modern Convex Optimization: Analysis, Algorithms, and Engineering Applications*. Society for Industrial Mathematics.

Bonet, J. & Kulasegaram, S. 2000 Correction and stabilization of smooth particle hydrodynamics methods with applications in metal forming simulations. *International Journal for Numerical Methods in Engineering* **47**, 1189–1214.

Borges, L. A., Zouain, N., Costa, C. & Feijoo, R. 2001 An adaptive approach to limit analysis. *International Journal of Solids Structures* **38**, 1707–1720.

Bottero, A., Negre, R., Pastor, J. & Turgeman, S. 1980 Finite element method and limit analysis theory for soil mechanics problems. *Computer Methods in Applied Mechanics and Engineering* **22**, 131–149.

Boulbibane, M. & Ponter, A. 2005 Limit loads for multilayered half-space using the linear matching method. *Computers and Geotechnics* **32**, 535–544.

Boulbibane, M. & Ponter, A. 2006 Extension of the linear matching method to geotechnical problems. *Computer Methods in Applied Mechanics and Engineering* **194**, 4633–4650.

Braestrup, M. W. 2008 Yield line theory and concrete plasticity. *Magazine of Concrete Research* **60**, 549–553.

Brion, A. & Hodge, P. G. 1967 Limit analysis of rotationally symmetric shells under central boss loading by a numerical method. *Journal of Applied Mechaincs* **34**, 644–650.

Capsoni, A. 1999 A mixed finite element model for plane strain limit analysis computations. *Communications in Numerical Methods in Engineering* **15**, 101–112.

Capsoni, A. & Corradi, L. 1997 A finite element formulation of the rigid-plastic limit analysis problem. *International Journal for Numerical Methods in Engineering* **40**, 2063–2086.

Capsoni, A. & Corradi, L. 1999 Limit analysis of plates -a finite element formulation. *Structural Engineering and Mechanics* **8**, 325–341.

Casciaro, R. & Cascini, L. 1982 A mixed formulation and mixed finite elements for limit analysis. *International Journal for Numerical Methods in Engineering* **18**, 211–243.

Chakrabarty, J. 1988 *Theory of plasticity.* McGraw-Hill international editions.

Chan, H. S. Y. 1972 The collapse load of reinforeced concrete plates. *International Journal for Numerical Methods in Engineering* **5**, 57–64.

Chen, H. F. & Ponter, A. R. S. 2001 Shakedown and limit analyses for 3-D structures using the linear matching method. *International Journal of Pressure Vessels and Piping* **78**, 443–451.

Chen, J. S., Pan, C. & Wu, C. T. 1997 Large deformation analysis of rubber based on a reproducing kernel particle method. *Computational Mechanics* **19**, 153168.

Chen, J. S., Pan, C. & Wu, C. T. 2001 Lagrangian meshfree formulation for analysis of geotechnical materials. *Journal of Engineering Mechanics* **127**, 440–449.

Chen, J. S., Pan, C., Wu, C. T. & Roque, C. 1998 A lagrangian reproducing kernel particle method for metal forming analysis. *Computational Mechanics* **21**, 289307.

Chen, J. S., Wu, C. T. & Belytschko, T. 2000 Regularization of material instabilities by meshfree approximations with intrinsic length scales. *International Journal for Numerical Methods in Engineering* **47**, 1303–1322.

Chen, J. S., Wu, C. T., Yoon, S. & You, Y. 2001a A stabilized conforming nodal integration for Galerkin mesh-free methods. *International Journal for Numerical Methods in Engineering* **50**, 435–466.

Chen, S., Liu, Y. & Cen, Z. 2008 Lower-bound limit analysis by using the EFG method and non-linear programming. *International Journal for Numerical Methods in Engineering* **74**, 391–415.

Chen, W. F. & Han, D. J. 1988 *Plasticity for structural engineers*. Springer-Verrlag, New York.

Chen, Y., Lee, J. & Eskandarian, A. 2006 *Meshless Methods in Solid Mechanics*. Springer.

Christiansen, E. 1980 Limit analysis in plasticity as a mathematical programming problem. *Calcolo* **17**, 41–65.

Christiansen, E. 1981 Computation of limit load. *International Journal for Numerical Methods in Engineering* **17**, 1547–1570.

Christiansen, E. 1996 *Limit analysis of collapse states*. Handbook of Numerical Analysis, Elsevier Science B.V.

Christiansen, E. & Andersen, K. D. 1999 Computation of collapse states with von Mises type yield condition. *International Journal for Numerical Methods in Engineering* **46**, 1185–1202.

Christiansen, E. & Kortanek, K. O. 1991 Computation of the collapse state in limit analysis using the LP affine scaling algorithm. *Journal of Computational and Applied Mathematics* **34**, 47–63.

Christiansen, E. & Larsen, S. 1983 Computations in limit analysis for plastic plates. *International Journal for Numerical Methods in Engineering* **19**, 169–184.

Christiansen, E. & Pedersen, O. S. 2001 Automatic mesh refinement in limit analysis. *International Journal for Numerical Methods in Engineering* **50**, 1331–1346.

Chung, H. J. & Belytschko, T. 1998 An error estimate in the EFG method. *Computational Mechanics* **21**, 91–100.

Ciria, H., Peraire, J. & Bonet, J. 2008 Mesh adaptive computation of upper and lower bounds in limit analysis. *International Journal for Numerical Methods in Engineering.* **75**, 899–944.

Cohn, M. Z. & Maier, G. 1979 *Engineering plasticity by mathematical programming*. Pergamon Press, New York.

de Berg, M., van Krefeld, M., Overmars, M. & Schwarzkopf, O. 2008 *Computational Geometry: Algorithms and Applications*. Springer.

de Borst, R. 1982 Calculation of collapse loads using higher order elements. *in: IUTAM Symposium on Deformation and Failure of Granular Materials, Rotterdam, Balkema* pp. 503–513.

Dolbow, J. & Belytschko, T. 1999 Volumetric locking in the Element-Free Galerkin method. *International Journal for Numerical Methods in Engineering* **46**, 925–942.

Donning, B. M. & Liu, W. K. 1998 Meshless methods for shear-deformable beams and plates. *Computer Methods in Applied Mechanics and Engineering* **52**, 47–71.

Drucker, D. C., Prager, W. & Greenberg, H. J. 1952 Extended limit design theorems for continuous medium. *Quarterly of Applied Mathematics* **9**, 381389.

Duan, Q. & Belytschko, T. 2009 Gradient and dilatational stabilizations for stress-point integration in the element-free Galerkin method. *International Journal for Numerical Methods in Engineering* **77**, 776–798.

Duarte, C. A. & Oden, J. T. 1996 An hp adaptive method using clouds. *Computer Methods in Applied Mechanics and Engineering* **139**, 237–262.

Duflot, M. & Nguyen-Dang, H. 2002 Dual analysis by a meshless method. *Communications in Numerical Methods in Engineering* **18**, 621–631.

Faccioli, E. & Vitiello, E. 1973 A finite element, linear programming methods for the limit analysis of thin plates. *International Journal for Numerical Methods in Engineering* **5**, 311–325.

Fortune, S. 1995 *Computing in Euclidean Geometry*. Lecture Notes Series on Computing, D.Z. Du and F. Hwang, Editors.

Fox, E. N. 1974 Limit analysis for plates: The exact solution for a clamped square plate of isotropic homogeneous material obeying the square yield criterion and loaded by uniform pressure. *Philosophical Transactions of the Royal Society of London, Series A* **277**, 121–155.

Fraeijs de Veubeke, B. 2001 Displacement and equilibrium models in the finite element method. *International Journal for Numerical Methods in Engineering, Reprinted* **52**, 287–342.

Fraeijs de Veubeke, B. & Zienkiewicz, O. C. 1967 Strain-energy bounds in finite element analysis by slab analogy. *Journal of Strain Analysis* **2**, 265–271.

Franco, J. R. Q., Ponter, A. R. S. & Barros, F. B. 2003 Adaptive F.E. method for the shakedown and limit analysis of pressure vessels. *European Journal of Mechanics - A/Solids* **22**, 525–533.

Fries, T. P. & Belytschko, T. 2008 Convergence and stabilization of stress-point integration in mesh-free and particle methods. *International Journal for Numerical Methods in Engineering* **78**, 1067–1087.

Fries, T. P. & Matthies, H. G. 2003 Classification and overview of meshfree methods. *Informatikbericht 2003-3, Technical University Braunschweig, Brunswick, Germany* .

Gaudrat, V. F. 1991 A Newton type algorithm for plastic limit analysis. *Computer Methods in Applied Mechanics and Engineering* **88**, 207–224.

Gingold, R. A. & Monaghan, J. 1977 Smooth particle hydrodynamics: theory and applications to non spherical stars. *Royal Astronomical Society, Monthly Notices* **181**, 375–389.

Grierson, D. E. 1977 Mathematical programming methods for deformation analysis at plastic collapse. *Computers and Structures* **7**, 599–612.

Haussler-Combe, U. & Korn, C. 1998 An adaptive approach with the Element-Free-Galerkin method. *Computer Methods in Applied Mechanics and Engineering* **162**, 203–222.

Hill, R. 1950 *Mathematical theory of plasticity*. Oxford Univ. Press, London.

Hodge, P. G. 1959 *Plastic analysis of structures*. Robert E. Krieger Publishing Co. Malabar, Florida.

Hodge, P. G. 1961 The Mises yield condition for ratationally symmetric shells. *Quarterly of Applied Mathematics* **18**, 305–311.

Hodge, P. G. 1963 *Limit analysis of rotationally symmetric plates and shells*. Prentice Hall, Englewwood, New Jersey.

Hodge, P. G. J. & Belytschko, T. 1968 Numerical Methods for the Limit Analysis of Plates. *Journal of Applied Mechanics* **35**, 796–802.

Hopkins, H. G. & Wang, A. J. 1954 Load-carrying capacities for circular plates of perfectly-plastic material with arbitrary yield condition. *Journal of the Mechanics and Physics of Solids* **3**, 117–129.

Huerta, A., Belytschko, T., Fernandez-Mendez, S. & Rabczuk, T. 2004 Meshfree methods. *Encyclopedia of Computational Mechanics* **1, Chapter 10**, 279–309.

Huerta, A. & Fernandez-Mendez, S. 2000 Enrichment and coupling of the finite element and meshless methods. *International Journal for Numerical Methods in Engineering* **48**, 1615–1636.

Huerta, A. & Fernandez-Mendez, S. 2001 Locking in the incompressible limit for the Element Free Galerkin method. *International Journal for Numerical Methods in Engineering* **51**, 1361–1383.

Hughes, T. J. R. 1980 Generalization of selective integration procedures to anisotropic and nonlinear media. *International Journal for Numerical Methods in Engineering* **15**, 1413–1418.

Jirasek, M. & Bazant, Z. P. 2002 *Inelastic analysis of structures*. John Wiley & Son, Ltd.

Johansen, K. W. 1962 *Yield-line theory*. London: Cement and Concrete Association.

Johnson, D. 1995 Yield-line analysis by sequential linear programming. *International Journal of Solids and Structures* **32**, 1395–1404.

Johnson, D. 2001 On the safety of the strip method for reinforced concrete slab design. *Computers and Structures* **79**, 2425–2430.

Jun, S., Liu, W. K. & Belytschko, T. 1998 Explicit reproducing kernel particle methods for large deformation problems. *International Journal for Numerical Methods in Engineering* **41**, 137–166.

Kamenjarzh, J. A. 1996 *Limit analysis of solids and structures*. CRC press.

Koopman, D. C. A. & Lance, R. H. 1965 On linear programming and plastic limit analysis. *Journal of the Mechanics and Physics of Solids* **13**, 77–87.

Krabbenhoft, K. & Damkilde, L. 2002 Lower bound limit analysis of slabs with nonlinear yield criteria. *Computers and Structures* **80**, 2043–2057.

Krabbenhoft, K. & Damkilde, L. 2003 A general nonlinear optimization algorithm for lower bound limit analysis. *International Journal for Numerical Methods in Engineering* **56**, 165–184.

Krabbenhoft, K., Lyamin, A. V., Hjiaj, M. & Sloan, S. W. 2005 A new discontinuous upper bound limit analysis formulation. *International Journal for Numerical Methods in Engineering* **63**, 1069–1088.

Krabbenhoft, K., Lyamin, A. V. & Sloan, S. W. 2007 Formulation and solution of some plasticity problems as conic programs. *International Journal of Solids and Structures* **44**, 1533–1549.

Krenk, S., Damkilde, L. & Hoyer, O. 1994 Limit analysis and optimal design of plates with equilibrium elements. *Journal of Engineering Mechanics* **120**, 1237–1254.

Krongauz, Y. & Belytschko, T. 1997 Consistent pseudo-derivatives in meshless methods. *Computer Methods in Applied Mechanics and Engineering* **146**, 371–386.

Krysl, P. & Belytschko, T. 1995 Analysis of thin plates by the Element-Free Galerkin method. *Computational Mechanics* **17**, 26–35.

Krysl, P. & Belytschko, T. 1996 Analysis of thin shells by the element-free Galerkin method. *International Journal of Solids and Structures* **33**, 30573080.

Lancaster, P. & Salkauskas, K. 1981 Surfaces generated by moving least squares methods. *Mathematics of Computation* **37**, 141158.

Laudiero, F. 1972 Limit analysis of plates with piecewise linear yield surface. *Meccanica* **7**, 105–110.

Le, C. V., Gilbert, M. & Askes, H. 2009 Limit analysis of plates using the EFG method and second-order cone programming. *International Journal for Numerical Methods in Engineering* **78**, 1532–1552.

Leitao, V. M. A. 2001 A meshless method for Kirchhoff plate bending problems. *International Journal for Numerical Methods in Engineering* **52**, 11071130.

Li, S., Hao, W. & Liu, W. K. 2000 Numerical simulations of large deformation of thin shell structures using meshfree methods. *Computational Mechanics* **25**, 102–116.

Li, S. & Liu, W. K. 1996 Moving least-squares reproducing kernel method Part ii: Fourier analysis. *Computer Methods in Applied Mechanics and Engineering* **139**, 159–193.

Li, S. & Liu, W. K. 1999 Reproducing kernel hierarchical partition of unity part ii: Applications. *International Journal for Numerical Methods in Engineering* **45**, 289–317.

Li, S. & Liu, W. K. 2000 Numerical simulations of strain localization in inelastic solids using mesh-free methods. *International Journal for Numerical Methods in Engineering* **48**, 12851309.

Li, S. & Liu, W. K. 2002 Meshfree and particle methods and their applications. *Applied Mechanics Reviews* **55**, 1–34.

Liu, G. R. 2003 *Mesh Free Methods: Moving Beyond the Finite Element Method*. CRC press.

Liu, G. R., Dai, K. Y. & Nguyen, T. T. 2007a A smoothed finite element method for mechanics problems. *Computational Mechanics* **39**, 859877.

Liu, G. R. & Gu, Y. T. 2005 *An Introduction to Meshfree Methods and Their Programming*. Springer.

Liu, G. R., Nguyen, T. T., Dai, K. Y. & Lam, K. Y. 2007b Theoretical aspects of the smoothed finite element method (SFEM). *International Journal for Numerical Methods in Engineering* **71**, 902–930.

Liu, G. R. & Tu, Z. H. 2002 An adaptive procedure based on background cells for meshless methods. *Computer Methods in Applied Mechanics and Engineering* **191**, 1923–1943.

Liu, W. K. & Chen, Y. 1995 Wavelet and multiple scale reproducing kernel methods. *International Journal for Numerical Method in Fluids* **21**, 901–931.

Liu, W. K., Chen, Y., Chang, C. T. & Belytschko, T. 1996a Advances in multiple scale kernel particle methods. *Computational Mechanics* **18**, 73–111.

Liu, W. K., Chen, Y., Uras, R. A. & Chang, C. T. 1996b Generalized multiple scale reproducing kernel particle methods. *Computer Methods in Applied Mechanics and Engineering* **139**, 91–158.

Liu, W. K., Hao, S., Belytschko, T., Li, S. & Chang, C. T. 1999 Multiple scale meshfree methods for damage fracture and localization. *Computational Materials Science* **16**, 197–205.

Liu, W. K. & Jun, S. 1998 Multiple-scale reproducing kernel particle methods for large deformation problems. *International Journal for Numerical Methods in Engineering* **41**, 1339–1362.

Liu, W. K., Jun, S., Sihling, D. T., Chen, Y. & Hao, W. 1997a Multi-resolution reproducing kernel particle method for computational fluid dynamics. *International Journal for Numerical Method in Fluids* **24**, 1–25.

Liu, W. K., Jun, S. & Zhang, Y. F. 1995a Reproducing kernel particle methods. *International Journal for Numerical Methods in Fluids* **20**, 1081–1106.

Liu, W. K., Li, S. & Belytschko, T. 1997 Moving least-square reproducing kernel methods (I) methodology and convergence. *Computer Methods in Applied Mechanics and Engineering* **143**, 113–154.

Liu, Y. H., Zen, Z. Z. & Xu, B. Y. 1995 A numerical method for plastic limit analysis of 3-D structures. *International Journal of Solids Structures* **32**, 1645–1658.

Liu, Y., Zhang, X. & Cen, Z. 2004 Numerical determination of limit loads for three-dimensional structures using boundary element method. *European Journal of Mechanics - A/Solids* **23**, 127–138.

Lobo, M., Vandenberghe, L., Boyd, S. & Lebret, H. 1998 Applications of second-order cone programming. *Linear Algebra and its Applications* **284**, 193–228.

Lu, Y. Y., Belytschko, T. & Gu, L. 1994 A new implementation of the Element-Free Galerkin method. *Computer Methods in Applied Mechanics and Engineering* **113**, 397–414.

Lu, Y. Y., Belytschko, T. & Tabbara, M. 1995 Element-free Galerkin method for wave propagation and dynamic fracture. *Computer Methods in Applied Mechanics and Engineering* **126**, 131–153.

Lubliner, J. 1990 *Plasticity theory*. Macmillan, New York.

Lucy, L. 1977 A numerical approach to testing the fission hypothesis. *The Astronomical Journal* **82**, 1013–1024.

Lyamin, A., Salgado, R., Sloan, S. W. & Prezzi, M. 2007 Two and three dimensional bearing capacity of footings in sand. *Geotechnique* **57**, 647–662.

Lyamin, A. V. & Sloan, S. W. 2002a Lower bound limit analysis using nonlinear programming. *International Journal for Numerical Methods in Engineering* **55**, 573–611.

Lyamin, A. V. & Sloan, S. W. 2002b Upper bound limit analysis using linear finite elements and non-linear programming. *International Journal for Numerical and Analytical Methods in Geomechanics* **26**, 181–216.

Lyamin, A. V. & Sloan, S. W. 2003 Mesh generation for lower bound limit analysis. *Advances in Engineering Software* **34**, 321–338.

Lyamin, A. V., Sloan, S. W., Krabbenhoft, K. & Hjiaj, M. 2005 Lower bound limit analysis with adaptive remeshing. *International Journal for Numerical Methods in Engineering* **63**, 1961–1974.

Lysmer, J. 1970 Limit analysis of plane problems in soil mechanics. *Journal of the Soil Mechanics and Foundations Division, ASCE* **96**, 1311–1334.

Mackenzie, D. & Boyle, J. T. 1992 A method of estimating limit loads by iterative elastic analysis. I – Simple examples. *International Journal of Pressure Vessels and Piping* **53**, 77–95.

Maier, G. 1968 A quadratic programming approach for certain classes of non linear structural problems. *Meccanica* **1**, 121–130.

Maier, G. 1970 A matrix structural theory of piecewise linear elasto-plasticity with interacting yield planes. *Meccanica* **5**, 54–66.

Maier, G., Pastor, J., Ponter, A. R. S. & Weichert, D. 2003 Direct Methods of Limit and Shakedown Analysis. *In: Comprehensive Structural Integrity* pp. 631–678.

Maier, G. & Polizzotto, C. 1983 A boundary element approach to limit analysis, 5th Int. Conference on Boundary Elements, Hiroshima, Japan, Springer-Verlag, pp. 551–556.

Makrodimopoulos, A. 2009 Remarks on some properties of conic yield restrictions in limit analysis. *Communications in Numerical Methods in Engineering* p. in press.

Makrodimopoulos, A. & Martin, C. M. 2006a Lower bound limit analysis of cohesive-frictional materials using second-order cone programming. *International Journal for Numerical Methods in Engineering* **66**, 604–634.

Makrodimopoulos, A. & Martin, C. M. 2006b Upper bound limit analysis using simplex strain elements and second-order cone programming. *International Journal for Numerical and Analytical Methods in Geomechanics* **31**, 835–865.

Makrodimopoulos, A. & Martin, C. M. 2008 Upper bound limit analysis using discontinuous quadratic displacement fields. *Communications in Numerical Methods in Engineering* **24**, 911–927.

Marcal, P. V. & King, I. P. 1967 Elasto-plastic analysis of two-dimensional stress systems by the element method. *International Journal of Mechanical Sciences* **9**, 143–155.

Markov, A. A. 1947 On variational principles in theory of plasticity. *Prik. Mat. Mekh* **11**, 339–350.

Martin, J. B. 1975 *Plasticity*. MIT Press, Cambridge.

Massonnet, C. & Save, M. 1967 *Calcul plastique des constructions*. Centre Belgo-Luxembourgeois d'Information de L'Acler.

Melenk, J. & Babuska, I. 1996 The partition of unity finite element method: basic theory and applications. *Computer Methods in Applied Mechanics and Engineering* **139**, 289–314.

Moes, N., Dolbow, J. & Belytschko, T. 1999 A finite element method for crack growth without remeshing. *International Journal for Numerical Methods in Engineering* **46**, 131–150.

Monaghan, J. 1988 An introduction to SPH. *Computer Physics Communications* **48**, 89–96.

Mosek 2008 *The MOSEK optimization toolbox for MATLAB manual. http://www.mosek.com*, version 5.0 edn, Mosek ApS.

Munoz, J. J., Bonet, J., Huerta, A. & Peraire, J. 2009 Upper and lower bounds in limit analysis: Adaptive meshing strategies and discontinuous loading. *International Journal for Numerical Methods in Engineering* **77**, 471–501.

Munro, J. & Fonseca, A. D. 1978 Yield line method by finite elements and linear programming. *The Structural Engineer* **56**, 37–44.

Nagtegaal, J. C., Parks, D. M. & Rice, J. C. 1974 On numerically accurate finite element solutions in the fully plastic range. *Computer Methods in Applied Mechanics and Engineering* **4**, 153–177.

Nayroles, B., Touzot, G. & Villon, P. 1992 Generalizing the finite element method: diffuse approximation and diffuse elements. *Computational Mechanics* **10**, 307–318.

Neal, B. G. 1968 Limit load of a cantilever in plane stress. *In: Engineering plasticity edited by J. Heyman and F. A. Leckkie* pp. 473–488.

Nguyen-Dang, H. 1976 Direct limit analysis via rigid-plastic finite elements. *Computer Methods in Applied Mechanics and Engineering* **8**, 81–116.

Nguyen-Dang, H. 1984 CEPAO-an automatic program for rigid-plastic and elastic-plastic analysis and optimization of frame structures. *Engineering Structures* **6**, 35–51.

Nguyen, P. V., Rabczuk, T., Bordas, S. & Duflot, M. 2008 Meshless methods: A review and computer implementation aspects. *Mathematics and Computers in Simulation* **79**, 763–813.

Nguyen-Xuan, H., Bordas, S. & Nguyen-Dang, H. 2008 Smooth finite element methods: Convergence, accuracy and properties. *International Journal for Numerical Methods in Engineering* **78**, 175–208.

Nielsen, M. P. 1964 *Limit analysis of reinforced concrete slabs*. Acta-Polytechnica. Danmark: Kobenhavn.

Nielsen, M. P. 1998 *Limit analysis and concrete plasticity*. CRC Press.

Owen, D. R. J. & Hinton, E. 1980 *Finite Elements in Plasticity: Theory and Practice*. Pineridge, Swansea.

Pannachet, T. 2006 *Error estimation and adaptive discretisation for quasi-brittle failure*, PhD thesis, Technical University Delft.

Panzeca, T. 1992 Shakedown and limit analysis by the boundary integral equation method. *European Journal of Mechanics - A/Solids* **11**, 685–699.

Ponter, A. R. S. & Carter, K. F. 1997 Limit state solutions, based upon linear elastic solutions with a spatially varying elastic modulus. *Computer Methods in Applied Mechanics and Engineering* **140**, 237–258.

Ponter, A. R. S., Fuschi, P. & Engelhardt, M. 2000 Limit analysis for a general class of yield conditions. *European Journal of Mechanics - A/Solids* **19**, 401–421.

Prager, W. 1972 *Limit analysis: The development of a concept*. Foundation of Plasticity 2 (edited by Sawczuk), Noordhoff.

Rabczuk, T. & Belytschko, T. 2005 Adaptivity for structured meshfree particle methods in 2D and 3D. *International Journal for Numerical Methods in Engineering* **63**, 1559–1582.

Save, M. 1995 *Atlas of limit loads of metal plates, shells and disks*. Elsevier.

Save, M. & Massonnet, C. 1972 *Plastic analysis and design of plates, shells and disks*. North-Holland publishing company.

Save, M., Massonnet, C. & Saxce, G. D. 1997 *Plastic analysis and design of plates, shells and disks*. North-Holland publishing company - second edition.

Simo, J. C. & Rifai, M. S. 1990 A class of mixed assumed strain methods and the method of incompatible modes. *International Journal for Numerical Methods in Engineering* **29**, 1595–1638.

Sloan, S. W. 1988 Lower bound limit analysis using finite elements and linear programming. *International Journal for Numerical and Analytical Methods in Geomechanics* **12**, 61–67.

Sloan, S. W. 1989 Upper bound limit analysis using finite elements and linear programming. *International Journal for Numerical and Analytical Methods in Geomechanics* **13**, 263–282.

Sloan, S. W. & Kleeman, P. W. 1995 Upper bound limit analysis using discontinuous velocity fields. *Computer Methods in Applied Mechanics and Engineering* **127**, 293–314.

Sloan, S. W. & Randolph, M. F. 1982 Numerical prediction of collapse loads using finite element methods. *International Journal for Numerical and Analytical Methods in Geomechanics* **6**, 47–76.

Smith, C. C. & Gilbert, M. 2007 Application of Discontinuity Layout Optimization to Plane Plasticity Problems. *Proceedings of the Royal Society A: Mathematical, Physical and Engineering Sciences* **463**, 2461–2484.

Sze, K. Y., Chen, J. S., Sheng, N. & Liu, X. H. 2004 Stabilized conforming nodal integration: exactness and variational justification. *Finite Elements in Analysis and Design* **41**, 147–171.

Thavalingam, A., Jennings, A., McKeown, J. J. & Sloan, D. 1998 A computerised method for rigid-plastic yield-line analysis of slabs. *Computers and Structures* **68**, 601–612.

Tin-Loi, F. 1990 A yield surface linearization procedure in limit analysis. *Mechanics of Structures and Machines* **18**, 135–149.

Tin-Loi, F. & Ngo, N. S. 2003 Performance of the p-version finite element method for limit analysis. *International Journal of Mechanical Sciences* **45**, 1149–1166.

Vicente da Silva, M. & Antao, A. N. 2007 A non-linear programming method approach for upper bound limit analysis. *International Journal for Numerical Methods in Engineering* **72**, 1192–1218.

Wagner, G. J. & Liu, W. K. 2000 Application of essential boundary conditions in mesh-free methods: a corrected collocation method. *International Journal for Numerical Methods in Engineering* **47**, 1367–1379.

Wang, D. & Chen, J. S. 2004 Locking-free stabilized conforming nodal integration for meshfree Mindlin-Reissner plate formulation. *Computer Methods in Applied Mechanics and Engineering* **193**, 1065–1083.

Wolfensberger, R. 1964 *Traglast und optimale Bemessung von Platten*. Zurich, Schweiz: ETH.

Wood, R. H. 1961 *Plastic and elastic design of slabs and plates*. London: Thames and Hudson.

Yoo, J. W., Moran, B. & Chen, J. S. 2004 Stabilized conforming nodal integration in the natural-element method. *International Journal for Numerical Methods in Engineering* **60**, 861–890.

You, Y., Chen, J. S. & Lu, H. 2003 Filters, reproducing kernel, and adaptive meshfree method. *Computational Mechanics* **31**, 316–326.

Yu, H. S. & Sloan, S. W. 1994 Limit analysis of anisotropic soils using finite elements and linear programming. *Mechanics Research Communications* **21**, 545–554.

Yu, H. S., Sloan, S. W. & Kleeman, P. W. 1994 A quadratic element for upper bound limit analysis. *Engineering Computations* **11**, 195–212.

Yu, X. & Tin-Loi, F. 2006 A simple mixed finite element for static limit analysis. *Computers and Structures* **84**, 1906–1917.

Yvonnet, J., Coffignal, G., Ryckelynck, D., Lorong, P. & Chinesta, F. 2006 A simple error indicator for meshfree methods based on natural neighbors. *Computers and Structures* **84**, 1301–1312.

Zavelani-Rossi, A. 1974 Finite element techniques in plane limit problems. *Meccanica* **9**, 312–324.

Zhang, X., Liu, Y. & Cen, Z. 2004 Boundary element methods for lower bound limit and shakedown analysis. *Engineering Analysis with Boundary Elements* **28**, 905–917.

Zhang, X., Lu, M. & Wagner, J. L. 2000 A 2-D meshless model for jointed rock structures. *International Journal for Numerical Methods in Engineering* **47**, 1649–1661.

Zhao, J. D., Sheng, D. C., Sloan, S. W. & Krabbenhoft, K. 2007 Limit theorems for gradient-dependent elastoplastic geomaterials. *International Journal of Solids and Structures* **44**, 480–506.

Zhu, J. Z. & Zhang, Z. 1999 The relationship of some a posteriori estimators. *Computer Methods in Applied Mechanics and Engineering* **176**, 463–475.

Zhu, T. & Atluri, S. N. 1998 A modified collocation method and a penalty formulation for enforcing the essential boundary conditions in the element free Galerkin method. *Computational Mechanics* **21**, 211–222.

Zienkiewicz, O. C. & Taylor, R. L. 2000 *The Finite Element Method, Volume 1: The Basis*. Butterworth-Heinemann; 5 edition.

Zienkiewicz, O. C., Taylor, R. L. & Too, J. M. 1971 Reduced integration technique in general analysis of plates and shells. *International Journal for Numerical Methods in Engineering* **3**, 275–290.

Zienkiewicz, O. C., Valliappan, S. & King, I. P. 1969 Elasto-plastic solutions of engineering problems "initial stress", finite element approach. *International Journal for Numerical Methods in Engineering* **1**, 75–100.

Zienkiewicz, O. C. & Zhu, J. Z. 1987 A simple error estimator and adaptive procedure for practical engineering analysis. *International Journal for Numerical Methods in Engineering* **24**, 337–357.

Zienkiewicz, O. C. & Zhu, J. Z. 1992 The superconvergent patch recovery (SPR) and adaptive finite element refinement. *Computer Methods in Applied Mechanics and Engineering* **101**, 207–224.

Zouain, N., Herskovits, J., Borges, L. A. & Feijoo, R. A. 1993 An iterative algorithm for limit analysis with nonlinear yield functions. *International Journal of Solids and Structures* **30**, 1397–1417.